



RODRIGO FIGUEIREDO ROMA

**CHEMICAL AND CREEP MODELS APPLIED FOR
CONCRETE AFFECTED BY ALKALI-AGGREGATE
REACTION**

Master's Thesis presented to the Graduate Program in Civil Engineering of the Catholic University of Pernambuco as a partial requirement to obtain the title of Master in Civil Engineering.

Concentration Area: Construction Engineering

Advisor: Prof. Dr. Fernando Artur Nogueira Silva

Co-Advisors: Prof. Dr. Mahfoud Tahlaiti and Prof. Dr. Khaled Bourbatache

RECIFE

2021

CATHOLIC UNIVERSITY OF PERNAMBUCO
GRADUATE PROGRAM IN CIVIL ENGINEERING

RODRIGO FIGUEIREDO ROMA

**Chemical and Creep Models Applied for Concrete
Affected by Alkali-Aggregate Reaction**

Examining Committee



Prof. Dr. Fernando Artur Nogueira Silva

Advisor – Catholic University of Pernambuco, Brazil - UNICAP



Prof. Dr. Joaquim Teodoro Romão de Oliveira

Internal Examiner – Catholic University of Pernambuco, Brazil - UNICAP



Prof. Dr. Abdelhafid Khelidj

Internal Examiner – University of Nantes – IUT de Saint Nazaire – France

Approved July 13, 2021

R756c Roma, Rodrigo Figueiredo.
Chemical and creep models applied for concrete
Affected by alkali-aggregate reaction / Rodrigo Figueiredo
Roma, 2021.
106 f. : il.

Orientador: Fernando Arthur Nogueira Silva.
Coorientador: Mahfoud Tahlaiti.
Coorientador: Khaled Bourbatache.
Dissertação (Mestrado) - Universidade Católica de
Pernambuco. Programa de Pós-graduação em Engenharia
Civil. Mestrado em Engenharia Civil, 2021.

1. Reação álcalis-agregado. 2. Concreto - Testes.
3. Engenharia civil - Métodos de simulação. I. Título.

CDU 666.972

Luciana Vidal - CRB 4/1338

**CATHOLIC UNIVERSITY OF PERNAMBUCO
GRADUATE PROGRAM IN CIVIL ENGINEERING**

“No matter how hard your problems seem to be, remember to be faithful, to don’t give up and to always be close to the ones you love. You’ll be rewarded”

ACKNOWLEDGEMENTS

Firstly, I would like to thank the institutions responsible for this project, both UNICAP and ICAM-Nantes, for all the support given to me.

Secondly, I would like to thanks my supervisors Prof. Dr. Mahfoud Tahlaiti and Prof. Dr. Fernando Arthur for the orientation and careful analysis of what I did through this period of my life, and especially Prof. Dr. Khaled Bourbatache who put a lot of effort in helping me to implement the numerical models in COMSOL Multiphysics®, spending many afternoons with me trying to solve the many problems that we had encountered in this journey. Also, and no less important, I would like to thanks Prof. Dr. Abdelhafid Khelidj for the brilliant insights and collaborations to this work.

Thirdly, a special thanks to my “fathers” in the engineering life, Prof. Dr. Alexandre Duarte Gusmão and the brilliant engineer Gilmar de Brito Maia, for making all of it possible, for believing in me, giving me the financial and moral support needed to finish this work, showing me the only way to ascend in life: study a lot, work hard, follow your dreams and never give up. A special thanks also to my co-workers at Gusmão Engenheiros Associados: Allan Leite, Marina Didier, Pedro Eugenio, Victor Hugo Rufino, Lindemberg Pereira, Sr. Cláudio, Laís Moura and Willians Perley, who cheered for me all this time, sending motivational speeches to help me to carry on.

Fourthly, to my friends in Nantes, Klayne Kattiley, Ícaro Ladeira, Marc Congolo, Ye Pyae Sone Oo, Chisom Bernard, Hicham El Maimouni, Anastasia Kovalenko and Celia Mir Alvarez, for sharing laughs, love, good food and awesome moments by my side. The journey was easier with you all.

Finally, all my love to my family and friends in Brazil, who supported me, cared about me even though they were more than 7.000 km away. You showed me the miracle of limitless love, and for showing me that I will always have a place where I can go back and start again. Sometimes we have to be very far away to really understand how special and necessary is to be close to the ones we love.

ABSTRACT

ROMA, R. F. **Chemical and Creep Models Applied for Concrete Affected by Alkali-Aggregate Reaction**. 2021. 111 p. Engineering Master's Thesis in Civil Engineering Graduate School, Catholic University of Pernambuco, Recife, Brazil.

Concrete structures suffering from Alkali Aggregate Reaction (AAR) are also affected by other deleterious mechanisms such as creep and shrinkage. In Brazil and many other countries worldwide, numerous cases of building foundations and concrete dams were investigated due to the damage associated to AAR. Macroscopic AAR models must have to consider the influence of the main environmental parameters, such as temperature, saturation degree and the speed of the evolution of the chemical reaction. To be relevant in structural applications, concrete creep models have to consider several important phenomena, such as non-linearity, multi-axiality, thermal and drying effects. In order to prevent those pathologies, plan rehabilitation works or create new design procedures, the numerical simulation through finite elements method (FEM) is recognized as a very useful tool. The aim of this work is to implement a chemical model to simulate the advancement of the reaction and a mechanical model to simulate creep and shrinkage phenomena in COMSOL Multiphysics®, as a way to reassess concrete structures suffering from those mechanisms. The model to represent the AAR was developed by Morenon (2017) and the creep and shrinkage models were developed by Sellier et al. (2016), currently in use on other commercial softwares like CAST3M and Code_Aster. The models were implemented in COMSOL separately in order to evaluate their responses, comparing to theoretical results and experimental benchmarks proposed by the developers of such models. The chemical model to reproduce AAR was compared to the theoretical results shown by the developer of the model (Morenon, 2017), and the creep model was compared to experimental data regarding creep strains in different directions of a specimen under various loads and different temperatures. The results of the simulations were in reasonable good agreements with the results taken from the literature, with a maximum error of 10%, showing that the implementation in COMSOL was a success. Although, the shrinkage model didn't show any good results, and some numerical instability was encountered when the coupling of such models was done, and to fully reproduce a concrete structure affected by those deleterious phenomena, a coupled chemo-mechanical-damage model in a rheological framework must be implemented, which will be the aim of the next research projects.

Keywords: Alkali-Aggregate Reaction; Creep; Shrinkage; Numerical Simulation; COMSOL Multiphysics®

RÉSUMÉ

ROMA, R. F. **Modèles chimiques et de fluage appliqués au Béton Affecté par la Réaction Alkali-Granulat**. 2021. 111 p. Thèse de Maîtrise en Génie Civil, Université Catholique de Pernambuco, Recife, Brésil.

Structures de béton que souffrent à cause de la réaction alkali-granulat sont aussi affectées par autres mécanismes de détérioration comme le fluage et le rétrécissement. Au Brésil et dans autres pays au monde, cas nombreux des fondations des constructions et béton DAMS ont été investigués à cause du dommage associé à la réaction alkali-granulat. Modèles macroscopiques de la réaction alkali-granulat doivent considérer l'influence des paramètres naturels principaux, comme température, degré de saturation et la vitesse d'évolution de la réaction chimique. Pour être relevant aux applications des structures, modèles de fluage béton doivent considérer plusieurs phénomènes importants, comme la non-linéarité, multi-axialité, et des effets thermaux et de séchage. Pour prévenir ces pathologies, réhabilitation des plans ou créer nouvelles procédures de design, la simulation numérique pour la méthode des éléments finis est reconnue comme un outil très utile. Le but de cette recherche est d'implémenter un modèle chimique pour simuler l'avancement de la réaction et un modèle pour simuler les phénomènes de fluage et le rétrécissement sur COMSOL Multiphysics®, comme un moyen de réévaluer des structures de béton qui souffrent de ces mécanismes. Le modèle pour représenter la réaction alkali-granulat a été développé pour Morenon (2017) et les modèles de fluage et de rétrécissement ont été développés pour Sellier et al. (2016), utilisés aujourd'hui pour autres logiciels commerciales comme CAST3M et Code_Aster. Les modèles ont été implémentés en COMSOL séparément afin d'évaluer les réponses, en comparaison avec les résultats théoriques et les repères expérimentaux proposées pour les développeurs de ces modèles. Le modèle chimique pour reproduire la réaction alkali-granulat a été comparé aux résultats théoriques montrés par le développeur du modèle (Morenon, 2017) et le modèle de fluage a été comparé aux données expérimentales concernant les déformations de fluage dans différentes directions d'un échantillon sous diverses charges et différentes températures. Les résultats de la simulation ont été en assez bon accord avec les résultats tirés de la littérature, avec une erreur limite de 10%, ce qui montre que l'implémentation en COMSOL a été un succès. Le modèle de rétrécissement n'a pas montré de bons résultats, et quelques instabilités numériques des modèles ont été trouvées quand le couplage des modèles est fini, et pour reproduire complètement une structure de béton affectée par ces phénomènes de détérioration, une comparaison chimio-mécanique-dommage dans un cadre rhéologique doit être mise en œuvre, ce qui sera l'objectif des prochains projets de recherche.

Mots Clés: Réaction Alkali-Granulat; Fluage; Rétrécissement; Simulation Numérique; COMSOL Multiphysics®

RESUMO

ROMA, R. F. **Modelo químico e de fluência aplicados ao concreto afetado pela reação álcali-agregado**. 2021. 111 p. Tese de Mestrado em Engenharia Civil, Universidade Católica de Pernambuco, Recife, Brasil.

Estruturas de concreto sofrendo de Reação Álcali-Agregado (RAA) são também afetadas por outros mecanismos deletérios como fluência e retração. No Brasil e em muitos outros países, um grande número de casos de fundações de edifícios e barragens de concreto foram investigados por causa do dano associado à RAA. Modelos macroscópicos de RAA devem considerar a influência das principais variáveis ambientais, como temperatura, grau de saturação e a velocidade de evolução da reação química. Para ser relevante em aplicações estruturais, modelos de fluência devem considerar diversos fenômenos importantes como a não linearidade e multi-axialidade, e efeitos térmicos e de secagem. Para prevenir estas patologias, planejar obras de reabilitação ou criar novas diretrizes de projeto, a simulação numérica através de Métodos de Elementos Finitos (MEF) é reconhecida como uma ferramenta muito útil. O objetivo deste trabalho é de implementar um modelo químico, para simular o avanço da reação, e um modelo mecânico para simular os fenômenos de fluência e retração no COMSOL Multiphysics®, como uma forma de reproduzir estruturas de concreto sofrendo destes mecanismos. O modelo para representar RAA foi desenvolvido por Morenon (2017) e os modelos de fluência e retração por Sellier et al. (2016), atualmente em uso por outros softwares comerciais como CAST3M e Code_Aster. Os modelos foram implementados no COMSOL separadamente de forma a avaliar seus resultados, comparando a resultados teóricos e benchmarks experimentais propostos pelos desenvolvedores dos modelos. O modelo químico para reproduzir RAA foi comparado aos resultados teóricos apresentados pelo desenvolvedor (Morenon, 2017), e o modelo de fluência foi comparado aos resultados experimentais de medição de deformação por fluência em diferentes direções em corpos-de-prova de concreto sob diferentes condições de carregamento e temperatura. Os resultados das simulações tiveram correlação razoável com os resultados obtidos na literatura, com discrepância máxima de 100%, mostrando que a implementação no software COMSOL foi bem executada. Entretanto, o modelo de retração não mostrou resultados aceitáveis, e instabilidades numéricas foram encontradas na tentativa de acoplar os modelos químicos e mecânicos, e para reproduzir totalmente a estrutura de concreto afetada pelos fenômenos deletérios, é necessário implementar um modelo químico-mecânico-dano acoplado, desenvolvido em estrutura reológica, que será o objetivo das próximas pesquisas.

Palavras-chave: Reação Álcali-Agregado; Fluência; Retração; Simulação Numérica; COMSOL Multiphysics®.

SUMMARY

| | |
|---|----|
| ACKNOWLEDGEMENTS | 3 |
| ABSTRACT | 4 |
| RÉSUMÉ | 5 |
| RESUMO | 6 |
| LIST OF FIGURES | 9 |
| LIST OF TABLES | 13 |
| 1. INTRODUCTION | 14 |
| 1.1. JUSTIFICATION AND RELEVANCE OF THE TOPIC | 15 |
| 1.2. OBJECTIVES | 16 |
| 1.2.1. General Objectives | 16 |
| 1.2.2. Specific Objectives | 17 |
| 1.3. METHODOLOGY | 17 |
| 1.4. OUTLINE OF THE MASTER THESIS | 18 |
| 2. LITERATURE REVIEW | 19 |
| 2.1. ALKALI-AGGREGATE REACTION (AAR) | 19 |
| 2.1.1. Historical Background and the Problem in Brazil | 19 |
| 2.1.2. The Formation of ASR Gel and its Chemistry | 23 |
| 2.1.3. Swelling and Cracking Mechanisms Related to ASR | 27 |
| 2.1.4. Factors Influencing on AAR | 29 |
| 2.1.4.1. Influence of the Concrete Composition | 29 |
| 2.1.4.2. Influence of the Environment | 32 |
| 2.1.4.3. Influence of the Confining Stresses | 35 |
| 2.1.5. Numerical Modelling of ASR | 36 |
| 2.1.5.1. Modelling of the Generated Volume of ASR Gel | 39 |
| 2.2. MECHANICAL BEHAVIOR OF CONCRETE | 44 |
| 2.2.1. Creep and Shrinkage | 44 |
| 2.2.1.1. Creep | 45 |
| 2.2.1.2. Shrinkage | 46 |
| 2.2.1.3. Factors Influencing Shrinkage and Creep | 49 |
| 2.2.1.4. Creep And Shrinkage Modelling | 55 |
| 2.2.2. Poro-mechanical Theory | 59 |
| 2.2.3. PORO-MECHANICAL MODELS FOR SWELLING IN CONCRETE STRUCTURES | 61 |
| 3. MATERIALS AND METHODS | 64 |

| | |
|---|----|
| 3.1 RHEOLOGICAL SCHEME (GRIMAL <i>et al.</i> , 2017) | 64 |
| 3.2 CHEMICAL MODEL (MORENON, 2017) | 65 |
| 3.3 CREEP AND SHRINKAGE MODELS (SELLIER <i>et al.</i> , 2016) | 68 |
| 3.3.1 Permanent Creep – Maxwell Strain | 69 |
| 3.3.2 Reversible Creep – Kelvin Strain | 72 |
| 3.3.3 Shrinkage | 73 |
| 3.4 IMPLEMENTATION IN COMSOL® | 74 |
| 3.4.1 Implementation of the Chemical Model | 75 |
| 3.4.2 Implementation of the Shrinkage Model | 76 |
| 3.4.3 Implementation of the Creep Model | 78 |
| 4. RESULTS AND DISCUSSION | 84 |
| 4.1 RESULTS OF THE CHEMICAL MODEL | 84 |
| 4.2 RESULTS OF THE CREEP MODEL | 87 |
| 5. CONCLUSIONS AND SUGGESTION FOR FUTURE WORKS | 94 |
| REFERENCES | 96 |

LIST OF FIGURES

| | |
|---|----|
| Figure 2.1: Thomas Stanton of the California State Division of Highways and a bridge parapet wall that is showing of damage due to Alkali-Silica Reaction (ASR) (THOMAS, FOURNIER & FOLLIARD, 2013). | 21 |
| Figure 2.2. Crackings caused by AAR on the foundation blocks (pile caps) of a public building with 13 floors (adapted from ANDRADE et al., 2006a). | 22 |
| Figure 2.3. Crackings caused by AAR on buildings at the RMR (adapted from ANDRADE, 2006). | 23 |
| Figure 2.4. General flowchart for use of aggregate on concrete (NBR 15577-1:2008). | 24 |
| Figure 2.5. Diagrammatic representation of AAR. | 25 |
| Figure 2.6. Conditions to generate ASR (PAN et al., 2012). | 25 |
| Figure 2.7. Alkali-Silica Reaction process (adapted from Deschenes, 2009). | 26 |
| Figure 2.8. Illustration of aggregate being attacked by alkali hydroxyls ions (POURBEHI, VAN ZIJL & STRASHEIM, 2018). | 26 |
| Figure 2.9. Petrographic interpretation of the evolution of ASR – S-shaped curve (SAOUMA et al., 2015). | 28 |
| Figure 2.10. Crack patterns due to different types of aggregates within ASR-affected concrete (addapted from PONCE & BATIC, 2006). | 29 |
| Figure 2.11. Final expansions of ASR-affected concrete specimens depending on their size and the size of the aggregates (GAO et al., 2013). | 31 |
| Figure 2.12. Final expansions of ASR-affected concrete specimens depending on their size and the size of the aggregates (OBERHOLSTER, 1983). | 32 |
| Figure 2.13. Swelling over time to 38°C and 60°C (LARIVE, 1997). | 34 |
| Figure 2.14. Influence of the temperature in the expansion by ASR (DYER, 2015). | 35 |
| Figure 2.15. Influence of the humidity in the expansion by ASR (POYET, 2003). | 36 |
| Figure 2.16. Evolution of the uniaxial expansion over time (CAPRA & BOURNAZEL, 1998). | 37 |
| Figure 2.17. Evolution of the uniaxial expansion over time (adapted from DUNANT & SCRIVENER, 2010; NGUYEAN, STROEVEN & SLUYS, 2012). | 38 |
| Figure 2.18. Schematic representation of the diffusion of alkalis in the reactive aggregate and the creation of a reaction zone (FURUSAWA et al., 1994). | 41 |
| Figure 2.19. Representation of the idealized spherical aggregate (POYET, 2003). | 42 |
| Figure 2.20. [Top] Definition of the REV for several reactive aggregate sizes; [Bottom] Diffusion of equivalent Na ₂ O in aggregate (adapted from MULTON et al., 2009). | 43 |

| | |
|---|----|
| Figure 2.21. Typical S-shaped curve of alkali-silica reaction expansion, obtained on the experimental tests from Larive (1998) (LEMARCHAND et al., 2005). | 44 |
| Figure 2.22. Total deformation of concrete subjected to constant loading (adapted from BALABUCH, 2018). | 45 |
| Figure 2.23. Total deformation of concrete over time subjected to a constant loading of 10 MPa (KUPERMAN, 2007). | 46 |
| Figure 2.24. Creep reversibility (MEHTA & MONTEIRO, 2014). | 47 |
| Figure 2.25. Cracking due to autogenous shrinkage (DYER, 2015). | 48 |
| Figure 2.26. Drying shrinkage reversibility (MEHTA & MONTEIRO, 2014). | 49 |
| Figure 2.27. The influence of w/c ratio on the creep strain (WENDER, HUBLER & BAZÄNT 2015). | 50 |
| Figure 2.28. The influence of w/c ratio and aggregate content on the shrinkage strain (NEVILLE & BROOKS, 2013). | 51 |
| Figure 2.29. Effect on shrinkage by the replacement of cement by admixtures (ZHANG & MALHOTRA, 1995). | 52 |
| Figure 2.30. Effect on shrinkage by the replacement of cement by admixtures (ZHANG & MALHOTRA, 1995). | 53 |
| Figure 2.31. Influence of the environmental conditions on the shrinkage (JOSHAGHANI, BALAPOUR & RAMEZANIANPOUR, 2018). | 54 |
| Figure 2.32. Influence of the environmental conditions on the compression strength (JOSHAGHANI, BALAPOUR & RAMEZANIANPOUR, 2018). | 54 |
| Figure 2.33. Influence of the theoretical thickness on creep and shrinkage (MEHTA & MONTEIRO, 2014). | 55 |
| Figure 2.34. Representation of the concrete in 3 zones (DORMIEUX et al., 2004). | 62 |
| Figure 3.2. Rheological scheme (GRIMAL et al., 2017). | 66 |
| Figure 3.2. Strains effect on gel pressure (GRIMAL et al., 2017). | 69 |
| Figure 3.3. Idealized rheological scheme for poro-mechanical creep model (SELLIER et al., 2016). | 70 |
| Figure 3.4. Stress field heterogeneity at meso-scopic scale and consequences in terms of shrinkage forces transmission to macroscopic scale, for two conditions: (1) free shrinkage and (2) shrinkage amplified by external mechanical loading (SELLIER et al., 2016). | 75 |
| Figure 3.5. General parameters – environmental conditions, loading and total time of simulation. | 76 |
| Figure 3.6. Chemical model parameters. | 76 |
| Figure 3.7. Internal variables of the chemical model. | 77 |
| Figure 3.8. Advancement of the reaction written as a domain ODE. | 77 |
| Figure 3.9. Shrinkage model parameters. | 78 |

| | |
|--|----|
| Figure 3.10. Internal variables of the shrinkage model. | 78 |
| Figure 3.11. Capillary pressure (shrinkage stress). | 78 |
| Figure 3.12. Maxwell module parameters. | 79 |
| Figure 3.13. Internal variables of the Maxwell module. | 80 |
| Figure 3.14. Internal variables of the function to consider the non-linearity dependance on loading level. | 80 |
| Figure 3.15. Discretization of the Maxwell module applied as an ODE. | 81 |
| Figure 3.16. Coded function of the Maxwell module applied as an ODE. | 81 |
| Figure 3.17. Maxwell strains applied External Strain. | 82 |
| Figure 3.18. Kelvin module parameters. | 82 |
| Figure 3.19. Internal variables of the Kelvin module. | 83 |
| Figure 3.20. Discretization of the Kelvin module applied as an ODE. | 83 |
| Figure 3.21. Coded function of the Maxwell module applied as an ODE. | 84 |
| Figure 3.22. Maxwell strains applied External Strain. | 84 |
| Figure 4.1. Effects of the characteristic time over the advancement of the reaction – comparison with the results shown by Morenon (2017). | 86 |
| Figure 4.2. Effects of the temperature over the advancement of the reaction – comparison with the results shown by Morenon (2017). | 86 |
| Figure 4.3. Effects of the saturation degree over the advancement of the reaction – comparison with the results shown by Morenon (2017). | 87 |
| Figure 4.4. Difference of the evolution of the advancement of the reaction for the same main parameters, shown by Morenon (2017). | 87 |
| Figure 4.5. (a) Geometry of the problem; (b) Boundary conditions for uniaxial compression; (c) Boundary conditions for biaxial compression. | 88 |
| Figure 4.6. Evolution of the total strain for concrete type C1 under uniaxial compression. | 90 |
| Figure 4.7. Evolution of the total strain for concrete type C2 under uniaxial compression. | 90 |
| Figure 4.8. Evolution of the total strain for concrete type C3 under uniaxial compression. | 91 |
| Figure 4.9. Evolution of the total strain for concrete type C1 under biaxial compression. | 91 |
| Figure 4.10. Evolution of the total strain for concrete type C2 under biaxial compression. | 92 |
| Figure 4.11. Evolution of the total strain for concrete type C3 under biaxial compression. | 92 |
| Figure 4.12. (a) Geometry of the problem; (b) Boundary conditions for uniaxial compression. | 93 |

Figure 4.13. Evolution of the total strain for the different temperatures in the creep test performed by Ladaoui et al. (2013).

94

LIST OF TABLES

| | |
|--|----|
| Table 1: Material parameters used to calculate the volume of gel (Morenon, 2017). | 68 |
| Table 2: Material parameters to calculate the intrapore pressure (Morenon, 2017). | 69 |
| Table 3: Material parameters to calculate the permanent creep (Sellier <i>et al.</i> , 2016). | 73 |
| Table 4: Material parameters to calculate the reversible creep (Sellier <i>et al.</i> , 2016). | 74 |
| Table 5: Loading scenarios for the multiaxial creep tests by Kim <i>et al.</i> (2005). | 88 |
| Table 6: Main material parameters to simulate the multiaxial creep tests performed by Kim <i>et al.</i> (2005). | 89 |
| Table 7: Main material parameters to simulate the creep tests performed by Ladaoui <i>et al.</i> (2013). | 93 |

CHAPTER 1

1. INTRODUCTION

The concrete is probably the most used civil construction material in the modern world. Developing countries such as China, India and Brazil stand out as the largest consumers of this material in the execution of buildings and infrastructure. The durability of concrete structures must be guaranteed in order to prevent expensive maintenance or even failure of those structures (METALSSI & TOUTLEMOND, 2012).

The behavior of concrete includes the viscosity, elasticity and plasticity, and it can be characterized as an elasto-viscoplastic material, which its strains can be due to shrinkage, creep and damage (LEONHARDT & MÖNNING, 1977). The strains linked to shrinkage and creep are known as the two main factors affecting the durability of the structures in the long term. To better understand how those strains occur over time, many experimental programs, formulations and models with the objective of predicting the concrete behavior were developed (ABDELLATEF et al., 2015).

In addition, expansion is another type of deformation affecting concrete. The chemo-physical expansion processes activated by certain environmental conditions can lead to significant loss in strength and stiffness of many concrete structures. When those environmental conditions are presented, damage due to expansion might appear, and those expansions are due to one or more pathologies affecting the concrete structures (SCRIVENER, 2009; COMI & PEREGO, 2011). The inadequate durability of the concrete is perceived by the pathological manifestations, whose agents can reside inside itself or come from the external environment. Internally, these agents can be found in the chemical and mineralogical composition of cement or aggregates. Externally, aggressive substances penetrate the interior of concrete structures through the capillary network (connected porous matrix) in the form of gases, vapors or liquids, leading to chemical deterioration, which may involve the formation of expansive products (e.g. the alkali-aggregate reaction).

Some pathologies such as Alkali-Aggregate Reaction (AAR) and Delayed Ettringite Formation (DEF), external sulfate attack and even frost, are considered as Internal Swelling Processes (ISP). The ISP cause expansion on the affected concrete, leading to cracking, decrease of its mechanical properties and loss of early durability (lifespan of concrete structures). These pathologies often cause severe problems in terms of serviceability, structural integrity and sustainable operation of the concrete structures. The two reactions (AAR and DEF) are often observed acting simultaneously on concrete structures, implying the precise understanding of these processes acting in two scenarios: alone and combined (MARTIN, OMIKRINE; TOUTLEMONDE, 2012; MARTIN, BAZIN & TOUTLEMONDE, 2012).

The AAR is a phenomenon involving chemical reactions in which some constituents of the aggregate react with the alkaline hydroxides dissolved in the solution of the concrete pores, and it leads to cracking and loss of durability in cement-based composites. AAR is a chemical reaction in either concrete or mortar between hydroxyl ions (OH^-) of the alkalis (sodium and potassium) from hydraulic cement (or others

sources), and certain constituents of some aggregates; under certain conditions deleterious expansion of concrete or mortar may result (RAJABIPOUR et al., 2015).

Basically, four conditions must be satisfied in order to generate AAR on concrete: the presence of reactive aggregate, an adequate level of alkalinity, sufficient moisture in the pores of concrete and high temperature. The understanding of AAR is very complex and such processes have an important role on the pathologies found on big structures such as bridges, railroads, dams and building foundations. The damage caused by AAR goes from localized cracking to generalized failure and performance degradation. The effective resolution of this problem is also very complex since the description of the mechanism of the reaction is not yet endorsed by conclusive theoretical formulation accepted by worldwide scientific associations, and the experimental tests for careful observation of the phenomenon requires considerable amount of time and resources.

As the AAR is a process that takes many years to produce visible damage, it is very important to predict the behavior of the AAR-affected concrete structures, done in a way that is possible to evaluate the stability and durability of such structures. In the other hand, the numerical simulations of AAR-affected concrete structures generally neglect the interactions between AAR, creep and shrinkage (GRIMAL et al., 2007; COMI & PEREGO, 2011; PAN et al., 2013).

1.1. JUSTIFICATION AND RELEVANCE OF THE TOPIC

As time goes by, the society needs larger and higher structures than before in order to continue the process of development of cities and their infrastructures. Such megastructures (e.g. large raft foundations, dams, long tunnels and bridges) use a huge volume of concrete in its execution, and such amount of concrete needs a large quantity of aggregate, but sometimes non-reactive aggregates aren't available locally – near to the construction site – and shipping it wouldn't be feasible. In addition, reactive aggregates are readily and abundantly available at lower cost and reduced environmental impact when compared with non-reactive materials (THOMAS; FOURNIER; FOLLIARD, 2013). But the usage of reactive aggregates may lead to the appearance of AAR if all the environmental conditions are satisfied.

The deterioration caused by the ISP leads to high cost maintenance or rehabilitation of the affected concrete structures, and many countries all over the world have been reporting evidences of DEF and AAR on these kinds of infrastructures and buildings. According to Taylor, Famy & Scrivener (2001) and Hobbs (1999), in many of these cases the DEF happened simultaneously with the AAR, when siliceous aggregates were used on concrete. In the literature there are a lot of reports showing those two phenomena – DEF and AAR – often manifested together since both are activated by high temperatures on the curing stage, followed by exposure in a high humidity environment.

In many countries a large amount of resources has been applied to the repair and maintenance of concrete structures affected by the AAR. For example, according to Oberholster, quoted by Kuperman (2007), South Africa had spent the amount of U\$ 350 million only between the 1970s and 1996. In the year of 2008, the organizers of the 13th International Conference on Alkali-Aggregate Reactions in Concrete (ICAAR) estimated

the annual cost to rehabilitate and substitution of constructions affected by ISR is U\$ 2.6 billion.

Another good example is the case of the Elgeseter Bridge, in Norway, built between 1949 and 1951 and costing kr\$1.5 million at the time. In 1989 the bridge was already damaged due to shrinkage, creep and corrosion of the reinforcements concrete columns, but in the early 90's many other damage due to AAR was also verified, and the cost to repair all the bridge in 5 years was around kr\$ 6.8 million at the time (JENSEN, 2004).

Such huge amounts of money are a big concern to the civil construction industry and also the governments all over the world, leading to the creation and funding of many research centers (e.g. LMDC-INSA) in order to develop technology suitable for characterization, mitigation and repairing of the affected structures. The main research centers are located in France, Canada, United Kingdom, Germany and United States of America.

According to Divet et al. (2003), there are three components to the investigation of structures suffering from ISP:

- Chemo-physical characterization focusing primarily on the materials (cement and aggregates);
- Computational modeling of the evolution of damage and assessing the structural response of the structure;
- Managing the structure.

The presenting research project, a partnership between UNICAP (Universidade Católica de Pernambuco – Recife, BR) and ICAM (Institut Catholique de d'Arts et Métiers – Nantes, FR) is focused on the computational modeling, as the numerical simulation is an adequate instrument to quantify the extension of the damage caused by the AAR, assisting on the decision making regarding structural recovery works and also serving as a basis to modify some structural design criteria. In possession of all the information shown above, the research of numerical modeling of ISP affecting concrete structures must be done with caution and precision in order to mitigate the effects of these phenomena still on the design project stage, avoiding the high costs of maintenance and rehabilitation on those affected structures.

This research program was done during the COVID-2019 pandemic scenario, a very hard time for everyone worldwide. The ones involved in this work had put a lot of effort in order to maintain the schedule of the program, and most of the weekly reunions were done in a virtual platform.

1.2. OBJECTIVES

1.2.1. General Objectives

This work aims to perform a numerical simulation of the chemical and creep behavior of concrete affected by Alkali-Aggregate Reaction (AAR) on an isotropic non-linear bidimensional model using the software COMSOL Multiphysics®. This software is

based on Finite Element Method (FEM) for the solution of mechanical analysis for linear and non-linear problems.

1.2.2. Specific Objectives

- Organize and present a literature review about AAR chemistry modelling, as well as creep and shrinkage modelling.
- Implement the chemical model proposed by Morenon (2017) in COMSOL Multiphysics®, which calculates the pressure of the gel regarding the volume of gel created and the advancement of the reaction, comparing the results in order to validate the implementation.
- Implement the creep and shrinkage models proposed by Sellier et al. (2016) in COMSOL Multiphysics®, which relates the permanent and reversible creep strains to the elastic strain in any direction and also to some fitting material parameters obtained in creep tests. The validation of the implementation was made by comparison with experimental benchmark proposed by the developers of the model.

1.3. METHODOLOGY

For the development of this work, primarily it was done a literature review in order to search for the most advanced and suitable numerical models related to AAR, creep and shrinkage. The models developed and published by the LMDC-INSA Toulouse, coordinated by the professors Alain Sellier, Stéphane Multon and others, were selected due to its background: they were calibrated by extensive experimental programs and experimental data found in literature. The very up-to-date models showed results in very good agreement to the experimental results.

For the chemical model, it was selected the model proposed by Morenon (2017), which takes into account the main environmental and material parameters that influence on the advancement of the reaction and the ASR gel pressure generated. For the creep and shrinkage behavior, it was selected the model proposed by Sellier et al. (2016).

Those models were implemented on COMSOL Multiphysics®, a commercial cross-platform finite element analysis, solver and multiphysics simulation software. It allows conventional physics-based user interfaces and coupled systems of partial differential equations (PDEs). COMSOL provides an ideal and unified workflow for electrical, mechanical, fluid, acoustics, and chemical applications.

When the models were successfully implemented, the modules were validated by comparison with experimental and numerical benchmark found in literature. The coupling of all the models showed numerical instability, therefore it's the full coupled chemo-mechanical model is not presented in this work.

For the readers, probably there is still a question remaining: why, amongst all the FEM softwares available, the author chose COMSOL? The answer for this question

remains on the procedures adopted to develop this research, as those chemo-mechanical models have already been implemented in other commercial softwares like CAST3M and Code_Aster. Also, COMSOL is able to simulate sensors in concrete structures, as seen on the works of Alcantara Jr. & Gonçalves Jr. (2015) and Pomarico et al. (2016), hence it would make possible – in the near future – to simulate a real concrete structure affected by ISP and the sensors inside of it, comparing the real data with the numerical simulations, providing an enormous contribution to the scientific community and civil construction industry.

1.4. OUTLINE OF THE MASTER THESIS

The first chapter is a general introduction about the problematic of the degradation of concrete structures, the importance of studying it and some costs related to those problems, which highlights the justification behind this research. Also, it's presented the objectives related to the research project and the methodology used in the development of this work. At least, it's shown the organization of the report.

The second chapter is about the literature review of this research, regarding the main concepts on the two subjects of the work: alkali-aggregate reaction (AAR) in concrete and the mechanical behavior induced by creep and shrinkage. The first part, which is about AAR, it's presented a historical background and the problem in Brazil, followed by a brief explanation about the formation of the gel produced by the reactions, a resume about the swelling and cracking mechanisms related to AAR, the factors which influence in this reaction and the main numerical models related to this problem. The second part, regarding the mechanical behavior of concrete, it's first presented the main concepts about creep and shrinkage, the factors which influence those phenomena and the main mathematical models, and secondly it's presented a brief concept about the poro-mechanical theory and the poro-mechanical models for swelling products in concrete structures.

The third chapter concerns about the materials and methods used in these research project, regarding the numerical models for both AAR (Morenon, 2017), creep and shrinkage (Sellier et al., 2013), explaining the required formulation and the main material parameters and its suggested values. Next, it's presented the implementation of those models in the software COMSOL Multiphysics®, and a simple step-by-step procedure for any researcher to do the same.

The fourth chapter concerns about the results of such simulations, according to the theoretical behavior and some experimental benchmarks available on the works of the developers of the models presented in Chapter 3.

The fifth and last chapter concerns the main conclusions about the work, regarding the limitations and the positive points encountered by the author, and of course some perspectives for future works.

CHAPTER 2

2. LITERATURE REVIEW

For well-designed concrete structures, the main source of damage is the shrinkage, creep and expansion processes, which can act combined or not. The expansion processes are often called Internal Swelling Processes (ISP), which are pathologies that degrade the concrete structures due to the formation of an intrapore product, and its swelling is responsible for damaging the solid skeleton of concrete.

This chapter is then divided in two parts, the first one is dedicated to the AAR and the second part is dedicated to the main mechanical behaviors of concrete which are necessary to numerically assess a concrete structure. Those mechanical behaviors can be resumed in creep and shrinkage, poro-mechanical theory and the main poro-mechanical models related to AAR.

In the subject of AAR, first is provided an historical background and an overview of the problem in Brazil, followed by the main reaction mechanisms and the most significant parameters on the formation of expansive product (AAR gel), and for the last is related the main mathematical models found in the literature related to the formation of the gel and its expansion.

In the subject of mechanical behavior, first is developed a brief concept of creep and shrinkage, followed by the theory of poro-elasticity and the models making it possible to numerically simulate the damage on concrete structures, and the effects of swelling stresses on the porous media of concrete.

2.1. ALKALI-AGGREGATE REACTION (AAR)

In this topic, it's presented a brief historical and theoretical review about the concepts linked to AAR. The factors which influence the occurrence of those phenomena are commented as well. This explanation is necessary in order to better understand the chemical model and its main material parameters presented in the Chapter 3 (Materials and Methods).

2.1.1. Historical Background and the Problem in Brazil

In the 1930's, a several number of pathological manifestations with expansive behavior were found on bridges and pavements in USA, and the real causes were not known at the time (HOBBS, 1988). Since Stanton (1940) – see Figure 2.1 – proved through experimental tests that aggregates derived from natural rocks aren't necessarily chemically inert materials (as they were supposed to be), the scientific community knows that the mineralogical constituents of the aggregates reacts with the alkalis from Portland cement. This chemical reaction was called Alkali-Aggregate Reaction (AAR).

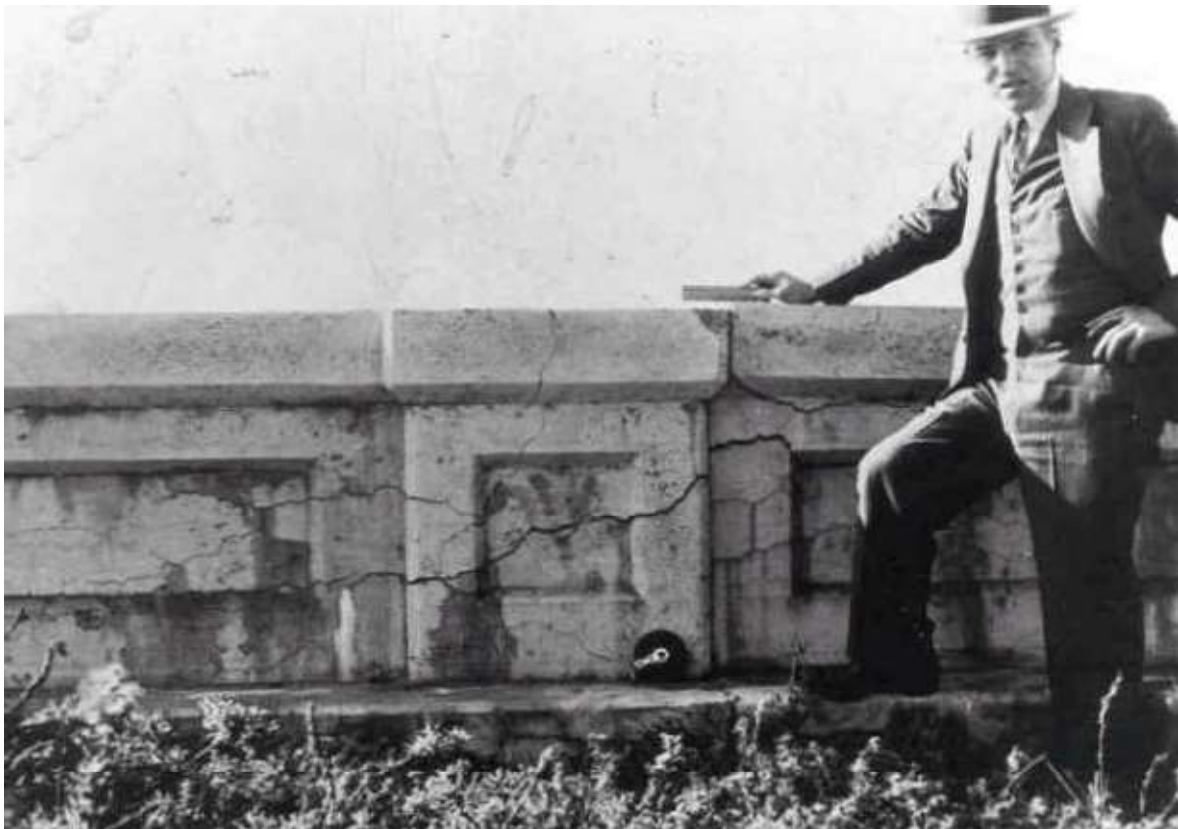


Figure 2.1. Thomas Stanton of the California State Division of Highways and a bridge parapet wall that is showing of damage due to Alkali-Silica Reaction (ASR) (THOMAS, FOURNIER & FOLLIARD, 2013).

At the beginning of 1980's, an important number of concrete structures had their damages associated to the expansive effect of Alkali-Silicate gel produced by AAR. At the time, the concern on the phenomenon's consequence motivated the beginning of more careful scientific investigations. The problem was put on the spotlight in a way that the volume and diversification of scientific research on this subject has been progressively expanded, leading to the growing discovery of new cases (THOMAS, FOURNIER & FOLLIARD, 2013).

The damage caused by AAR can be found without difficulties in concrete structures throughout the world, and today more than 50 countries have reported the occurrence of this phenomenon. In fact, some researchers believe that there are characteristic damages produced by AAR in concrete structures that are erroneously attributed to other causes, and it leads the scientific community to think that the seriousness of this problem (AAR) is even greater than they thought it was.

In Brazil, the firsts scientific works about the reactive potential of the aggregates are dated from 1960's when Heraldo Gitahy did extensive research on pozzolanic materials for the CESP's Urubupungá complex, which used calcined clay to mitigate AAR (PACELLI, 1999). This technique was a success because until now there are no registries of this kind of reaction affecting the buildings. However, it was only in 1997 that the problematic of AAR gained more attention with the creation of the 1st Symposium on Alkali-Aggregate Reactivity in Concrete Structures. Silveira (1997) showed that in Brazil,

the first records of concrete structures affected by AAR are dated from 1946 in the CEMIG's Peti Dam, and the aggregate used to fabricate the concrete was originally from gneiss rock.

Since 2004, the attention of the scientific community in Pernambuco (PE-BR) has turned to civil constructions in the Recife's Metropolitan Region (RMR) that was motivated by the collapse of the building Areia Branca. An extensive inspection was carried out on the foundation structures and at the end of several diagnoses made by many professionals, some signs of AAR were verified, although this pathological manifestation was not the cause of the collapse of the building. In Pernambuco there is a significant number of constructions proven to be affected by AAR. The cases registered are: i) six foundation slabs for refrigeration towers; ii) Tapacurá's Dam; iii) Paulo Guerra's bridge; iv) dozens of foundation blocks (pile caps) from buildings situated on the RMR (ANDRADE, 2006; ANDRADE et al., 2006a; ANDRIOLO, 2000; BRITO JÚNIOR; FERRO, 2016).

The expansions of the aforementioned structures can be attributed to the usage of a large rock deposit located very close to a geological fault, and such deposit is a source of extraction of aggregates for concrete. It is known that quartz minerals in regions subjected to tectonic movements present their crystals with a deformed geometric arrangement, which is one of the varieties responsible for the slowest expansion rates that can last for many years (MADUREIRA, 2007).

Since the collapse of the building Areia Branca until 2006, more than 30 cases of AAR were found on the RMR. According to Andrade (2006), Andrade et al. (2006a), Andrade et al. (2006b) and Pecchio et al. (2006), the major causes are: i) the existence of aggregates containing extremely deformed, microcrystalline and recrystallized quartz; ii) low depth of the water table (near to the ground surface); iii) availability of soluble alkalis (specially potassium); iv) high ambient temperatures. Unlike the classic cases in the literature, where deleterious expansions occur over long periods of time, some constructions on the RMR showed deleterious cracks just in three years of construction.

In some cases, the expansion caused by the AAR is so severe that the internal tensile stresses in the concrete reached extremely high values (PECCHIO et al., 2006), as can be seen by the rupture of the stirrup shown in Figure 2.2. The magnitude of these expansions caused by the AAR in the constructions of RMR can also be visualized in the photographs shown in Figure 2.3.



Figure 2.2. Crackings caused by AAR on the foundation blocks (pile caps) of a public building with 13 floors (adapted from ANDRADE et al., 2006a).



Figure 2.3. Crackings caused by AAR on buildings at the RMR
(adapted from ANDRADE, 2006).

After 80 years since Stanton's first works, many other researches programs had been done throughout the world. A significant number of works approach the problem in a very efficient and clear way on how to avoid the reaction before it is consolidated, using techniques which consists on the use of mineral and chemical additions, limitation of the alkali content of cement, showing the importance on the prevention of the phenomenon. With regard to the treatment of AAR in concrete structures, what has been seen are empirical measures such as: i) injection of cementitious materials in the cracks; ii) monitoring of the expansions; iii) cuts to relieve tension caused by the expansive products of AAR; iv) restructuring of structural members etc.

The Brazilian Standard ABNT NBR 15577 (2008) shows how to perform a risk analysis on the possibility of the occurrence of AAR by taking into account the conditions of exposure, dimensions and the importance of the structure or the concrete member, in order to indicate a possible preventive action. However, the document does not yet include repairs and/or mitigating actions in situation where the AAR pathological manifestations are already happening.

To decide on which aggregate should be used on concrete mixture and possibly some mitigating actions, the Brazilian Standard ABNT NBR 15577 (2008) recommends the use of the flowchart presented in Figure 2.4, taking into account the risk analysis and its factors.

According to the flowchart, whenever it is necessary to classify the degree of reactivity of an aggregate, petrographic analysis must be carried out, and subsequently, it must be done the reactivity test by MABA – *Método Acelerado em Barras de Argamassa* (Accelerated Mortar Bar Test - ABT NBR 15577-4), which classifies the aggregate as potentially reactive when its expansion limit is equal to or greater than

0.19%, at 30 days of testing. To confirm the results obtained by MABA and/or there is a necessity for more accurate assessment of the reactivity of an aggregate, the use of the MPC – *Método dos Primas de Concreto* (Concrete Prisma Test - ABNT NBR 15577-4) – is required. For the aggregate to be considered potentially reactive by the MPC, the expansion limit has to be equal to or greater than 0.04%, at one year of testing. Values below those limits suggest that the aggregate is potentially innocuous. If there is a discrepancy in the results provided by MABA and MPC, it is suggested that only the results on concrete specimens must be used.

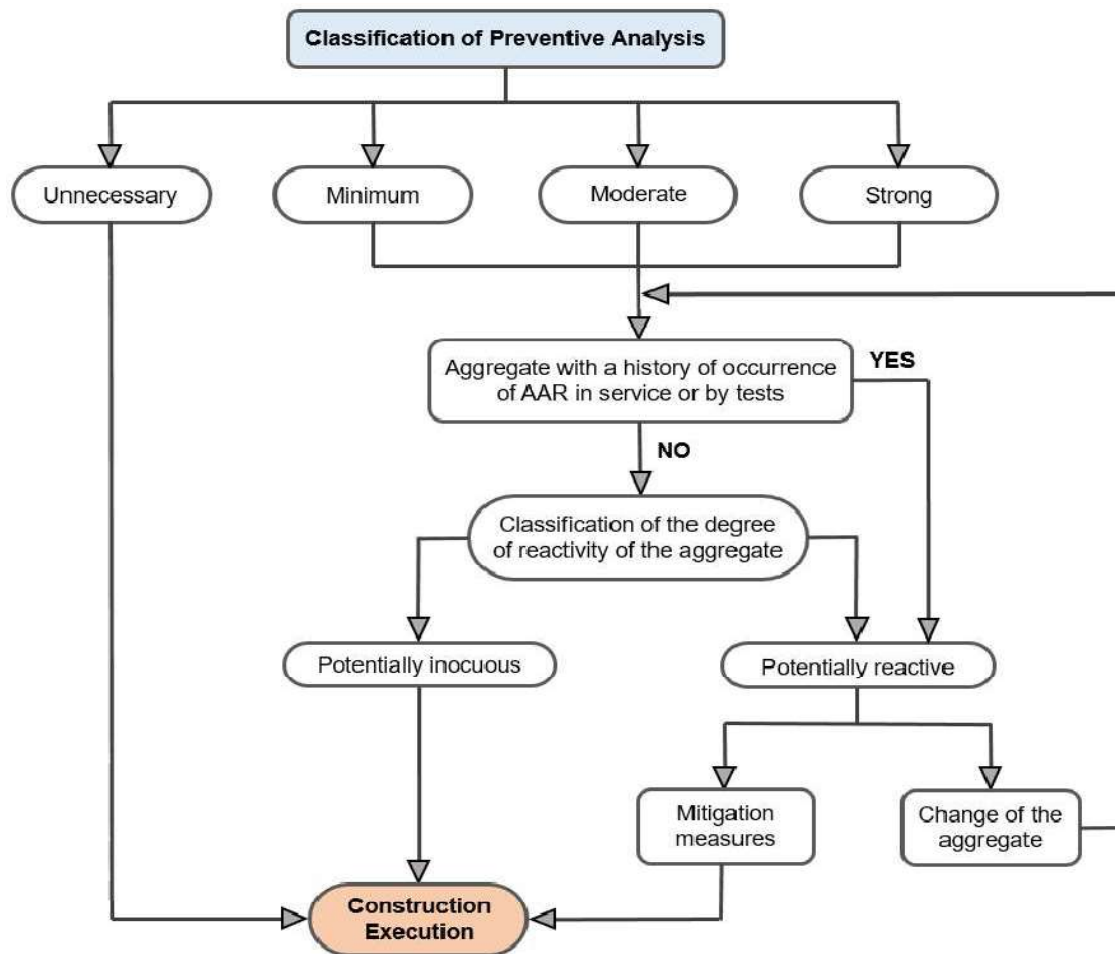


Figure 2.4. General flowchart for use of aggregate on concrete (NBR 15577-1:2008).

2.1.2. The Formation of ASR Gel and its Chemistry

In a general way, Alkali-Aggregate Reaction (AAR) can be considered as a chemical reaction which occurs inside of a concrete structure, and this reaction involves four agents (Figure 2.5 and Figure 2.6): i) reactive minerals located on the aggregates; ii) the alkalis located on the concrete pores moisture; iii) water; iv) high temperature.

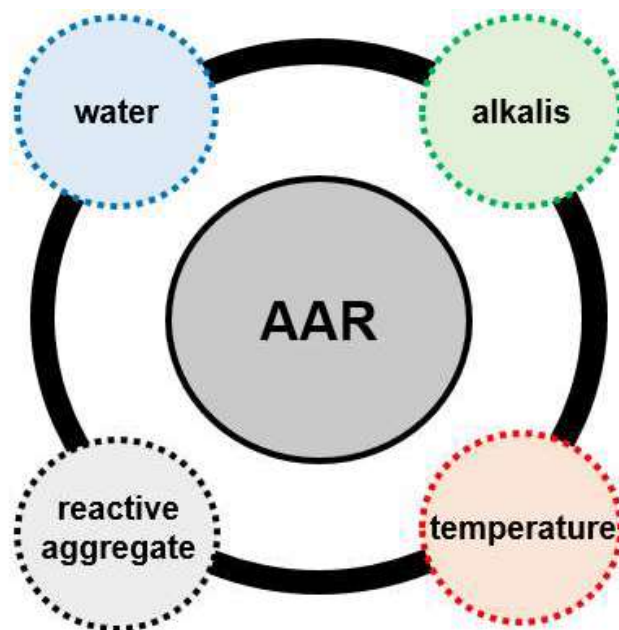


Figure 2.5. Diagrammatic representation of AAR.

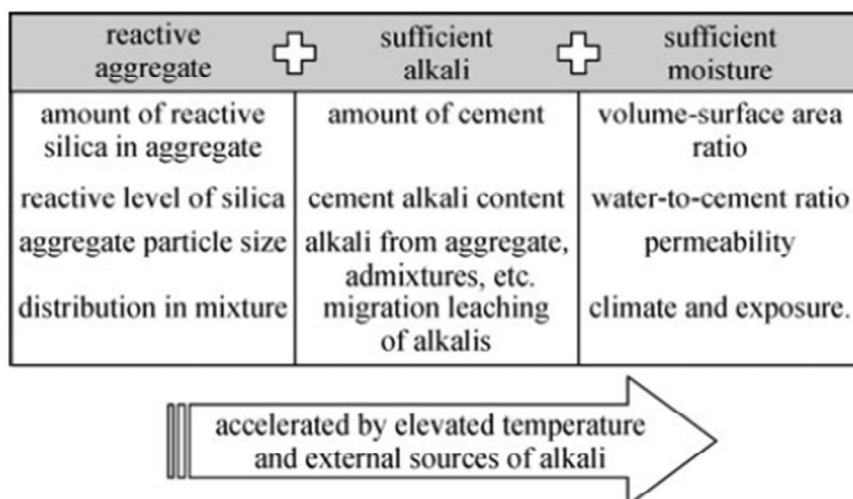


Figure 2.6. Conditions to generate ASR (PAN *et al.*, 2012).

The product of this reaction causes expansion and consequently cracking, drastically interfering on the structure durability (HASPARYK, 2011). Commonly, AAR is divided into two different types: Alkali-Silica Reaction (ASR) and Alkali-Carbonate Reaction (ACR). There is also a particular case of the ASR which is the Alkali-Silicate Reaction (ASSR). ASR is derived from certain siliceous rocks and minerals, such as opal, chert, microcrystalline quartz, and acidic volcanic glass, present in some aggregates. In the other hand, ACR is derived from certain carbonate rocks, particularly calcitic dolostone and dolomitic limestones, present in some aggregates. However, ASR is far more widespread than ACR, and now is recognized as a major cause of concrete deterioration in the USA and numerous countries worldwide (THOMAS, FOURNIER & FOLLIARD, 2013).

ASR is derived from certain siliceous rocks and minerals, such as opal, chert, microcrystalline quartz, and acidic volcanic glass present in some aggregates. In the other hand, ACR is derived from certain carbonate rocks, particularly calcitic dolostone and dolomitic limestones.

The ASR process happens in several stages and it's also very complicated to understand and exposed, but the works of Glasser & Kataoka (1981; 1982) proposed that the phenomenon can be summarized in two steps (Figure 2.7). The first step is the rupture of the aggregate siloxane networks ($Si-O-Si$) caused by the attack of hydroxyl ions (Figure 2.8), which produces alkali silicate and silicic acid, immediately reacting with further hydroxyl ion, and as a result the product of this reaction (the alkali silicate or alkali-silica gel) is amorphous and hygroscopic. The second step is the expansion of the alkali-silica gel by absorption of free water, causing cracking on the cement paste and on the aggregate (depending on the type of the aggregate).

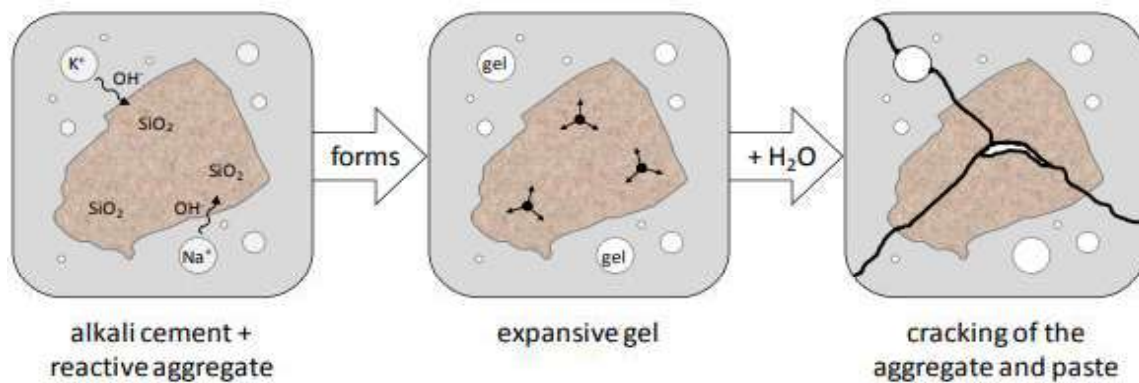


Figure 2.7. Alkali-Silica Reaction process (adapted from Deschenes, 2009).

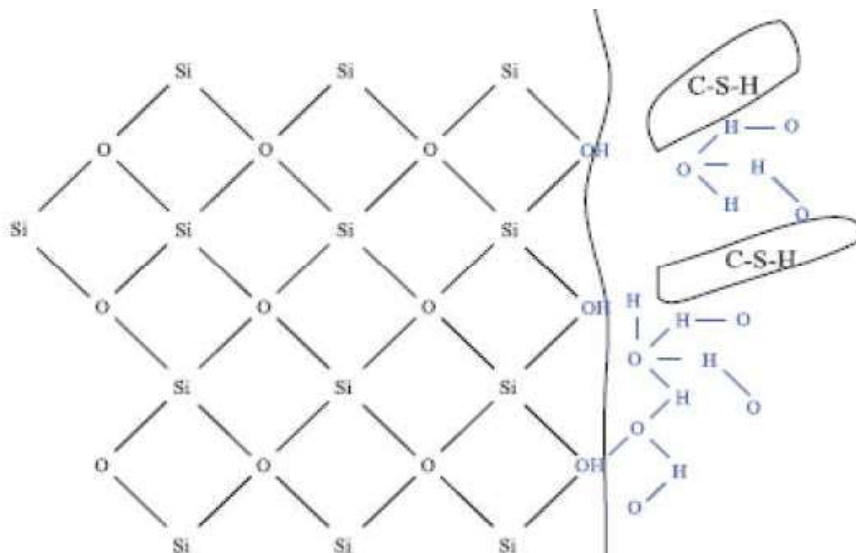


Figure 2.8. Illustration of aggregate being attacked by alkali hydroxyls ions (POURBEHI, VAN ZIJL & STRASHEIM, 2018).

According to Powers & Steinour (1955a), the ASR product is a solid in the absence of water, and this solid can be called basic gel, which has the capacity to imbibe water molecules, generating extensive swelling of the gel and transforming it on a fluid. The authors stated that:

“Hydrous silica aggregates, as already mentioned, may of course already contain substantial silanol bonding. These silanol groups react readily with further hydroxyls. As more siloxane bonds are attacked, a gel-like layer forms on the surface of the aggregate. Some silica may even pass into the solution.

The negatively charged species of this gel attract positive charges, which are present in the pore solution in the form of mobile species such as sodium, potassium, and calcium. They diffuse into the gel in sufficient numbers to balance the negatively charged groups.

The presence of these ions determines important properties of the gel. If the gel is formed in an environment rich in Ca^{2+} , mainly this species will be taken up by the gel, soon forming particles of C-S-H as a separate constituent. Thus, the gel is transformed into a rigid and unreactive structure. This process may be considered similar to the pozzolanic reaction in concrete. If the pore solution, however, is low in Ca^{2+} , the gel takes up mainly Na^{+} and K^{+} . This results in a more viscous consistence of the gel. This gel will also imbibe further water, which will cause its large expansion.

If the gel is in contact with CO_2 , which occurs when it is exposed to the atmosphere, it carbonates. This is observed on the surface of cut concrete specimens that have undergone ASR. The ability to imbibe water and ionic species as Na^{+} and K^{+} cause the water contents, densities, and other physical properties to vary over wide ranges. It is very difficult to predict the species of gel that may form in a certain concrete.”

Saouma *et al.* (2015) detail the ASR in stages, taking as reference the petrographic interpretations on the evolution of the reaction (Figure 2.9). For the stage I (*Micro-Nucleation*), the reaction starts around the aggregate causing no expansion. On the stage II (*Development*) occurs the formation of the gel in the pores of the reactive aggregates which starts the expansion, and the pressure exerted by this expansion to cracking in the aggregate. On the stage III (*Acceleration*), the process of deterioration becomes more noticeable as the cracking in the reactive aggregate starts to propagate to the cement paste. This cracking grows in size and quantity, and the gel permeates through them, reaching distant voids in the cement paste. For the stage IV (*Deterioration*), severe damage occurs in the structure, for example rupture of the rebar reinforcement and total loss of structural integrity.

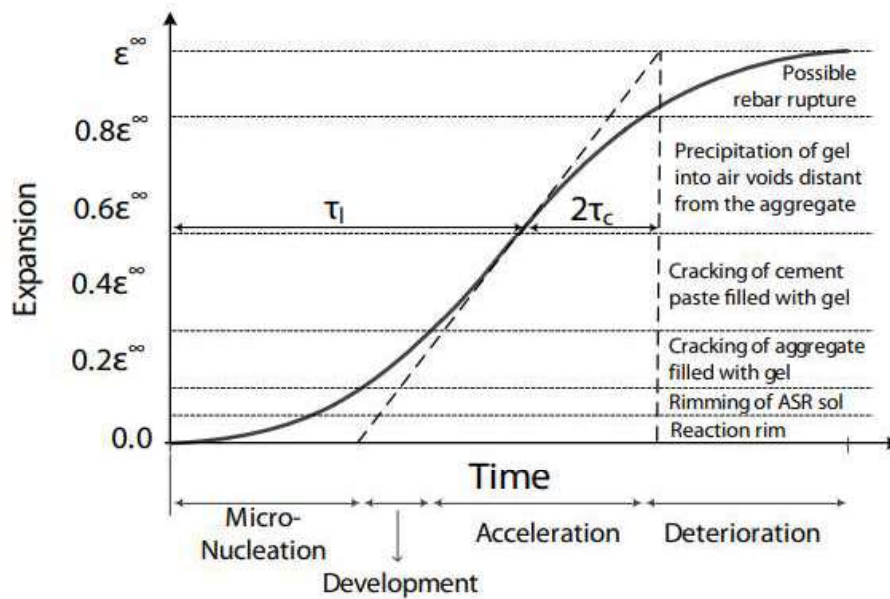


Figure 2.9. Petrographic interpretation of the evolution of ASR – S-shaped curve (SAOUMA *et al.*, 2015).

2.1.3. Swelling and Cracking Mechanisms Related to ASR

The mechanism of expansion and cracking is still not clearly understood, but is widely accepted that the deleterious process of ASR on concrete structures is due to water absorption by the gel, causing its expansion and increasing internal stress. When the tensile strength of the concrete skeleton is exceeded, the swelling of gel creates and propagates cracking.

The osmotic pressure theory suggests that the cement paste act as a semipermeable membrane when it's surrounding the reactive aggregate, preventing the diffusion of alkali-silicate ions from the reactive sites into the surrounding cement paste, while water is still able to pass through the pore solution. Therefore, an osmotic pressure cell forms and the alkali-silica gel swells with increasing hydrostatic pressure, inducing cracking in the cement paste (HANSEN, 1944; DENT GLASSER, 1979; POOLE, 1992).

The mechanical expansion theory, proposed by McGowan & Vivian (1952), suggests that a solid alkali-silicate layer is formed on the reactive aggregate surface. This layer absorbs water from the pore solution and changes from solid to a gel, followed by the absorption of more water by the gel and then it swells, inducing cracking on the cement paste.

Powers & Steinour (1955a) claimed that both of the theories aforementioned – the osmotic pressure theory and mechanical expansion theory – are fundamentally the same. The amount of absorbed water strongly influences on the forms of the alkali-silica gel, and it can be solid or colloidal fluid. Both phenomena, the osmotic pressure cell of fluid gel and solid gel swelling, primarily generates the expansion of concrete. According to Durand *et al.* (1992), the gel is capable to absorb in volume of water approximately 200 to 400% of its weight in a saturated atmosphere. In that case, it's possible to calculate the volume and the mass of the gel formed on the surface of the reactive aggregate as the gel can occupy the porous media.

In addition to the theories shown before, the works of Bazănt & Steffens (2000) and Dron & Brivot (1993) assumed that the expansion is caused by the swelling pressure accumulated in the Interfacial Transition Zone (ITZ), and the dissolved silica is diffused far away from the reactive aggregates into the connected porous matrix of the cement paste. A pressure in the gel is generated by the imbibition of water, which is initially released by pushing the gel to permeate the micropores in the cement paste located near the surface of the aggregate. The pores around the reactive aggregate and inside the cement paste get fully filled by the gel, and further formation of even more gel induces the increasing internal pressure, leading to cracking of the cement paste.

Although the aforementioned works affirm that the cracking only occurs in the cement paste and not on the aggregate, the researchers Ponce & Batic (2006) found that cracking patterns of ASR-affected concrete depend on the mineralogical nature of aggregate. Those researchers carried out the petrographic examination in aggregates with gel formation and expansion at the aggregate-paste interface, leading to two main conclusions:

- a) Some aggregates – opal and vitreous volcanic rocks – caused cracking only in the cement paste;
- b) Mixed mineralogy aggregates – more common in the field – generated cracks in both the cement paste and the aggregates.

On the Figure 2.10 it's shown the two examples listed before. The Figure 2.10 (a) shows the cracking on the cement paste within concrete with vitreous volcanic rocks on its mixture. The Figure 2.10 (b) shows the cracking in both cement paste and siliceous aggregate.

Some researchers validated the conclusions of Ponce & Batic (2006), and they stated that when hydrate gel starts to be formed inside the reactive aggregate, it develops an expansive pressure causing tensile stress in the aggregate, and such pressure is finally released by cracking both the aggregate and the surrounding cement paste (IDORN, 2001; GARCIA-DIAZ, *et al.*, 2006).

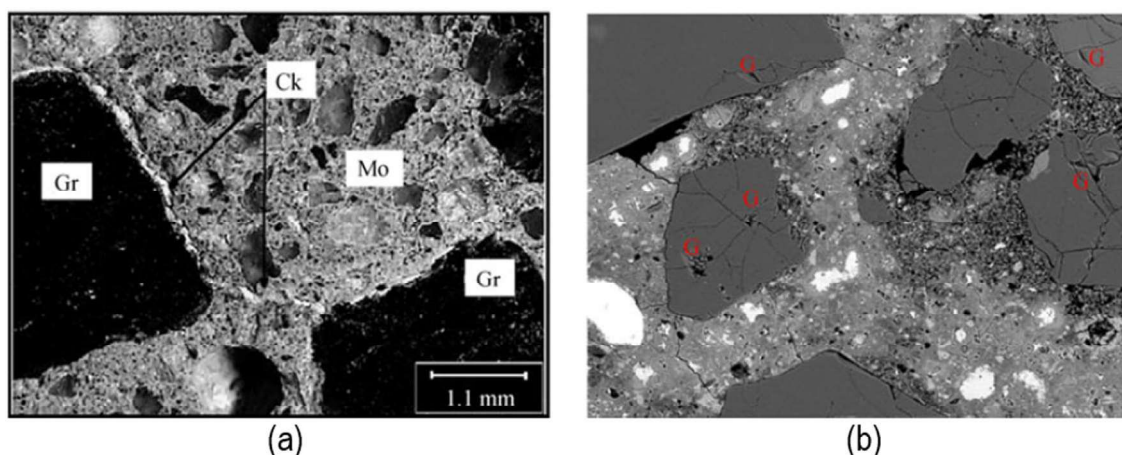


Figure 2.10. Crack patterns due to different types of aggregates within ASR-affected concrete (**addapted from PONCE & BATIC, 2006**).

Other cracking mechanism was proposed by Ichikawa & Miura (2007), suggesting that the diffusion of the viscous alkali-silicate gel doesn't happen because the reactive aggregate is tightly packed with an insoluble and rigid reaction rim, although it allows the alkaline solution to penetrate. After the formation of the rim, the excess of alkali-silica gel generated is stored inside the aggregate, thereby generating expansive pressure and when the strength of material is exceeded, the cracking of the aggregate and the surrounding cement paste occurs.

2.1.4. Factors Influencing on AAR

To better understand the AAR phenomena, it is important to highlight the main factors which have influence on the reaction. As mentioned before, for AAR to occur is needed the presence of reactive aggregates, alkalis on the pore moisture in the cement paste, sufficient humidity and high temperature.

But there are also other factors which play significant role on the expansion due to AAR, such as the porosity of the cement paste and confining stresses on the concrete structure. Therefore, those factors can be divided in three groups: **i)** influence of the concrete composition; **ii)** influence of the environment; **iii)** influence of the confining stresses (MORENON, 2017; BALABUCH, 2018).

2.1.4.1. Influence of the Concrete Composition

The Type of Aggregate:

The rocks which contain potential reactive silica can react in different velocities, and as a consequence of this variation, the aggregates can be classified by the alkaline reactivity as “fast reactive” to “normal reactive” (5 to 20 years), “slow reactive” (more than 15 to 20 years) and “non-reactive” (LINDGÅRD *et al.*, 2010). The aggregate reactivity is directly linked to the velocity which the reaction occurs as well as the type of the reaction. The increase on the permeability of the aggregates with higher porosity may lead to an increase in the aggregate reactivity (ZHANG *et al.*, 1999; BROEKMANS, 2002).

According to LCPC recommendations (LCPC, 1994; FD P18-464 – *Béton – Dispositions pour prévenir les phénomènes d'alcali-réaction*, 2014), aggregates can be classified into three groups: **i)** non-reactive siliceous aggregates (NR); **ii)** potentially reactive aggregates (PR); **iii)** potentially reactive aggregates but with a pessimum effect (PRP). Indeed, for some aggregates a maximum swelling can be observed depending on the content of the reactive aggregate (HAWLETT, 2003). The peak of the pessimum expansion varies according to the aggregates used. The kinetics of the reactions also strongly depend on the nature of the aggregates.

Tiecher (2006) analyzed 40 samples of Brazilian aggregates, where 30 of them were rocks (granites, rhyolites, basalts, limestone and gneiss) and the other 10 were sand. Using the petrographic analysis, the author verified that all the analyzed aggregates (without exceptions) showed potential reactive mineralogical constitutions. The analyzed aggregates in general had deformed silicate minerals in its matrix, which may lead to the occurrence of AAR.

The Granulometry:

The specific surface of the aggregates has an influence on the swelling, more gel can migrate into the connected porosity for a small size aggregate than for a larger one (GAO *et al.*, 2013). In addition, a pessimum effect is observed depending on the size of the aggregates (MULTON *et al.*, 2010; GAO *et al.*, 2013) (Figure 2.11). Multon *et al.* (2010) stated that the size of the aggregate which causes the highest AAR expansion depends on the nature and composition of the aggregate. For fast reactive aggregate it was verified that the quantity of soluble silica was similar for the different particle sizes of a certain aggregate, and the expansion varied to different sizes as the higher expansions was verified to coarse particles (MULTON *et al.*, 2008).

This phenomenon could be explained by the quantity of silica consumed during the cracking of the aggregate. If the aggregate is small, cracking will take place for an aggregate which silica will be strongly attacked. For a larger aggregate, its core won't have reacted yet at the time of cracking. The produced ASR gel will only cause a small increase in pressure due to the space created by the cracking (GAO *et al.*, 2013).

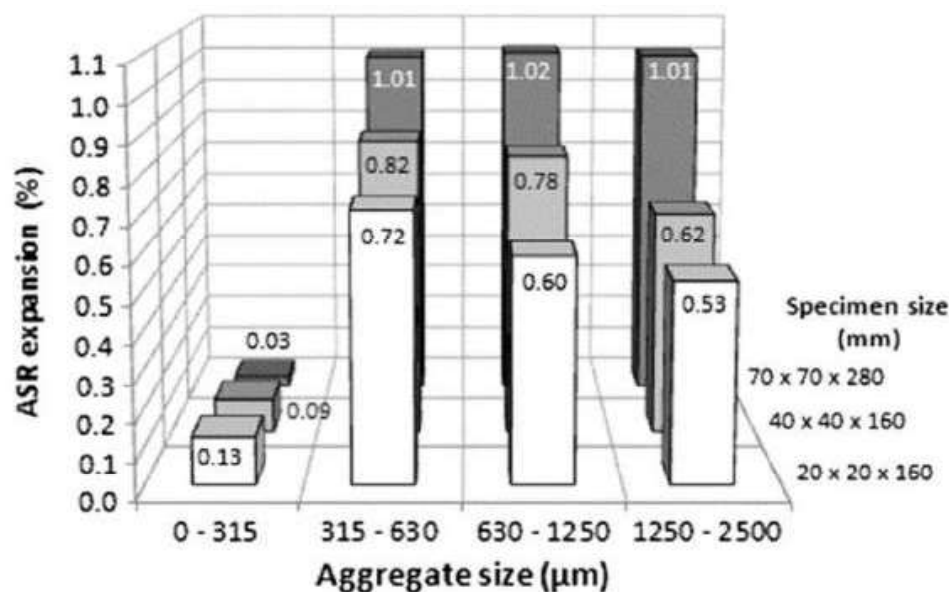


Figure 2.11. Final expansions of ASR-affected concrete specimens depending on their size and the size of the aggregates (GAO *et al.*, 2013).

A scale effect is also observed: the larger the size of the aggregates in relation to the size of the test pieces, lower will be the final swelling. Gao *et al.* (2013) explains this phenomenon by the production of the gel in the created cracking, as the crack depends on the size ratio of the swelling inclusions and the test specimen.

The difference on the kinetics of the reaction between the gravel and the sand is used to determine the advancement of the reaction on testimonial blocks extracted from concrete structures (GRIMAL, 2007).

The Alkalies Content:

The alkali content provides an increase in the concentration of OH^- ions in the concrete pore moisture, which are responsible for the attack to the silica in the reactive aggregates (HASPARYK, 2011). This content must be sufficient to allow the reaction (POOLE, 1992; BERRA *et al.* 2005).

The Portland cement is the main source of alkalis in the concrete, and higher is the alkalis content in the cement or higher the cement consumption, higher will be the expansions. But the Portland cement is not the only source of alkalis in the concrete, as some minerals in the aggregates (feldspar or mica) can also provide the alkalis (DIAMOND, 1989; BÉRUBÉ *et al.*, 2002).

Oberholster (1983) proposed some guidelines in terms of cement content in concrete and active alkalis content of cement to evaluate in which conditions a concrete specimen would suffer from ASR-expansion (Figure 2.12). Posteriorly, in order to avoid the occurrence of AAR, it was established a limit in the alkali content of 0.6% of equivalent Na_2O ($Na_2O + 0,658K_2O$) (ABNT NBR 15577-1:2008; MEHTA & MONTEIRO, 2014).

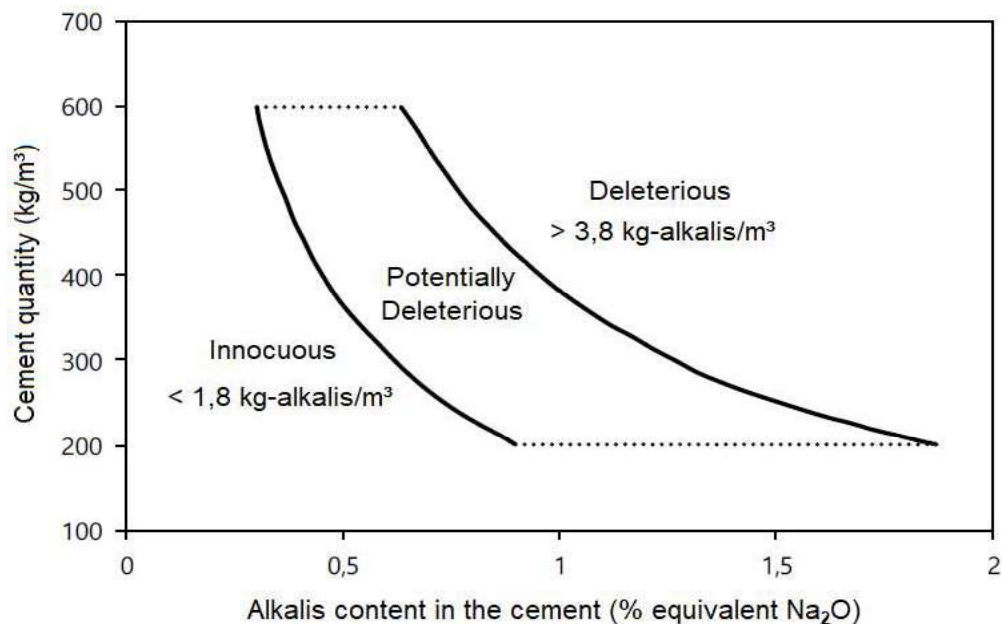


Figure 2.12. Final expansions of ASR-affected concrete specimens depending on their size and the size of the aggregates (OBERHOLSTER, 1983).

The leaching of alkalis is an important phenomenon to take into account in testes with small concrete specimens (LINDGÅRD *et al.*, 2013). In fact, Multon & Sellier (2016) specified that a competition between alkali leaching and the diffusion of alkalis in the aggregates can participate in the scale effect observed in the case of test specimens stored in high humidity conditions.

The Porosity of the Cement Paste:

A high value of porosity of the paste plays two confronting roles when related to AAR. Greater is the porosity, greater is the volume of available moisture on the pores and greater is the space which the gel has to permeate without causing damage to the concrete, because the available voids would be larger, although the diffusion would be accelerated.

In the other hand, lower is the porosity, lower will be the velocity of the AAR, delaying the advancement of the reaction, because the gel and the water would be restricted in their mobility, causing a reduction on the expansion of the gel and even preventing the formation of the gel. Jensen *et al.* (1984) show a technique to reduce the pessimum expansion using air-entraining in the concrete mixture, and for values of 4% of air insertion there is a reduction about 40% of the pessimum expansion, although the technique of air-entraining can drastically reduce the structural properties (e.g. compression strength) of concrete (SILVA *et al.*, 2009; WAWRZECZYK & MOLENDOWSKA, 2017).

The impact of the permeability of the gel (in the cement paste) on the expansions before cracking is limited to few cases of very reactive aggregates. In most cases, significant expansions are generated before the detection of the gel in the cement paste (SANCHEZ *et al.*, 2015). This phenomenon occurs because once AAR has begun, it rapidly generates an intra-porous stress (Sellier *et al.*, 1995a; Capra *et al.*, 1996).

2.1.4.2. Influence of the Environment

The Temperature:

The temperature is directly linked to the advancement of the reaction: higher is the temperature, faster is the reaction. This effect (Figure 2.13) is simulated on the laboratory tests to accelerate the AAR which would take years in the room temperature (DIAMOND *et al.*, 1981; LARIVE, 1997).

As the temperature is increased, the solubility of the silica is also increased and also is perceived a decrease on the solubility of the calcium hydroxide. Making the silica more suitable for reaction and decreasing the capacity of the calcium hydroxide to combine with the gel, is obtained an increase in the velocity of the expansion by AAR (COLLINS & BAREHAM, 1987).

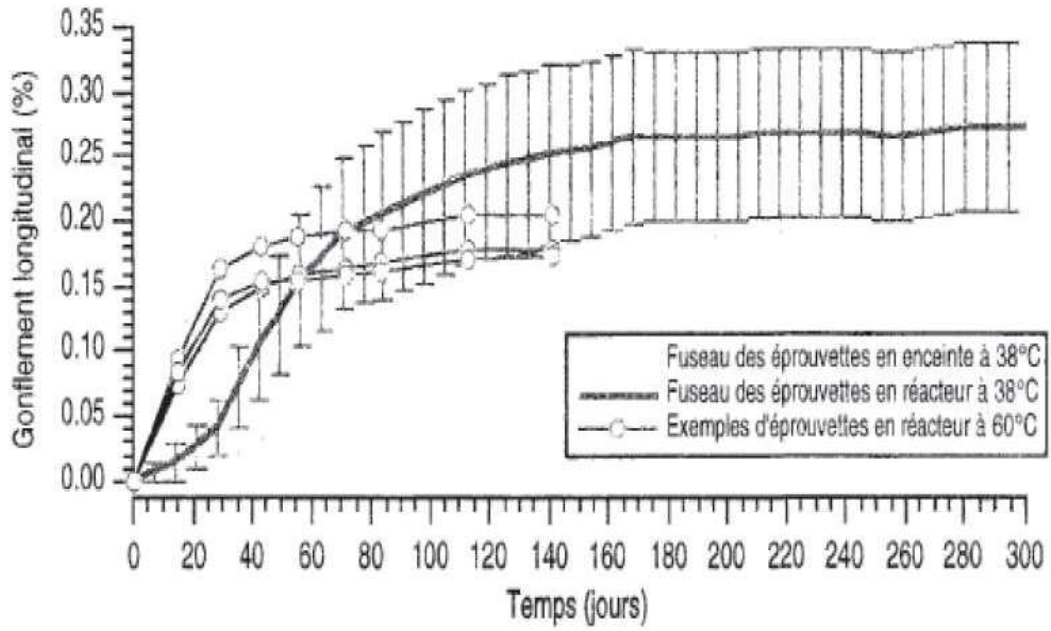


Figure 2.13. Swelling over time to 38°C and 60°C (LARIVE, 1997).

The effect of the temperature on the kinetics of the reaction can be modeled with an Arrhenius law (Eq. 1), where the term “ Ea ” is the activation energy, which varies from 40 and 53 kJ/mol, and the term “ R ” is the perfect gas constant, which the value is equal to 8.1314 J/(mol.K) (LARIVE, 1997; ULM *et al.*, 2000; POYET, 2003; GRIMAL, 2007).

$$\varepsilon_{AAR}^{calcul} = \exp \exp \left[-\frac{Ea}{R} \cdot \left(\frac{1}{T_{ref}} - \frac{1}{T_{calcul}} \right) \right] \cdot \varepsilon_{AAR}^{ref} \quad (1)$$

Lombardi *et al.* (1997) stated that the increase in the temperature promotes an increase in the number of moles of gel created, and Furusawa *et al.* (1994) also affirms that the increase in temperature causes a change in the coefficient of apparent diffusion in the aggregates.

Larive (1997) stated that apparently the swelling asymptote is not modified by the temperature, although other researchers (Diamond *et al.*, 1981; Wood *et al.*, 1987) showed results that confront this point. Wood *et al.* (1987) even found swellings 4 times greater at low temperatures (around 13°C) than at high temperatures (around 38°C). Disturbing effects may had occurred on these experimental tests, such as alkalis leaching, gel permeation in cracks, the chemistry of the gel and even thermal damage.

The concrete expansion caused by ASR shows picks at temperatures close to 40°C as shown in Figure 2.14, and this phenomenon might be related to the lower viscosity of the gel for temperatures higher than 40°C, which would result in the decreasing of the expansion as the gel can permeate more easily through the pores of the cement matrix (DYER, 2015).

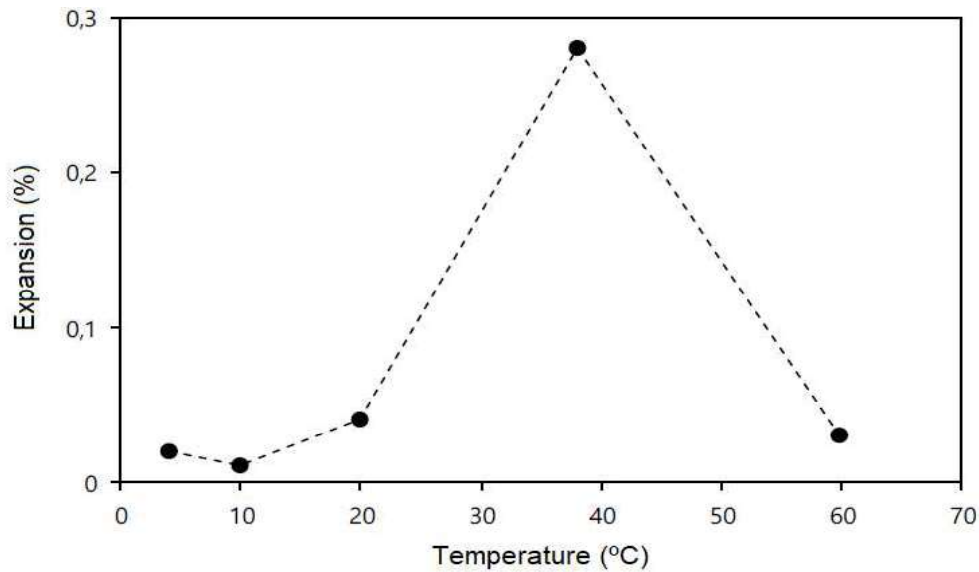


Figure 2.14. Influence of the temperature in the expansion by ASR (DYER, 2015).

The Humidity:

The water inside the concrete pores is also considered as one of the main factor to the developing of AAR, because the expansion induced by ASR is a consequence of the water imbibition by the gel and therefore the extension of the expansion depends on the amount of available water in the pores. Basically, the water acts in three different ways: **i)** on the transportation of alkali ions in the interstitial solution to the reaction sites by diffusion; **ii)** on the silica dissolution; **iii)** on the expansive mechanism of the gel (MEHTA & MONTEIRO, 2014).

The ASR gel is hydrophilic which absorbs a lot of water molecules. Some experimental data showed that the expansion was directly linked to the relative humidity (RH) of the environment (LARIVE, 1997; POYET, 2003; MULTON, 2003). Although the modeling of this effect became more precise when the RH was replaced by the saturation degree of the concrete.

Poyet (2003) shows that is a threshold at approximately 70% of relative humidity which above this value the swelling is no longer negligible (Figure 2.15). The final swelling seems less important for a RH of 100% than for the value of 96%, and this phenomenon can be due to the alkalis leaching. Larive (1997) states that a late addition of water can accelerate the kinetics of the reaction. According to Bazănt & Steffens (2000), for ASR takes place in the concrete, is necessary a RH of 85%. To Léger *et al.* (1996) this value is around 75%.

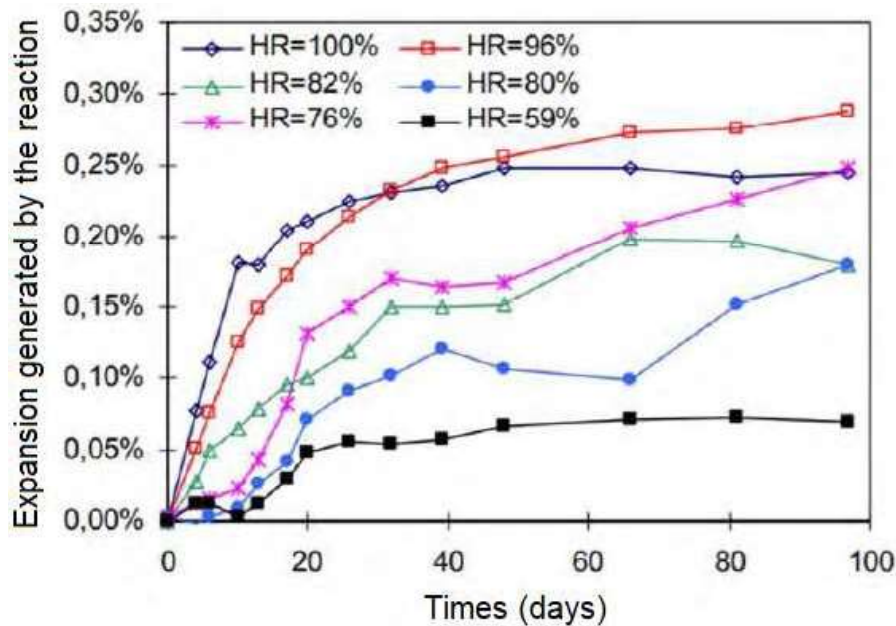


Figure 2.15. Influence of the humidity in the expansion by ASR (POYET, 2003).

The water is an important factor on the process of hardening and curing of concrete, which are used water/cement ratios varying from 0.35 to 0.60 to conventional concrete. Therefore, the humidity resulting from the water used on the concrete production (found on the pores of hardened concrete) is enough to react, contributing to the development of AAR (MEHTA & MONTEIRO, 2014).

2.1.4.3. Influence of the Confining Stresses

The confining stresses are considered as one of the most important factor which influences on the expansion induced by AAR, because they can limit the free expansion of the concrete structure or even prevent it. A compression stress causes a reduction in the value of the expansion on the direction which the stress is applied, and in the same way, a tensile stress can increase the expansion on the direction which the stress is applied (CARRAZEDO, 2004).

Capra & Bournazel (1998) showed that when a compression stress is applied in one of the main directions, the expansion in the orthogonal direction of the applied stress is a sum of the expansion that would occur normally in this direction and the expansion related to the restricted direction, as illustrated on the Figure 2.16, where the direction which the stress is applied is the direction 1. The curve of free expansion was calculated as a sum of the expansions on the direction 1 and 2 in the free stress condition.

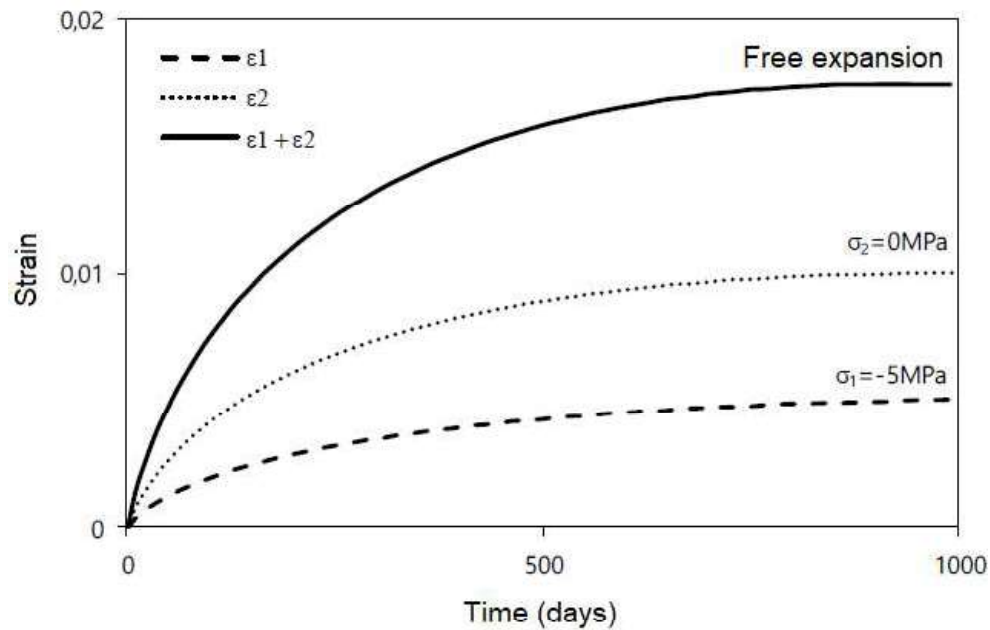


Figure 2.16. Evolution of the uniaxial expansion over time (CAPRA & BOURNAZEL, 1998).

2.1.5. Numerical Modelling of ASR

Numerical models able to describe the AAR have been developed since the 1980's (Carasek, Cascudo & Caetano, 2016), but the scientific community hasn't yet reached a consensus on a model able to fully describe and reproduce the effect of the evolution of AAR-affected concrete structures, nor for which parameters should be considered in the model (GAMELEIRA et al., 2016).

In literature, there is a several number of mathematical models to represent the expansion of ASR-affected concrete structures, and it's because of the complexity of this phenomenon: the heterogeneity of concrete, random distribution of reactive sites, dependence on the environmental conditions and a large number of theories to describe the mechanisms associated to the reaction (CAPRA & SELLIER, 2003; PIGNATELLI, 2012). In addition, the complexity of simulating AAR using numerical methods gets even higher because of the large amount of physical phenomena to consider, such as concrete reactivity, thermal activation, moisture (depends on the rheology of concrete) and the damage interaction (GRIMAL et al., 2007).

According to Bazant et al. (2000), to perform an ASR-affected concrete structure simulation, some basics aspects must be modelled first and then combined:

- Chemical reaction kinetics and diffusion process: determines the degree of ASR and potential expansion;
- Mechanical fracture, expansion and deterioration of concrete structures: describes the material and structural degradation.

One of the difficulties to simulate AAR-affected concrete relies on the fact that the concrete is a very complex heterogeneous material which has random microscopic

structure, with different scales of length (Figure 2.17). In the macroscopic scale, the concrete is considered as a homogeneous material. In the mesoscopic scale, there is the inclusion of the cement matrix, aggregates, pores (voids) and the ITZ, with sufficient length distribution. The microscopic scale is the finest structural scale, represented by the microstructure of the hardened cement paste, composed by the hydration products, micropores and non-hydrated residual clinker (DUNANT & SCRIVENER, 2010; NGUYEN, STROEVEN & SLUYS, 2012).

According to Pan et al. (2012), the existing mathematical models can be classified based in its scale:

- **Microscopic Models:** Those models deal with the chemical reactions only and the theoretical approach generally examines a Representative Volume Element (RVE), which consists of a cement-aggregate system. They were widely developed to predict the pessimum size of aggregate, and such size is responsible for generating the maximum expansion of ASR gel in affected concrete structures.
- **Mesoscopic Models:** Those models represent the mechanism of mechanical deterioration of ASR in a material scale, proposing to establish an interface with large structures. Anisotropy in concrete is expressed through the coupling of the multiphase of concrete (aggregate, cement paste, pores and ASR gel). ASR swelling is represented as a dilatation of gels randomly distributed or an equivalent expansion of aggregate particles.
- **Macroscopic Models:** Those models deal with the coupled chemo-mechanical behavior of ASR-induced expansion of the affected concrete structures, combining the chemical reaction kinetics with linear or non-linear mechanical constitutive, formulated in the framework of Finite Element Method (FEM). This type of model aims to reproduce and predict the long-term behavior observed in real AAR-affected concrete structures.

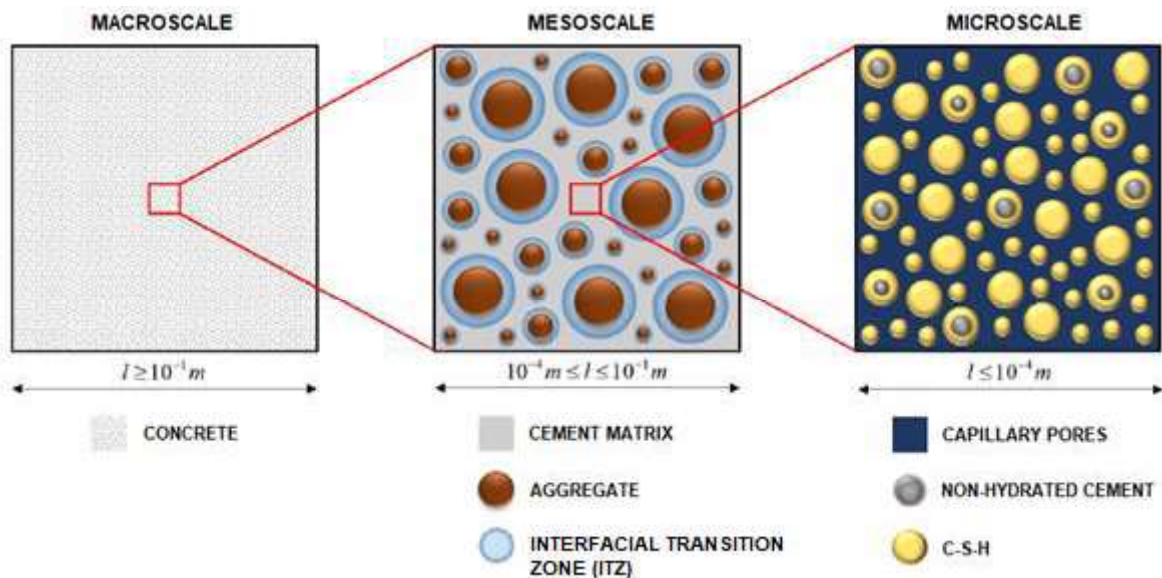


Figure 2.17. Evolution of the uniaxial expansion over time (adapted from DUNANT & SCRIVENER, 2010; NGUYEN, STROEVEN & SLUYS, 2012).

Later, the review work of Esposito & Hendriks (2019) brings a new classification for the available AAR-models, categorizing them based on their starting scale, which is defined as the level at which the input parameters are defined. The authors summarized as follows:

*“The chemical process involves silica ions, available in the aggregates, and alkali ions, mainly present in pore solution together with water (**reaction products level**). The formed alkali-silica gel, when exposed to moisture, tends to swell. Its expansion, while confined in the pore structure of concrete, builds up an internal pressure with the consequent formation of cracks in the aggregates and in the cement paste (**aggregate level**). As a consequence, the concrete is expanding and its mechanical properties are degrading (**concrete level**). The reduction in material resistance compromises the performance of the structure in terms of both capacity and durability (**structural level**)”.*

Several modelling approaches were developed with different aims as the AAR is considered a multiscale phenomenon, which takes place at the reaction products level and may implies consequences up to the structural level, this reaction had been studied by experts from different areas (e.g. structural engineers, material engineers, geologists) in the main fields of material sciences and structural mechanics. (ESPOSITO & HENDRIKS, 2019).

- Models based on concrete expansion (concrete level): Those models focus on the analysis of massive structures (e.g. concrete arch-dams). An imposed expansion strain in concrete is used to simulate the effects of ASR, and the evolution of this strain over time was derived from reaction kinetics laws (based on thermodynamic principles) and phenomenological laws linked to the environmental conditions. Examples of this type of modelling can be found in the works of Larive (1997), Léger et al. (1996), Capra & Bournazel (1998), Ulm et al. (2000) and Comi et al. (2009).
- Models based on internal pressure (aggregate level): Those models were developed thanks to the technological advancement in microscopic investigation on the ASR mechanisms at aggregate level, performed at the beginning of this century. The concrete was represented as a heterogeneous material composed by coarse and fine aggregates, cement paste and the ITZ, defining the microstructure of concrete and the mechanical properties of each phase. The gel swelling was direct related to the expansion of concrete. Example of this type of modelling can be found on the works of Bazănt et al. (2000), Dormieux et al. (2004), Comby-Peyrot et al. (2009), Wu et al. (2014) and Esposito & Hendriks (2016).
- Models based on gel production (reaction products level): Those models were developed at reaction products level with the aim to couple the physical chemistry of ASR with the mechanical behavior of concrete. The kinetics of the reaction were expressed as a function of the change in volume or mass of the ASR gel, and this change in volume/mass was translated into an imposed pressure or strain at aggregate level. Some models were developed in the framework of micro-poro-mechanical theory to investigate the connection between the swelling products at aggregate level and the consequent concrete expansion. Examples of this type of modelling can be found on the works of

Ulm et al. (2002), Grimal et al. (2007), Dunant & Scrivener (2010), Pignatelli et al. (2013) and Charpin & Ehrlacher (2014).

- Models based on ions diffusion-reaction (reaction products level): Those models were developed based on the chemical process translated as ions diffusion-reaction mechanisms, at reaction products level, and they aim to explain why and how the chemical reaction leads to the formation of ASR gel. The phenomena of pessimum size effect and the alkali leaching could be explained by postulating the diffusion of alkali ions via the pore solution and the following chemical reaction. Examples of this type of modelling can be found on the works of Bazănt & Steffens (2000), Suwito et al. (2002), Poyet et al. (2007), Multon et al. (2009), Sanchez et al. (2014), Nguyen et al. (2014), Multon & Sellier (2016) and Morenon (2017).

As mentioned before, this work will implement the model presented in the last technical report provided by the LMDC (SELLIER, 2018), which was firstly developed by Morenon (2017). The chemical model is based on the pressure exerted by the generated volume of ASR gel based in the poro-mechanical framework. Such model is described with more details on the next chapter (Chapter 3), but to understand its main assumptions and hypothesis, is necessary to give to the reader a brief review on the models based on the generated volume of gel.

The models responsible for describing the mechanical behavior of the swelling in concrete structures are discussed in this chapter, in the Section 2.2.4 (Poro-mechanical Models for Swelling in Concrete Structures), after a brief review of the main mechanical behaviors presented on concrete structures.

2.1.5.1. Modelling of the Generated Volume of ASR Gel

Some models were developed based on the diffusion of ions in a Representative Volume Element (REV) which incorporates the aggregate (FURUSAWA et al., 1994; BAZĂNT & STEFFENS, 2000; POYET, 2003).

As one of the pioneers works which applied the concept of REV in ASR modelling, Furusawa et al. (1994) developed a model based on the diffusion of alkali ions and hydroxides in the aggregate (Figure 2.18), and such model was able to describe a porous area around the aggregate which becomes filled with the generated volume of ASR gel. The expansion takes place after the vessel gets fulfilled by the gel, and the volume of this vessel varies according to how much of reactive silica was consumed.

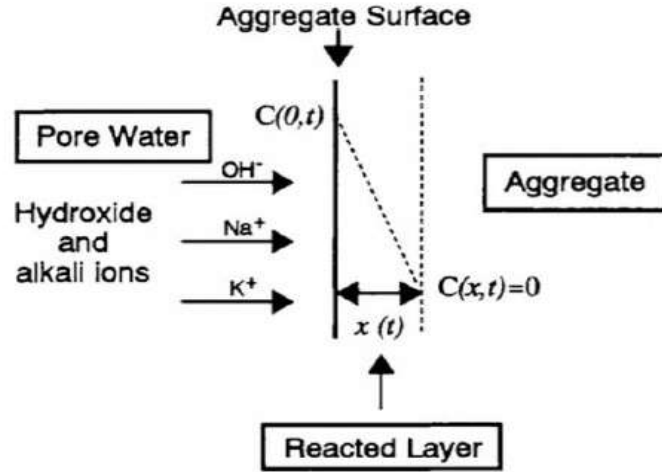


Figure 2.18. Schematic representation of the diffusion of alkalis in the reactive aggregate and the creation of a reaction zone (FURUSAWA *et al.*, 1994).

The mathematical model for the kinetics of ASR, presented by Bazănt & Steffens (2000), was developed aiming to predict the pessimum size of ground waste glass aggregate. It was a simplified approach on the complex chemical reactions and micro-diffusion processes with a good agreement with the experimental tests results, and the ingress of water into the concrete is modelled by a classical Fick law. Although the model was not available for regular concrete (e.g. crushed stones as aggregates) and the fracture mechanics were not taken into account (this model was developed separately in Bazănt *et al.* (2000).

Nonetheless, the assumption is that the species migrate towards the aggregate, therefore the silica is dissolved and reacts. A gel is formed around the aggregate, subsequently it's filled with water and the expansion is generated. Water is imbibed by the gel through diffusion. The water content in the gel (ξ_w) is then calculated as (Eq. 2):

$$\xi_w(x, t) = w_s \cdot \left(\frac{1 - \frac{z(t)}{x}}{1 - \frac{2z(t)}{D}} \right) \quad (2)$$

Where: w_s is the water content around the aggregate; $z(t)$ is the radius of the aggregate that remained unreacted; D is the initial diameter of the aggregate.

It was assumed that two molecules of water are needed to dissolve a reactive silica molecule. Therefore, the equation to calculate the mass concentration of the gel (ξ_g) is then expressed as (Eq. 3):

$$\xi_g = \frac{4\pi}{3} \left(\frac{D^3}{8} - z^3 \right) \cdot \rho_s \cdot \frac{m_g}{m_s} \cdot \frac{1}{s^3} \quad (3)$$

Where: ρ_s is the mass density of the reactive silica; m_g is the molar mass of the ASR gel; m_s is the molar mass of the reactive silica; s is the number of moles of the reactive silica.

The generated gel will then combine with water, when the RH is equal or higher than 85%, resulting in a swelling product. The water imbibition by the gel is expressed as an Ordinary Differential Equation (ODE) and can be written as (Eq. 4):

$$\frac{\partial w_i}{\partial t} = \dot{w}_i = \frac{n(P) \cdot m(RH) \cdot \xi_g - w_i}{\left(\frac{\delta_c^2}{C_{w_i}}\right)} \quad (4)$$

Where: w_i is the mass of water imbibed by the gel; δ_c is the thickness of the area where the diffusion takes place; C_{w_i} represents the diffusivity of water into the gel; $n(P)$ is the empirical function to represent the decrease of " \dot{w}_i " with the increase of pressure; $m(RH)$ is empirical function to represent the decrease of water imbibition by the gel with the increase of RH.

Poyet (2003) assumed that the aggregates can be represented by spheres (REV) and it is attacked by different chemical species (Na^+ , K^+ , Ca^{2+}), also the granular distribution directly impacts the kinetics of the reaction and the amplitude of the swelling (Figure 2.19). The mass conservation equation (Eq. 5) for any of the aforementioned species (specie X) makes it possible to manage the degradation of the aggregate by a diffusion mechanism. From this equation, written for any chemical compound X, the volume of gel is calculated and the subsequent swelling is evaluated by an energetic method which takes into account the volume of the connected porosity.

$$\frac{\partial}{\partial t} (\underline{p_g} \cdot \underline{Sr_g} \cdot \underline{X_g}) = -\text{div} [\underline{D_g^x} \cdot \underline{\text{grad}} (\underline{X_g})] + \underline{S_g}(X) \quad (5)$$

Where: $\underline{p_g}$ is the porosity of the aggregate; $\underline{Sr_g}$ is the degree of saturation of the aggregate; \underline{X} is the concentration of the chemical specie X; $\underline{D_g^x}$ is the coefficient of diffusion; $\underline{S_g}$ is the coefficient to permit the consumption of the chemical species by the reaction (at the exterior of the aggregate, this term corresponds to the consumption of the specie X into other aggregates).

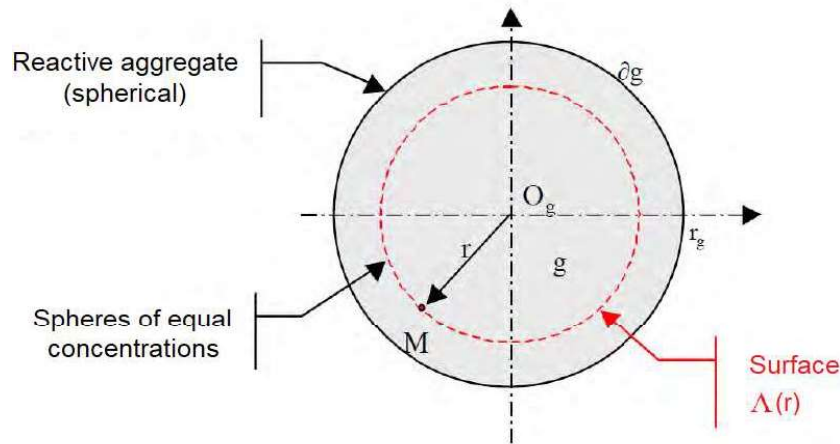


Figure 2.19. Representation of the idealized spherical aggregate (POYET, 2003).

With the aim to enhance the model developed by Poyet (2003), Multon et al. (2009) added a kinetic law for the alkalis fixation. Therefore, the swelling may be influenced by the diffusion or alkalis fixation (Figure 2.20). This model integrated to a finite element code (FEC) was able to reproduce the experimental data obtained in concrete specimens subjected to alkali gradient by external leaching.

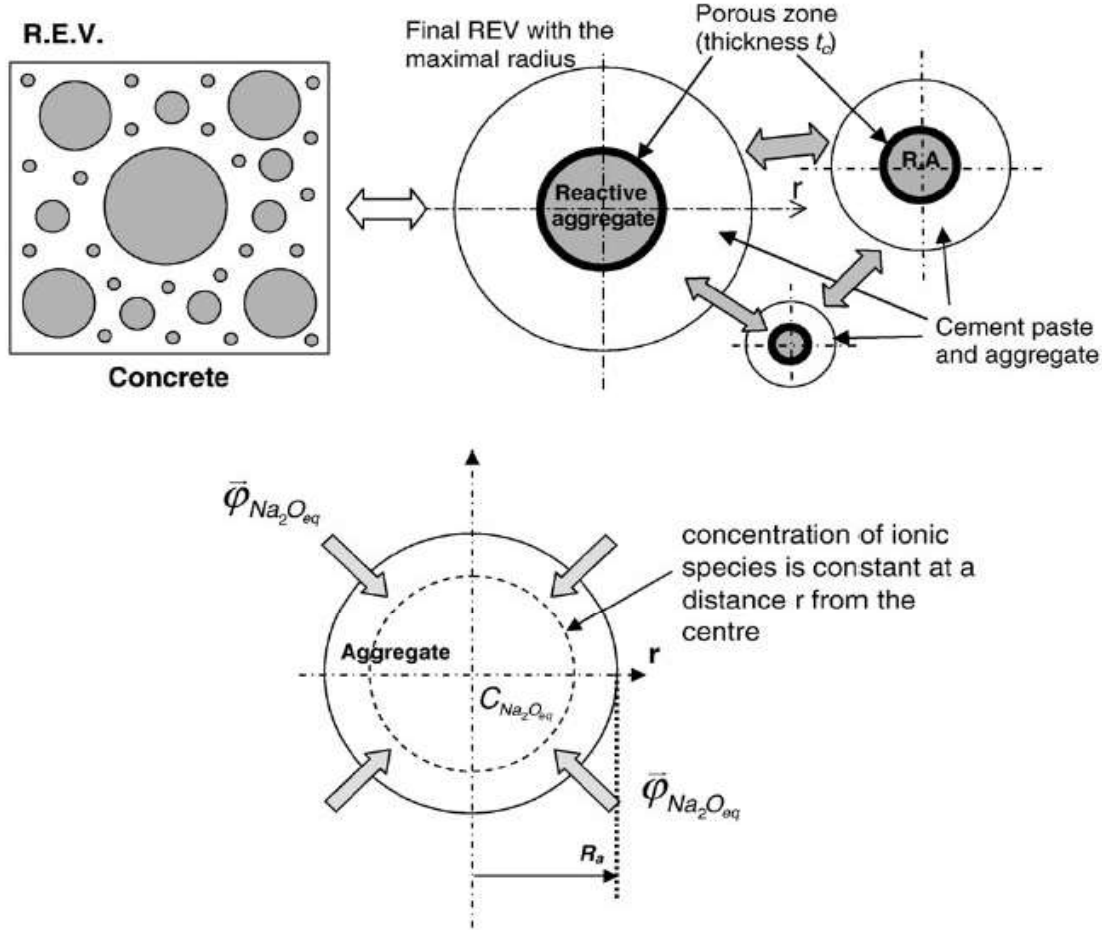


Figure 2.20. [Top] Definition of the REV for several reactive aggregate sizes; [Bottom] Diffusion of equivalent Na_2O in aggregate (adapted from MULTON *et al.*, 2009).

The most used model to reproduce the kinetics of the ASR gel swelling is the empirical model proposed by Larive (1998), which the advancement of the reaction (ξ) is used to assess the volume of gel created over time (Eq. 6). The main assumptions are that the ASR gel is considered as an incompressible fluid and the expansion is proportional to the advancement of the reaction, the term ξ is then multiplied by the final deformation to calculate the deformation for any given time (t). The term τl is the latency time which is responsible for managing the start of the swelling. The term τc is the characteristic time which is responsible for defining the kinetics of the reaction between the beginning and the end of the swelling, establishing the asymptote.

$$\xi(t) = \frac{1 + e^{-\frac{t}{\tau c}}}{1 + e^{-\frac{t - \tau l}{\tau c}}} \quad (6)$$

This type of curve “S” (Figure 2.9 and Figure 2.21) is typical of the internal swelling reactions. However, the parameters cannot be linked to measurable physical properties.

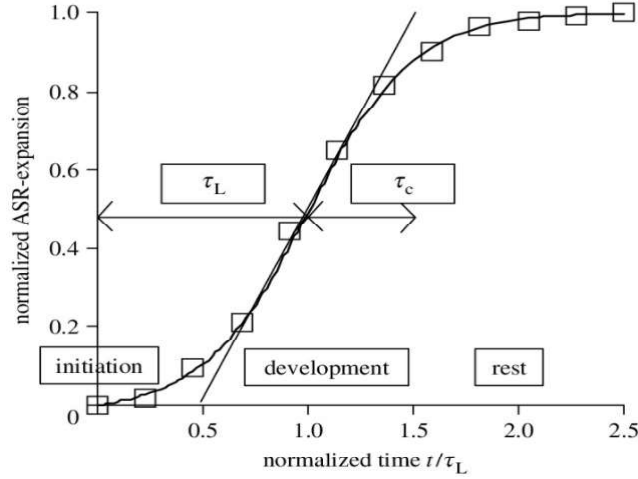


Figure 2.21. Typical S-shaped curve of alkali-silica reaction expansion, obtained on the experimental tests from Larive (1998) (LEMARCHAND *et al.*, 2005).

A differential law for the advancement of the reaction was proposed by Grimal *et al.* (2008). The advancement was calculated (Eq. 7) based on the temperature T (Arrhenius law) and the saturation degree Sr (POYET *et al.*, 2006). The advancement A goes from 0 (reaction not started) to 1 (reaction totally finished). Then, the advancement of the reaction is multiplied by a maximum volume of ASR gel that can be created (calibrated by the user regarding the expansion curves), allowing to obtain the volume of ASR gel for any given time.

$$\frac{\delta A}{\delta t} = \alpha_0 \cdot e^{\frac{Ea}{R} \left(\frac{1}{T_{ref}} - \frac{1}{T} \right)} \cdot \left(\frac{\langle Sr - Sr^0 \rangle^+}{1 - Sr^0} \right) \cdot \langle Sr - A \rangle^+ \quad (7)$$

Where: α_0 is a parameter to calibrate the kinetics; Ea is the ASR activation energy (47000 J/mol/K); R is the perfect gas constant (8,314 J/mol); T_{ref} is the reference temperature (K) of the experimental test; $\langle \rangle^+$ represents the Macaulay brackets, which are the positive part of the terms inside.

The majority of those presented models needs the previous knowledge on the free expansion of a concrete specimen in order to calibrate the parameters which cannot be directly measured. In general, three parameters are necessary to reproduce the curves admitted as representative of ASR-expansion.

In the Chapter 3 (Materials and Methods) it's presented the chemical model proposed by Morenon (2017) which follows the work of Grimal *et al.* (2008), using the advancement of the reaction (A) to generate the volume of gel. This volume exerts a pressure that is computed in the poro-mechanical framework.

2.2. MECHANICAL BEHAVIOR OF CONCRETE

In this topic is presented a brief theoretical review about the concepts linked to creep, shrinkage, poro-mechanical theory and the main mechanical models for AAR-affected concrete structures. The factors which influence the occurrence of those phenomena are commented as well. This explanation is necessary in order to better understand the numerical models and its parameters presented on the Chapter 3 (Materials and Methods).

2.2.1. Creep and Shrinkage

Time-dependent strains of concrete – at constant temperature – may be subdivided into a load-independent part, called **shrinkage**, and a load-dependent part, called **creep** (BAZĄNT & PANULA, 1978). The total deformation related to these phenomena is the sum of the strain related to shrinkage and the strains related to creep (Figure 2.22).

A concrete creep model to be relevant in structural applications must consider several important phenomena, such as non-linearity, multi-axiality, hydration, and thermal and drying effects (SELLIER et al., 2016). In order to consider the long-term mechanical behavior of concrete presenting delayed strains is necessary to split the total delayed strain into five different strains: basic creep, drying creep, plastic shrinkage, autogenous shrinkage and drying shrinkage. A poro-mechanical framework used on FEA softwares may be very useful to develop these type of numerical modelling, because it can distinguish the role of water and the constitutive behavior of solid phases.

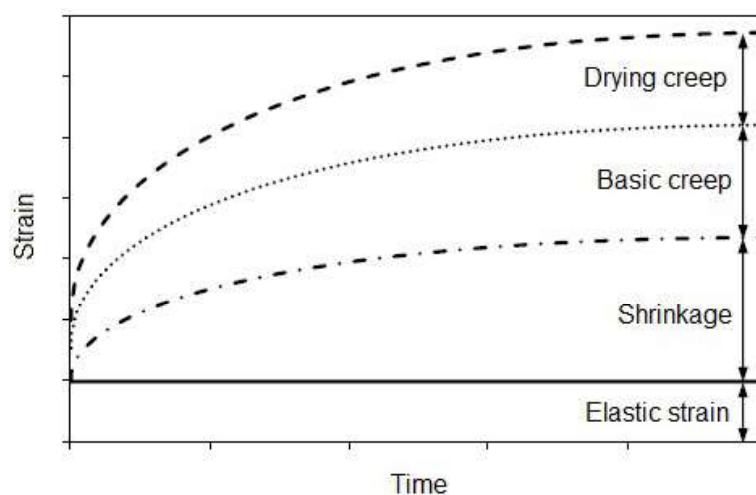


Figure 2.22. Total deformation of concrete subjected to constant loading (adapted from BALABUCH, 2018).

2.2.1.1. Creep

A perfect elastic material is the one which the deformation appears and disappears immediately after the application or removal of loading. It's important to note that an elastic material does not imply in a linear relation on the stress x strain graphic. The elastic characteristics of a certain material are a measure of its stiffness.

Rüsch, Jungwirth & Hilsdorf (1983) stated that the velocity at which the load is applied also influences the instantaneous strain recorded on the experimental test. The strain which occurs immediately or concomitantly to the load application is considered elastic, and its later increase when the load application is constant is treated as a slow deformation, also known as creep. There are two types of creep: basic and drying creep. The total creep is calculated as the sum of the basic and drying creep.

When the drying shrinkage is neglected, the **basic creep** can be taken as the increase in the strain over time, with an applied constant load, under conditions of 100% of RH and no water flux between the concrete and the environment. The **drying creep** is an additional type of creep which occurs when the concrete is under loading and it's simultaneously exposed to an environment with low RH.

Sellier et al. (2016) stated that at a microscopic scale, the fundamental cause of creep is the constitutive properties of hydration products, generating a viscous behavior due to the instability of the bond between C-S-H sheets. At a macroscopic scale, the cause of creep can be related to other non-linear phenomena such as water content variation and micro cracking of anhydrous phases.

To highlight the importance of such deformation, Kuperman (2007) showed the results of an experimental test where concrete specimens with cement consumption of 350 kg/cm³ were subject to a constant loading of 10 MPa for 7 days, under RH of 50%. In 4 days, the concrete specimens showed total strains almost 3 times higher than the elastic strain, and at the end of 3 years, the total strain was more than 6 times higher (Figure 2.23).

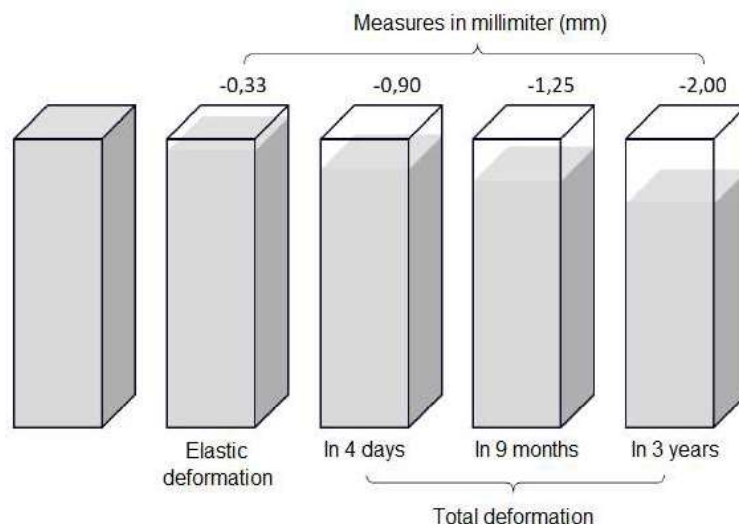


Figure 2.23. Total deformation of concrete over time subjected to a constant loading of 10 MPa (KUPERMAN, 2007).

In concrete structures, creep is capable of reducing the internal stresses due to non-uniform or restrained shrinkage. On the other hand, considering a huge volume of concrete, the creep alone may cause cracking when the restrained concrete suffers a temperature changing cycle caused by the hydration heat and the subsequent cooling.

Mehta & Monteiro (2014) illustrated the phenomenon of reversible creep of concrete when the loading is ceased. In the Figure 2.24 is observed a concrete specimen subjected to constant loading for 100 days, followed by the removal of the load which lasts for 40 days. After the instantaneous elastic strain, the deformation keeps rising over time as the loading is maintained. When the loading is removed, the instantaneous elastic recovery has approximately the same order of magnitude as the instantaneous elastic strain (for the first application of the loading). As time goes by, there is a gradual reduction in the strain, known as creep recovery or plastic recovery. This plastic recovery occurs faster than the creep, but it eventually stops, leaving a permanent deformation (irreversible creep).

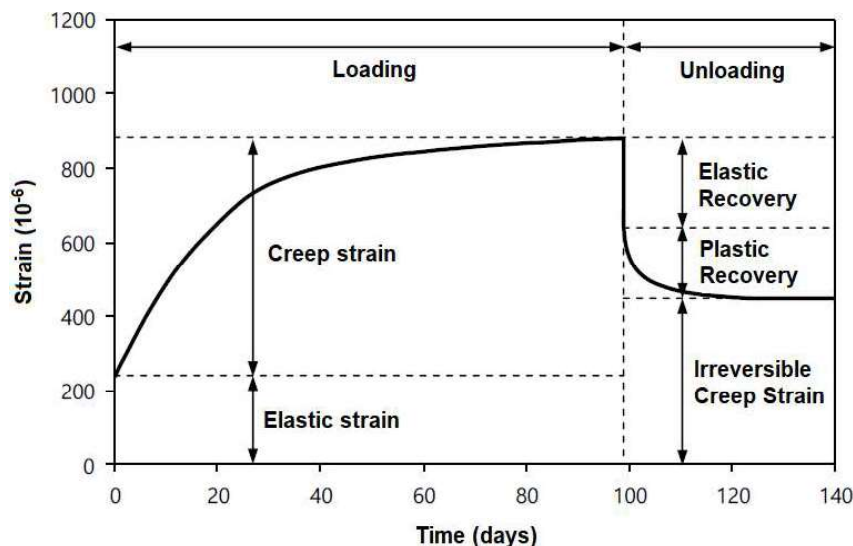


Figure 2.24. Creep reversibility (MEHTA & MONTEIRO, 2014).

2.2.1.2. Shrinkage

Sellier et al. (2016) stated that the water has complex effects in porous media because it can be adsorbed on porous walls, react with the solid skeleton, and exert capillary and disjoining forces on the solid skeleton. In concrete, the water molecules are found in nanoscopic inter-sheets, causing repulsive or attractive forces depending on the environmental conditions (temperature, RH and mechanical loading), but such effects have several consequences in macroscopic scale.

In a resumed way, shrinkage is caused by the water capillary pressure which exerts a tension perpendicular to the pore walls, and it is balanced by orthogonal compressions forces which are parallel to the pore walls. This water capillary pressure may occur only in a high RH environment, but other forces, like disjoining force variations (occurring in a low RH environment), can have similar consequences on drying cement pastes (SELLIER et al., 2016).

Shrinkage can be divided in three: **plastic shrinkage**, **autogenous shrinkage** and **drying shrinkage**. The first occurs when the concrete is on the curing process, and the second one occurs when the concrete is already hardened (BALABUCH, 2018).

Plastic Shrinkage:

According to Dyer (2015), during the process of curing of a concrete structure, it can be observed two simultaneous processes happening on the surface of the concrete (Figure 2.25 (a)). Firstly, the solid constituents have the tendency to settle which leads to the formation of a water layer on the surface of the concrete (Figure 2.25 (b)). Secondly, the free water on the surface gets evaporated, leading to the **plastic shrinkage** when the evaporation rate overcomes the transpiration rate. This happens because the cement particles on the surface of the concrete are no more covered by water, inducing tensile stresses on the superficial layer which is restrained by internal layers of the concrete, leading to the formation of water meniscus between the cement particles (Figure 2.25 (c)). With the progressive water evaporation, the radius of the water meniscus gets shorter, and for a certain instant of time, the radius are going to be so small that they won't fulfill the space between the cement particles in such a way that the water surface will need to rearrange in a point below the initial surface, leading to air penetration (Figure 2.25 (d)). Higher is the evaporation velocity, higher will be the plastic shrinkage.

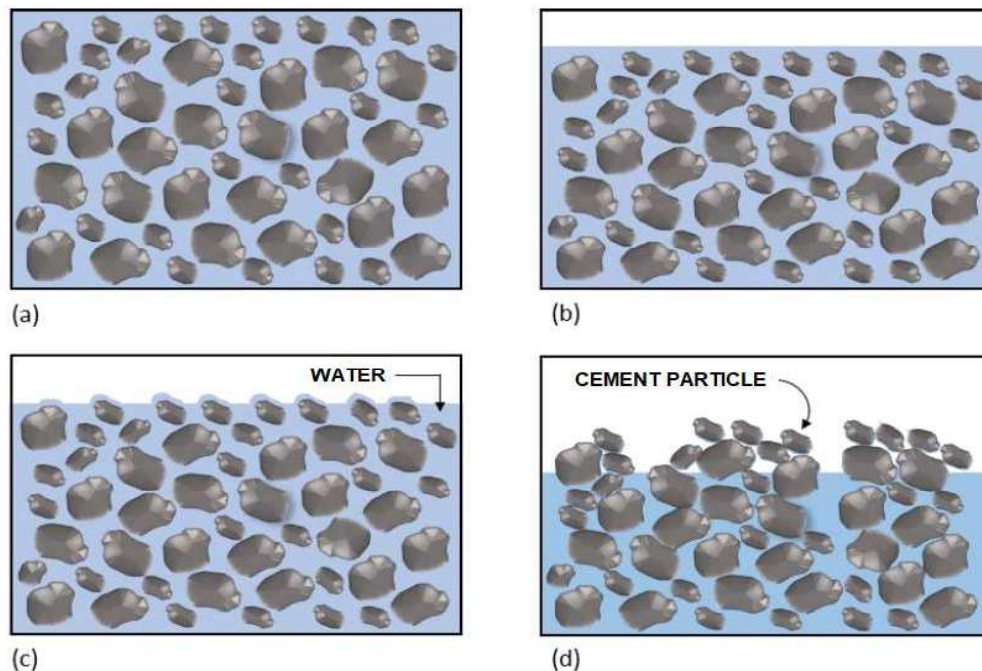


Figure 2.25. Cracking due to autogenous shrinkage (DYER, 2015).

Drying Shrinkage:

The **drying shrinkage** occurs in the hardened concrete due to the loss of the physically adsorbed water from the C-S-H, which represents 50 to 60% of the total volume of solids in an entirely hydrated cement paste. When the saturated cement paste

is exposed to lower environmental humidity, it will lead to a dimensional instability which will result in the deformation by shrinkage. The **drying shrinkage** can be classified as reversible or irreversible (Figure 2.26). The first one is due to the humidity diffusion, which part of the total shrinkage can be reproduced by wetting-drying cycles. On the other hand, at the second one there is no recovery of the deformation due to shrinkage, even after a long storage period in water (MEHTA & MONTEIRO, 2014).

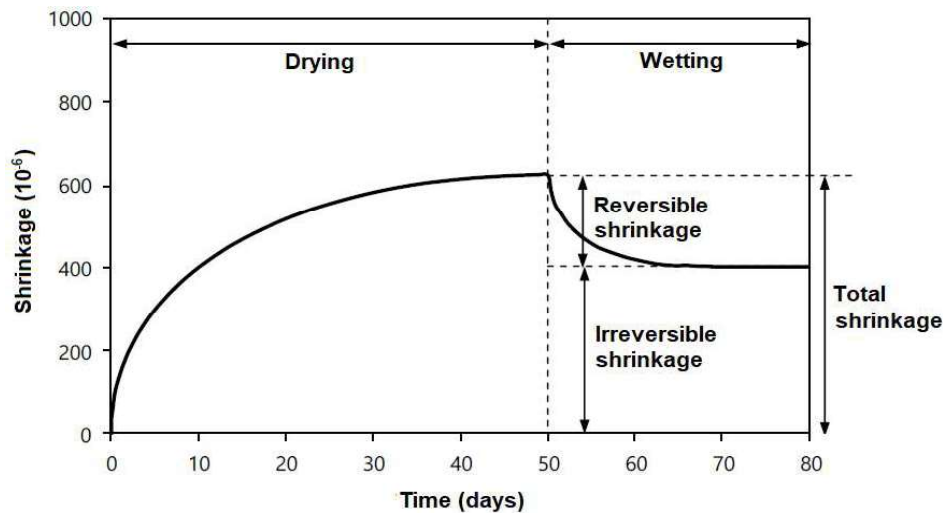


Figure 2.26. Drying shrinkage reversibility (MEHTA & MONTEIRO, 2014).

Mehta & Monteiro (2014) stated that the shrinkage reversibility depends on the duration of the wetting-drying cycles, where the drying occurs significantly faster than the wetting. Therefore, the small period of rains can be sufficient to reverse the consequences of the drying cycle.

The irreversible shrinkage is linked to the formation of chemical and physical bonds in the C-S-H when the adsorbed water is removed. Initially on the drying cycle, there is the loss in free water which induces internal humidity gradients in the cement paste, moving the water molecules over time from the superficial area of C-S-H to the capillaries pores, and then to the concrete exterior leading to the shrinkage of the cement paste (MEHTA & MONTEIRO, 2014).

Autogenous Shrinkage:

The **autogenous shrinkage** can occur even if there is no migration of water from inside or outside of concrete, because evaporation is not the only way that water can be removed from the pores of concrete. When the hydration reactions occurs on the cement, the free water is converted into chemically combined water, in a way which this loss of water due to the hydration can lead to autogenous shrinkage (Dyer, 2015).

This type of shrinkage consists of the macroscopic reduction of the volume of the cementitious materials which occurs when the cement is hydrated after the initial setting time. The autogenous shrinkage occurs in many different types of concrete and is considered as almost negligible for concrete with conventional strength, but it's very important for high-strength concretes and concrete mass. This phenomenon is not

related to volume variation due to loss or gain of substances, variation on temperature, application of mechanical loading or restrictions to the structure.

2.2.1.3. Factors Influencing Shrinkage and Creep

In the literature (Troxell, Raphael & Davis, 1958; Brooks, 1989; Zhang & Malhotra, 1995; Mazloom, Ramezaniapour & Brooks, 2004; Ayub, Khan & Memon, 2014; Wendner, Hubler & Bazănt, 2015; Joshaghani, Balapour & Ramezaniapour, 2018), the main factors influencing shrinkage and creep can be divided in 4 main groups:

- **Concrete composition:** water/cement ratio, type of cement, type of aggregate, admixtures and additives;
- **Environmental conditions:** relative humidity and temperature;
- **Concrete characteristics:** element geometry and age of the concrete;
- **Mechanical loading:** Intensity and age of the loading.

Water/cement ratio:

Wendner, Hubler & Bazănt (2015) affirms that the w/c ratio plays a major role on the porosity of the cement paste and subsequently on the resistance properties of the concrete. Lower is the w/c ratio, higher will be the concrete resistance. Considering a constant cement paste content, an increase in the w/c ratio will result in an increase of the creep strain (Figure 2.27).

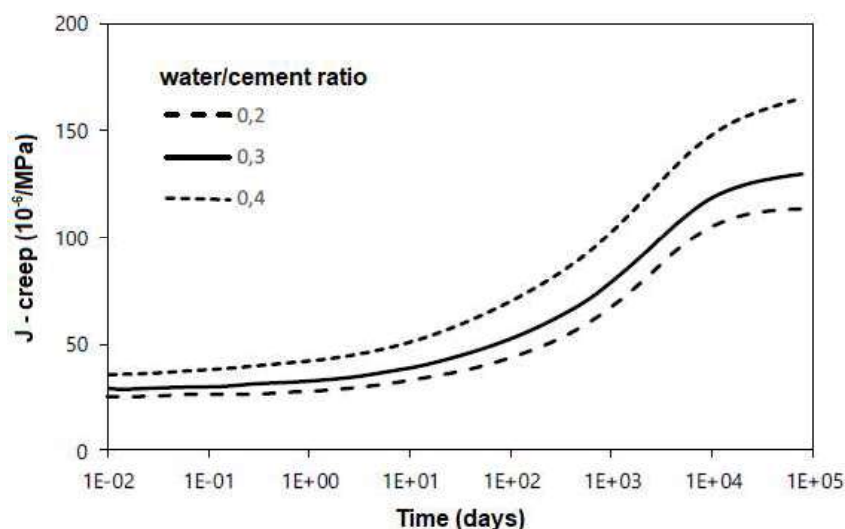


Figure 2.27. The influence of w/c ratio on the creep strain (WENDER, HUBLER & BAZĂNT 2015).

According to Neville & Brooks (2013), the w/c ratio also influences the quality of the cement paste, which may impact on the shrinkage intensity. Higher is the w/c ratio, higher will be the shrinkage. Considering a certain aggregate content, the shrinkage will be a function of the w/c ratio (Figure 2.28).

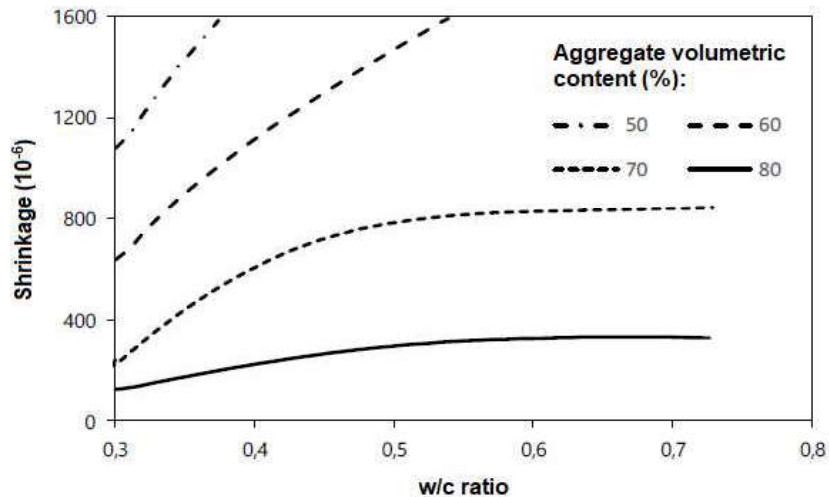


Figure 2.28. The influence of w/c ratio and aggregate content on the shrinkage strain (NEVILLE & BROOKS, 2013).

Type of Cement:

The hydration of the matrix of the cement paste is influenced by the type of cement used in the mixture, also the creep is influenced by the type of cement as it impacts on the strength of a concrete structure under loading. When the concrete which uses conventional Portland cement is subjected to loading in the early age, it will present a creep strain higher than for a concrete using cement with high initial strength (Mehta & Monteiro, 2014).

According to Neville & Brooks (2013), the cement consumption directly affects the shrinkage once the loss of the water from the cement paste is responsible for the occurrence of such phenomenon. Therefore, higher is the cement consumption, higher is the shrinkage intensity. Also, finer is the cement, higher is the risk of cracking, because the hydration reactions will happen slower leading to a retardation on the hardening process.

Type of Aggregate:

The granulometry, maximum dimension, shape and texture of the aggregate are factors which influence creep and drying shrinkage, as can be observed in Figure 2.28 (NEVILLE & BROOKS, 2013).

The maximum dimension plays a trick role, because it alone doesn't impact on the shrinkage intensity. On the other hand, larger aggregates allow the usage of concrete with low w/c ratio, leading to a lower shrinkage. One of the main important characteristics of the aggregate is its Young's modulus which is responsible for controlling the deformations, and the values of creep and shrinkage strains can increase up to 2.5 times

when the concrete uses a low Young's modulus aggregate rather than a high modulus one. The other factors (shape and texture) indirectly influence creep and shrinkage, for example in the densification capacity of the concrete mixture (NEVILLE & BROOKS, 2013).

Admixtures and Additives:

According to Ayub, Khan & Memon (2014), the mineral admixtures reduce the pore sizes in the cement paste with the increase in the pore size distribution, which reduces the porosity and permeability, and subsequently the creep and shrinkage strains. The reduction in the average pore diameter is highly and inversely dependent on the replaced cement volume and also on the age of the concrete or cement paste.

Zhang & Malhotra (1995) showed through experimental tests that the admixtures such as metakaolin and active silica can reduce the porosity and permeability of concrete, leading to a reduction on the drying shrinkage (Figure 2.29). Almost a decade later, Mazloom, Ramezaniapour & Brooks (2004) verified that with the increase on the replacement ratio of cement by active silica leads to an equivalent decrease rate of total creep and basic creep (Figure 2.30).

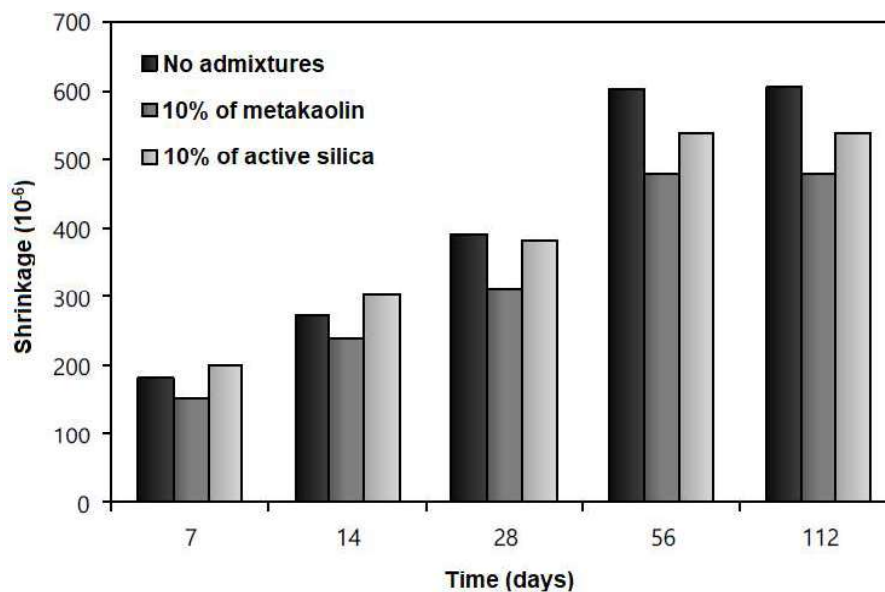


Figure 2.29. Effect on shrinkage by the replacement of cement by admixtures (ZHANG & MALHOTRA, 1995).

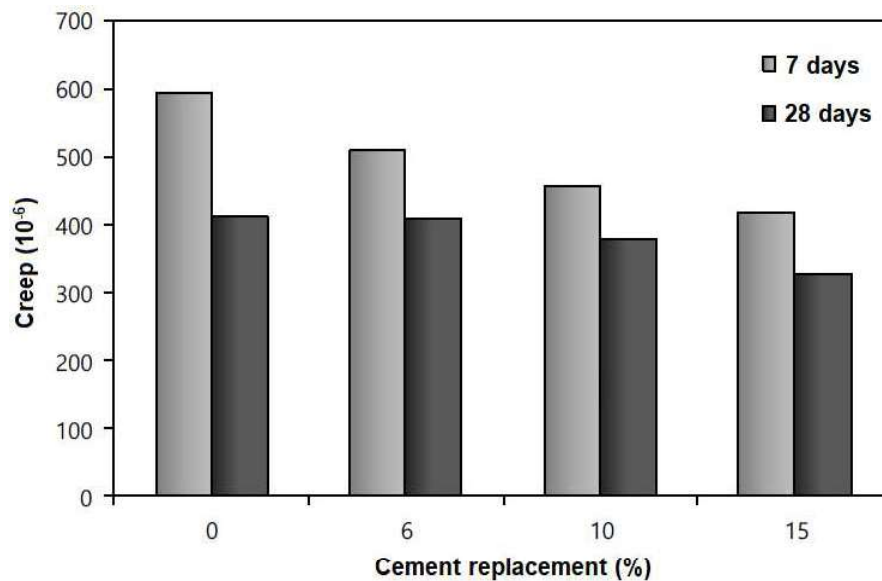


Figure 2.30. Effect on shrinkage by the replacement of cement by admixtures (ZHANG & MALHOTRA, 1995).

The setting retarders and water reduce additives are the best in order to cause dispersion of the cement particles into water, leading to a refining in the pores of the cement paste. It's believed that those types of additives increase the basic creep and drying shrinkage strains. The main effect is indirect because the usage of additives modifies the w/c ratio, which impacts on shrinkage (DYER, 2015).

According to Brooks (1989), a special care must be taken in order to evaluate the influence of additives, because when the usage of such materials are done simultaneously (with alteration on the initial concrete recipe), the comparison between two different mixtures becomes invalid. In order to obtain a valid analysis, it would be necessary to use the additives only to enhance the mixture workability.

Relative Humidity and Temperature:

The shrinkage potential varies under certain environmental conditions, as observed by Joshaghani, Balapour & Ramezaniapour (2018) in their experimental tests (Figure 2.31). High levels of RH may limit the loss of water from the cement paste leading to a mitigation in the effects of shrinkage. Low temperatures also reduced the drying shrinkage, probably due to the slower evaporation when compared to higher temperatures. On the other hand, it was observed a contradictory behavior as the temperature was increased, the direct effect of it was the increase in the evaporation rate and also an increase in the shrinkage strain. Although, an increase in the temperature accelerates the hydration process, which can avoid the evaporation of the free water and also leads to high strength at early age, indirectly resulting in the decrease of the measured values of shrinkage strain.

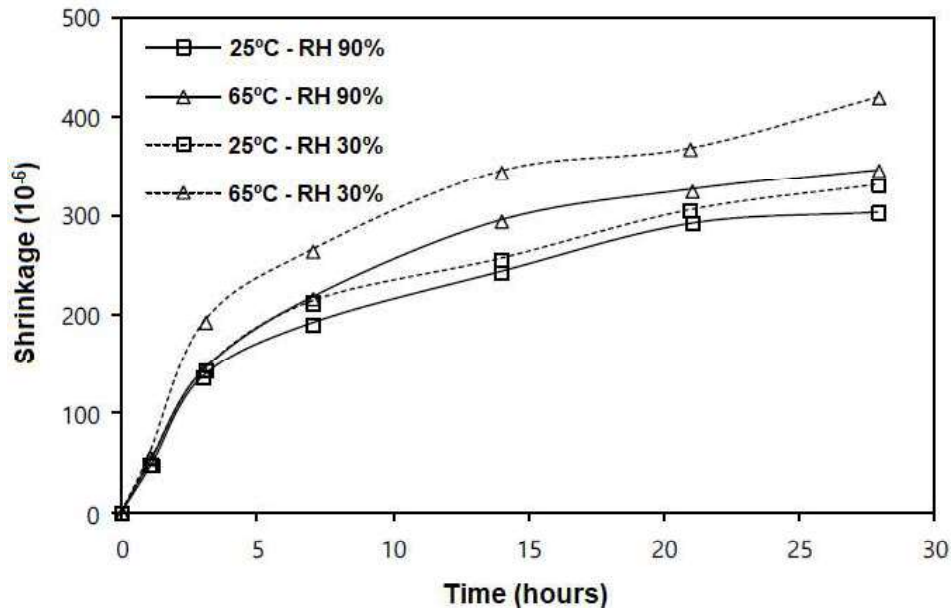


Figure 2.31. Influence of the environmental conditions on the shrinkage (JOSHAGHANI, BALAPOUR & RAMEZANIANPOUR, 2018).

As the creep is directly linked to the compressive strength, Joshaghani, Balapour & Ramezaniapour (2018) verified the increase in the compression strength at early age for an increase in the temperature, maintaining the RH as constant (Figure 2.32). Although, for concrete specimens with 28 days which was cured at high temperature (65°C) showed values of compressive strength lower when compared to specimens cured at lower temperatures. It may be explained by the increase in the C-S-H production at early age, which helps to develop compression strength. It was also verified that the concrete has higher compressive strength at low RH.

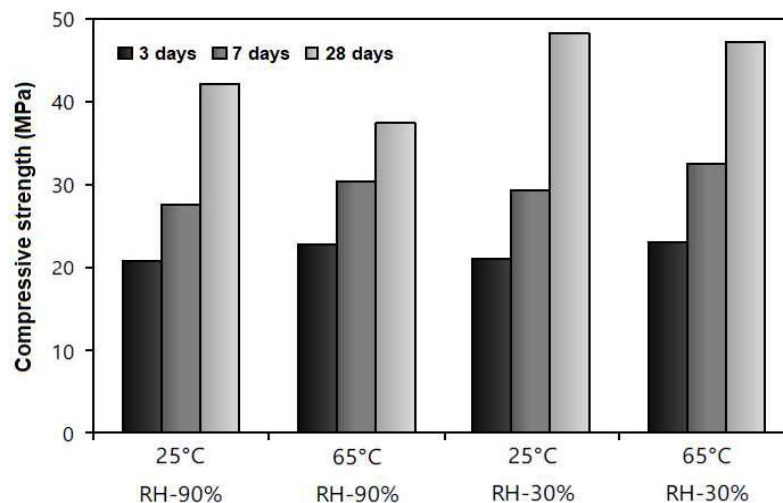


Figure 2.32. Influence of the environmental conditions on the compression strength (JOSHAGHANI, BALAPOUR & RAMEZANIANPOUR, 2018).

Element Geometry:

According to Mehta & Monteiro (2014), the rate of the loss of water is controlled by the length of the path that water must go through to get expelled from concrete during creep and/or shrinkage. This phenomenon is due to the resistance to the water diffusion from inside of concrete to the environment. Therefore, the dimension and shape of a concrete element – under constant RH – determine the creep and shrinkage rate.

The dimension and shape factors can be expressed by one single value, known as theoretical or effective thickness, which is equal to the ratio between the section area and the semi-perimeter in contact with the atmosphere (MEHTA & MONTEIRO, 2014). The relation between the creep coefficient and the theoretical thickness of the concrete element is presented in the Figure 2.33 (a). The shrinkage behavior over time for different theoretical thickness is presented in the Figure 2.33 (b).

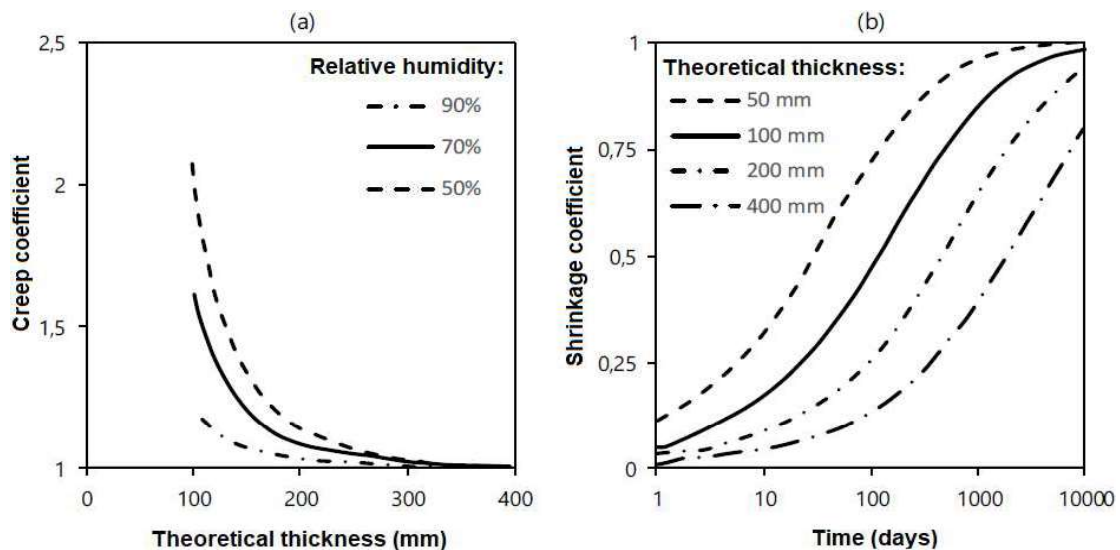


Figure 2.33. Influence of the theoretical thickness on creep and shrinkage (MEHTA & MONTEIRO, 2014).

Age of the Concrete:

The shrinkage may occur over a long period of time, although the shrinkage rate will decrease rapidly over time. Considering a concrete specimen constantly loaded for 20 years under constant environmental conditions, it's believed that 14 to 34% of the total shrinkage strain occurs in the first two weeks, 40 to 80% in three months, and 66 to 85% in one year. In the same way, it's believed that 25% of the total creep strain occurs in the first two weeks, 50% in three months and 75% in one year (MEHTA & MONTEIRO, 2014).

Intensity and Age of the Loading:

According to Troxell, Raphael & Davis (1958) stated a direct proportionality between the magnitude of the constant stress applied to the structure and the measured creep strain. This affirmative was made based in the experimental data which had shown that for concrete specimens with 90 days, the measured creep strain was two times

higher for a loading of 4 MPa when compared to 8 MPa. Also, lower values of creep were found for concrete specimens with 3 months when compared to specimens with 28 days.

2.2.1.4. Creep And Shrinkage Modelling

In the civil engineering practice, the time dependent average behavior of concrete is related to the physical phenomena of creep and shrinkage, and it's commonly predicted using two types of models: **design code models** or **academic models**. Examples of design code models are the *Model Code 2010* (FIB, 2012), *ACI 209* (ACI 209, 2008) and *JSCE* (JSCE, 2010). Examples of academic models are the *GL2000* (Gardner, 2004), *B4* (Baz ant & RILEM, 2015) the model proposed by *Sellier et al.* (2016) which will be discussed in the Chapter 3 (Materials and Methods).

GL2000 (GARDNER, 2004):

The model *GL2000* was firstly developed by Gardner & Lockman (2001) and then modified by Gardner (2004). This model can be used independently from the chemical additives and minerals admixtures used to produce the concrete, and also doesn't depend on the temperature and the curing. The shrinkage strain is then given by the following expression (Eq. 8):

$$\varepsilon_{sh}(t, t_c) = 900 \cdot k \cdot \left(\frac{30}{f_{cm28}} \right)^{\frac{1}{2}} \cdot (1 - 1,18h^4) \cdot \beta(t - t_c) \cdot 10^{-6} \quad (8)$$

Where: k is the shrinkage constant which depends on the type of cement; t is the age of the concrete; t_c is the age when the shrinkage begins or the end of the curing; f_{cm28} is the compression strength in 28 days; h is the relative humidity; $\beta(t - t_c)$ is a function which depends on the volume/surface ratio and the age when the shrinkage takes place (t_c).

Also, in the model *GL2000* is possible to calculate the consolidation function, which considers the creep in concrete, and it can be expressed as (Eq. 9):

$$J(t, t_0) = \frac{1}{E_{cm t_0}} + \frac{\phi_{28}(t, t_0)}{E_{cm28}} \quad (9)$$

Where: $E_{cm t_0}$ is the Young's modulus measured at the age when the loading was applied; E_{cm28} is the Young's modulus in 28 days; $\phi_{28}(t, t_0)$ is a function which depends on the volume/ratio, RH and the age when the loading was applied (t_0).

ACI 209 (ACI, 2008):

The model *ACI 209* was developed by the American Concrete Institute (ACI, 2008) and has the aim to predict the stress produced by shrinkage and creep over time,

presenting the same behavior: a hyperbolic curve with an asymptotic value called as final value. The curve shape and the final value depends on the curing conditions, age when the loading was applied, mixture proportions, environmental temperature and RH, and other factors. The shrinkage strain is then given by the following expression (Eq. 10):

$$\varepsilon_{sh}(t, t_c) = \frac{(t - t_c)^\alpha}{f + (t - t_c)^\alpha} 780 \cdot (\gamma_{sh,tc} \cdot \gamma_{sh,RH} \cdot \gamma_{sh,VS} \cdot \gamma_{sh,S} \cdot \gamma_{sh,\psi} \cdot \gamma_{sh,C} \cdot \gamma_{sh,\alpha}) \cdot 10^{-6} \quad (10)$$

Where: $(t - t_c)$ is the time to initiate drying; f and α are constants which depends on the shape and size of the structural member, respectively; $\gamma_{sh,tc}$, $\gamma_{sh,RH}$, $\gamma_{sh,VS}$, $\gamma_{sh,S}$, $\gamma_{sh,\psi}$, $\gamma_{sh,C}$ and $\gamma_{sh,\alpha}$ are parameters to represent the initial curing, environmental RH, size of the structural member in terms of volume/surface ratio, slump, fine aggregates, cement content and voids percentage, respectively.

Also, in the model ACI 209 is possible to calculate the consolidation function, which considers the creep in concrete, and it can be expressed as (Eq. 11):

$$J(t, t_0) = \frac{1 + \phi(t, t_0)}{E_{cmt0}} \quad (11)$$

Where: E_{cmt0} is the Young's modulus measured at the age when the loading was applied; $\phi(t, t_0)$ is the creep coefficient.

The creep coefficient may be calculated by the following expression (Eq. 12):

$$\phi(t, t_0) = \frac{(t - t_0)^\psi}{d + (t - t_0)^\psi} \cdot 2,35 \cdot (\gamma_{c,t0} \cdot \gamma_{c,RH} \cdot \gamma_{c,VS} \cdot \gamma_{c,S} \cdot \gamma_{c,\psi} \cdot \gamma_{sh,\alpha}) \quad (12)$$

Where: $(t - t_0)$ is the time since the loading was applied; d and ψ are constants to a certain shape and size of structural member; $\gamma_{c,t0}$, $\gamma_{c,RH}$, $\gamma_{c,VS}$, $\gamma_{c,S}$, $\gamma_{c,\psi}$ and $\gamma_{sh,\alpha}$ are parameters to represent the age loading factor, environmental RH, size of the structural member, slump, fine aggregates, cement content and voids percentage, respectively.

JSCE (JSCE, 2010):

The model JSCE developed by the Japan Society of Civil Engineers (JSCE, 2010) can be found on the book **Standard specifications for concrete structures**, takes into account the properties of the aggregate and the cement, the consolidation of the concrete and its curing conditions, the shape and dimensions of the transversal section of the concrete members, the materials proportion in the mixture, and also the environmental temperature and RH. The shrinkage strain is then given by the following expression (Eq. 13):

$$\varepsilon_{cs}(t, t_0) = \{1 - \exp \exp [-0,108 \cdot (t - t_0)^{0,56}]\} \cdot \varepsilon_{sh} \quad (13)$$

Where: $(t - t_0)$ is the time to initiate drying; ε_{sh} is the final value of the shrinkage strain.

The final value of the shrinkage strain can be calculated as (Eq. 14):

$$\varepsilon_{sh} = -50 + 78. \left[1 - \exp \exp \left(\frac{RH}{100} \right) \right] + 38. \ln \ln (W) - 5. \left[\ln \ln \left(\frac{V/S}{10} \right) \right]^2 \quad (14)$$

Where: RH is the relative humidity; W is the water content in concrete; V/S is the volume/surface ratio.

Also, in the model *JSCE* is possible to calculate the creep strain by the following expression (Eq. 15):

$$\frac{\varepsilon_{cc}(t, t', t_0)}{\sigma_{cp}} = \left\{ 1 - \exp \exp \left[-0.09. (t - t')^{0.06} \right] \right\}. (\varepsilon_{bc} + \varepsilon_{dc}) \quad (15)$$

Where: t , t' and t_0 represent the begin of drying, begin of loading and the loading duration, respectively; ε_{bc} and ε_{dc} represent the final values due to basic creep and drying creep, respectively; σ_{cp} is the applied stress.

The final values of the basic creep and drying creep strains can be calculated as (Eq. 16 and Eq. 17):

$$\varepsilon_{bc} = 15. (C + W)^2. (w/c)^{2.4}. [\ln \ln (t')]^{-0.67} \quad (16)$$

$$\varepsilon_{dc} = 4500. (C + W)^{1.4}. (w/c)^{4.2}. \left[\ln \ln \left(\frac{V/S}{10} \right) \right]^{-2.2}. \left(\frac{1 - RH}{100} \right)^{0.36}. t_0^{-0.30} \quad (17)$$

Where: C is the cement content; w/c is the water/cement ratio.

The equations shown are valid only for conventional concrete. For high-strength concrete, there are some modifications in the formulation.

Model Code 2010 (FIB, 2012):

The *Model Code 2010* was developed by the International Federation for Structural Concrete (FIB, 2012) which calculates the creep and shrinkage strain with empirical equations calibrated by experimental tests. The total creep and total is divided in basic and drying creep, and the total shrinkage is divided in drying and autogenous shrinkage, regarding their different related mechanisms.

Basically, both creep strains decrease when: **i)** decreasing in w/c ratio; **ii)** decreasing in the cement content; **iii)** increasing in the aggregate stiffness; **iv)** increase of the hydration degree.

On the other hand, a decrease in the w/c ratio produces a decrease in the drying shrinkage and an increase in the autogenous shrinkage. Although a decrease in the cement content produces a decrease in both shrinkage strains.

The total creep strain is then calculated by the following expression (Eq. 18):

$$\varepsilon_{cc}(t, t_0) = \frac{\sigma_c(t_0)}{E_{ci}} \cdot \varphi(t, t_0) \quad (18)$$

Where: $\sigma_c(t_0)$ is the compressive stress; E_{ci} is the Young's modulus in 28 days; t is the age of the concrete; t_0 is the age when the loading starts; $\varphi(t, t_0)$ is the creep coefficient, which is the sum of the basic creep $[\varphi_{bc}(t, t_0)]$ and drying creep $[\varphi_{dc}(t, t_0)]$.

The basic and drying creep are then expressed as (Eq. 19 and Eq. 20):

$$\varphi_{bc}(t, t_0) = \beta_{bc}(f_{cm}) \cdot \ln \ln \left(\left(\frac{30}{t_{0,adj}} + 0,035 \right) (t - t_0) + 1 \right) \quad (19)$$

$$\varphi_{dc}(t, t_0) = \beta_{dc}(f_{cm}) \cdot \beta(RH) \cdot \left(\frac{30}{0,1 + t_{0,adj}^{0,2}} \right) \ln \ln \left(\left(\frac{30}{t_{0,adj}} + 0,035 \right) (t - t_0) + 1 \right) \quad (20)$$

Where: $\beta_{bc}(f_{cm})$ and $\beta_{dc}(f_{cm})$ are the parameters related to the average compressive strength in 28 days; $\beta(RH)$ is the parameter related to the RH; $t_{0,adj}$ is the adjustment in the age of concrete related to the type of cement.

The total shrinkage strain $[\varepsilon_{cs}(t, t_s)]$ is then calculated as the sum of the drying shrinkage $[\varepsilon_{cds}(t, t_s)]$ and the autogenous shrinkage $[\varepsilon_{cas}(t)]$. Both strains can be expressed by the following expressions (Eq. 21 and Eq. 22):

$$\varepsilon_{cds}(t, t_s) = [(220 + 110 \cdot \alpha_{ds1}) \cdot \exp \exp(-\alpha_{ds2} \cdot f_{cm})] \cdot \left[\frac{(t - t_s)}{0,035 \cdot h^2 + (t - t_\sigma)} \right] \cdot \beta(RH) \cdot 10^{-6} \quad (21)$$

$$\varepsilon_{cas}(t) = -\alpha_{as} \cdot \left[\frac{\frac{f_{cm}}{10}}{6 + \left(\frac{f_{cm}}{10} \right)} \right]^{2,5} \cdot [1 - \exp(-0,2 \cdot \sqrt{t})] \cdot 10^{-6} \quad (22)$$

Where: α_{ds1} , α_{ds} and α_{as} are the coefficients related to the type of cement; t_s is the age when drying begins; h is a coefficient linked to the geometry of the structural member.

B4 (BAZĂNT & RILEM, 2015):

The model B4 (Bazănt & RILEM, 2015) was developed as an enhancement of the model B3 (Bazănt & Baweja, 2000), calibrated with a huge experimental tests database provided by the Northwestern University (Illinois, USA). The model is able to divide the total creep strain in basic and drying creep, and also is able to divide the total shrinkage strain in drying and autogenous shrinkage.

The total shrinkage strain $[\varepsilon_{sh,total}(t, t_0)]$ is then calculated as the sum of the drying shrinkage $[\varepsilon_{sh}(t, t_0)]$ and the autogenous shrinkage $[\varepsilon_{au}(t, t_0)]$. Both strains can be expressed by the following expressions (Eq. 23 and Eq. 24):

$$\varepsilon_{sh}(t, t_0) = -\varepsilon_0 \cdot k_{\varepsilon a} \cdot \frac{E \cdot (7 \cdot \beta_{Th} + 600 \cdot \beta_{Ts})}{E(t_0 + \tau_{sh} \cdot \beta_{Ts})} \quad (23)$$

$$\varepsilon_{au}(t, t_0) = \varepsilon_{au\infty} \cdot \left[1 + \left(\frac{\tau_{au}}{t + t_0} \right)^\alpha \right]^{r_t} ; \quad \alpha = r_a \cdot \left(\frac{w/c}{0.38} \right) \quad (24)$$

Where: $k_{\varepsilon a}$ is a factor linked to the type of aggregate; τ_{sh} is the shrinkage time interval; β_{Th} and β_{Ts} are the parameters linked to RH and temperature, respectively; ε_0 is the parameter linked to the proportion of the materials in the concrete mixture; w/c is the water/cement ratio; $\varepsilon_{au\infty}$ is the maximum autogenous shrinkage strain, calculate based on the aggregate/cement ratio and w/c ratio; τ_{au} is the autogenous shrinkage time interval; r_a and r_t are parameters linked to the type of cement.

Also, in the model B4 is possible to calculate the consolidation function, which considers the creep in concrete, and it can be expressed as (Eq. 25):

$$J(t, t_0) = q_1 + C_0(t, t_0) + C_d(t, t_0, t_c) \quad (25)$$

Where: q_1 is the instantaneous strain due to unitary stress; $C_0(t, t_0)$ and $C_d(t, t_0, t_c)$ is the consolidation function for basic and drying creep, respectively; t , t_0 and t_c are the age of concrete, the age when the drying begins (curing end) and the loading age, respectively.

The two consolidation functions can be expressed as (Eq. 26 and Eq. 27):

$$C_0(t, t_0) = q_2 \cdot Q(t, t_0) + q_3 \cdot \ln \ln [1 + (t - t_0)^n] + q_4 \cdot \ln \ln (t/t_0) \quad (26)$$

$$C_d(t, t_0, t_c) = q_5 \cdot \{ \exp \exp [-p_{5H} \cdot H(t, t_c)] - \exp \exp [-p_{5H} \cdot H_c(t_0, t_c)] \}^{1/2} \quad (27)$$

Where: q_2 , q_3 , q_4 and q_5 are parameters linked to the cement content, viscoelastic consolidation, aging flux consolidation and drying creep consolidation, respectively; $Q(t, t_0)$ is the function related to the beginning of drying; $H(t, t_c)$ and $H_c(t_0, t_c)$ are the functions related to the RH, compressive strength and theoretical thickness; p_{5H} is a parameter linked to the type of cement.

2.2.2. Poro-mechanical Theory

As previously mentioned, the swelling of the AAR gel exerts a pressure into the cement matrix. This pressure depends on the volume of gel created, on the porosity of the cement paste and also on the stiffness of each phase (fluid and solid). The behavior of the concrete over time, when subjected to a porous pressure (AAR or water), can be described applying the poro-mechanical theory.

Biot (1941) developed the poro-elasticity law (Eq. 28), which relates the effective stress and the total stress inside the porous media to the pressure exerted and also to the solid skeleton compressibility.

$$\bar{\sigma} = \sigma^{\bar{}} - b.p.\bar{I} \quad (28)$$

Where: $\bar{\sigma}$ is the total stress in the material; $\sigma^{\bar{}}$ is the effective stress in the solid skeleton considering the porosity; p is the pressure exerted by the fluid inside the pores; b is the Biot coefficient which weights the influence of the fluid pressure over the solid skeleton in function of their correspondent stiffness.

Almost 50 years later, Coussy (1991) presented a theory to answer the continuous mechanics theory. He proposed the poro-mechanical theory with many configurations of pore-solid matrix interaction, considering a multiphase medium where the different behaviors of the fluid and the solid skeleton are taken into account. The main hypothesis of this theory are: **i)** the small transformations deformations of the solid skeleton; **ii)** the small variations on the porosity.

In order to describe this multiphase system, it was used the combination of balance equations, mechanical equilibrium equations (Eq. 29) and state equations (of the fluid, skeleton and fluid transport). The state equations were represented with Darcy's law and the balance equations were represented with a conservation law for fluid mass (Eq. 30).

$$\text{div} \bar{\sigma} + (m_s + m_f). \underline{g} = 0 \quad (29)$$

$$\frac{\delta m_f}{\delta t} = \frac{\delta(\rho_f \phi)}{\delta t} = -\text{div} \underline{w} \quad (30)$$

Where: $\bar{\sigma}$ is the total stress; m_s is the skeleton mass; m_f is the fluid mass, which is equal to the product of the fluid volume by the porosity ($\rho_f \phi$); w is the water content.

The total stress can be written with the poro-elasticity theory for a linear isotropic media (Eq. 31):

$$\bar{\sigma} = \lambda_0. \text{tr}(\varepsilon_e^{\bar{}}). \bar{I} + 2.\mu. \bar{\varepsilon} - b.p.\bar{I} \quad (31)$$

Where: $\bar{\sigma}$ is the total stress; λ_0 and μ are the drained Lamé's coefficients (first coefficient and shear modulus); b is the Biot coefficient; p is the fluid pressure exerted on the solid skeleton.

The elastic strain (ε_e) is written as (Eq. 32):

$$\varepsilon_e = \varepsilon_{total} - \varepsilon_{pl} - \varepsilon_{cr} - \varepsilon_{th} \quad (32)$$

Where: ε_{total} is the total strain; ε_{pl} is the plastic strain; ε_{cr} is the creep strain; ε_{th} is the thermal strain.

According to the hypothesis of small variations on fluid mass and uniform porosity, the volume variation of fluid mass can be written as follows (Eq. 33):

$$v_f = b. \text{tr}(\varepsilon_e^{\bar{}}) + \frac{p}{M} = \frac{m_f - m_{f0}}{\rho_{f0}} \quad (33)$$

Where: M is the Biot modulus.

Assuming that the pressure is homogeneously exerted by the fluid, the Biot modulus (M) characterizes the variations of fluid mass in a triaxial test with zero volumetric deformation (Eq. 34):

$$\frac{1}{M} = \frac{b - \varphi_0}{K_s} + \frac{\varphi_0}{K_f} \quad (34)$$

Where: φ_0 is the initial porosity accessible by the fluid; K_s is the compressive modulus of the solid; K_f is the isothermal compressive modulus of the fluid.

The effective stress (σ') may reach an anisotropic state depending on the external stress, which can be due to structural loading in the case of concrete structures.

2.2.3. PORO-MECHANICAL MODELS FOR SWELLING IN CONCRETE STRUCTURES

In order to link the chemical models and mechanical models aforementioned, in this section is presented the main poro-mechanical models which includes the swelling reactions (e.g. AAR).

In order to numerically reproduce the AAR expansions, Dormieux *et al.* (2004) proposed a model based in a micro-poro-mechanical framework, where the concrete is divided in 3 different zones (Figure 2.34): **i)** the pores not filled with gel; **ii)** the pores filled with gel; **iii)** solid matrix (solid skeleton).

The volume of gel increases until it fills the pores, then the swelling of the solid matrix begins. Therefore, in order to use this model, it's necessary to establish the elasticity of the material and to define its microstructure (shape and volume of the pores). After, Lemarchand *et al.* (2005) enhanced this model through the addition of the kinetics of the gel production based on the work of Larive (1998).

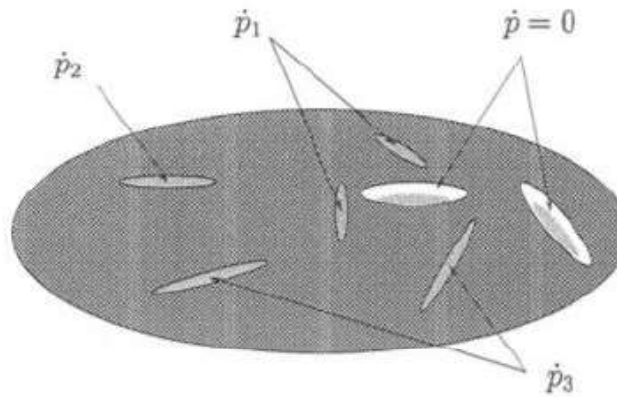


Figure 2.34. Representation of the concrete in 3 zones (DORMIEUX *et al.*, 2004).

Following the works of Capra & Sellier (2002), a poro-mechanical model was proposed by Grimal *et al.* (2008), where a phenomenological model was coupled with a damage model. The advancement of the reaction is calculated through the main environmental parameters, which are the temperature and the saturation degree (as shown in Eq. 7). Once the value of the advancement of the reaction (A) is determined for a given time, the intrapore pressure of gel (P_g) is then calculated as (Eq. 35):

$$P_g = M_g \cdot \langle A \cdot V_g - \langle A_0 \cdot V_g + b_g \cdot tr(\varepsilon) \rangle \rangle \quad (35)$$

Where: M_g is the Biot modulus which is responsible for the elastic interaction between the gel and the solid matrix; V_g is the maximum volume of gel that can be created, which is calibrated by the user; A_0 is the threshold of the advancement of the reaction, which the swelling begins; b_g is the Biot coefficient of the gel; $tr(\varepsilon)$ is the volume created by the swelling strains; $\langle \rangle$ is the Macaulay brackets.

The pressure of gel increases from a certain advancement and the state of deformation of the material influences the evolution of the pressure. The volume of the available pores to the expansion of the gel is then changed. In order to realistically reproduce the behavior of the concrete structures, this chemical model was coupled with a rheological model which takes into account creep, orthotropic damage and external stresses. The model was validated through comparison with the experimental data provided by Multon & Toutlemond (2006), which submitted AAR-affected concrete specimens to stresses and confinement, and also by the experimental data provided by Multon *et al.* (2005), which analyzed concrete beams subjected to AAR, under different reinforcements distributions and water gradients.

Comi *et al.* (2009) proposed a poro-mechanical coupled to a chemo-thermo-damage model. The gel pressure is calculated with the advancement of the reaction which is described with the equations from Larive (1998). The anelastic effective stress (σ'') is then calculated as (Eq. 36):

$$\sigma'' = \bar{\sigma} + (\beta - b) \cdot p \cdot \bar{I} \quad (36)$$

Where: $\bar{\sigma}$ is the external stress; p is the gel pressure; b is the Biot coefficient; β is a coefficient to link the pressure and the damage ($\beta < b$).

Two scalars allow to take into account two isotropic damages, one for tension and other for compression. The hardening law allows producing an elastic domain in function of the damages. The model was validated through comparison with the experimental data provided by Multon & Toutlemond (2006), and after it was applied to two concrete dams under AAR-degradation and the results were in very good agreement with the in-situ measures of cracking.

Some years later, Charpin & Ehrlacher (2014) proposed a micro-poro-mechanical model coupled with AAR orthotropic damage located in the ITZ and in the cement paste. Thus, the concrete was discretized in 4 different zones: i) the cement paste; ii) Interfacial transition zone (ITZ); iii) the attacked zone of the aggregate; iv) the unreacted aggregate.

The gel is formed in the attacked zone of the aggregate and can spread into the ITZ. The damage criteria are described by an energetic approach. Two phenomena are possible, which are a decohesion between the aggregate and the ITZ and a cement paste cracking. This model takes into account the effects of the stress in the swelling anisotropy, and it was validated through comparison with the experimental data provided by Multon & Toutlemond (2006).

In order to enhance the model developed by Grimal et al. (2008), Salgues et al. (2014) proposed a model that could reproduce the concrete behavior under ISR (e.g. AAR and DEF). The main difference in the intrapore pressure (P_{AFt}) calculation between this model and the previous one, is the addition of the plastic strain (Eq. 37), calculated through an anisotropic plastic criterion (Eq. 38) which depends on the effective stress in the main direction.

$$P_{AFt} = M_{AFt} \cdot \langle V_{ARt} - \langle V_{0,ARt} + b_0 \cdot tr(\varepsilon) + (1 - b_0) \cdot tr(\varepsilon^p) \rangle \rangle \quad (37)$$

$$f_I = \langle \tilde{\sigma}'_I - b_0 p^{rgi} \rangle + b_1 p^{rgi} - b_1 p^{lim} \quad (38)$$

Where: M_{AFt} is the Biot modulus; V_{ARt} is the volume of the swelling product for a given time; $V_{0,ARt}$ is the pore volume to be filled by the product to initiate the swelling; b_0 is the Biot coefficient; $tr(\varepsilon)$ is the volume created by the swelling strains; $tr(\varepsilon^p)$ is the volume created by the plastic strains; p^{li} is the maximum pressure acceptable by the unconfined concrete; b_1 is a characteristic material parameter; $\langle \rangle$ is the Macaulay brackets.

If p^{lim} is overwhelmed, $f_I > 0$ which implies that a plastic strain is propagated in one direction until the criterion becomes zero (or negative) again. Therefore, a positive hardening law allows calculating the corresponding plastic strain. The corresponding damage is then calculated with the formula (Eq. 39) proposed by Capra & Sellier (2002). This damage also affects on the strength and Young's modulus of the concrete.

$$\varepsilon_i^{AAR} = \varepsilon_0^{AAR} \cdot \frac{d_i^+}{1 - d_i^+} \quad (39)$$

Where: ε_i^{AAR} is the swelling strain due to AAR in one direction i ; ε_0^{AAR} is the characteristic swelling strain (fixed as 0.3%); d_i^+ is the damage due to the swelling in one direction i .

Lastly, Morenon (2017) developed a poro-mechanical model to describe the swelling of AAR and DEF. This model is coupled with a rheological model proposed by Grimal et al. (2017). The full numerical implementation of these combined works can be found in Sellier (2018). The model proposed by Morenon (2017) is described in the Chapter 3 (*Materials and Methods*).

CHAPTER 3

3. MATERIALS AND METHODS

In this chapter is presented an explanation of the models used to analyze the chemo-mechanical behavior on AAR-affected concrete. The first part is a presentation of the rheological scheme (Grimal *et al.*, 2017) that couples all the following models presented in this chapter. The second part is dedicated to describe the chemical model proposed by Morenon (2017) which shows how the advancement of the reaction creates a volume of gel, and such volume exerts an intrapore pressure in the solid skeleton. However, in order to calculate this gel pressure, the user needs the creep and shrinkage strains, and also the diffuse cracking produced by the gel (micro-plastic strains).

Therefore, the third part is dedicated to describe the creep and shrinkage models proposed by Sellier *et al.* (2016), in order to obtain the associated strains. The fourth and last part is dedicated to how those implementations were made in the software COMSOL Multiphysics®, showing the main features used in the software to add the models aforementioned.

3.1 RHEOLOGICAL SCHEME (GRIMAL *et al.*, 2017)

As previously mentioned, the concrete behavior is modelled in the poro-mechanical framework. The rheological scheme (Figure 3.1) couples the damage model (Sellier *et al.*, 2013), chemical model (Morenon, 2017) and the creep and shrinkage models (Sellier *et al.*, 2016), in order to consider the realistic interaction between ASR, creep, shrinkage and damage.

In the Figure 3.1, P_g is the pressure induced by AAR gel, P_w is the equivalent capillary pressure causing shrinkage in non-saturated conditions, σ_{ij} is the total stress, $\tilde{\sigma}_{ij}$ is the effective stress in the sense of damage and $\tilde{\sigma}_{ij}'$ is the effective stress in the sense of poro-mechanics.

The interstitial pressures (P_g and P_w) are taken into account with a Biot coefficient for both ASR (b_{asr}) and capillary pressure (b_w). The effective stress in the sense of damage ($\tilde{\sigma}_{ij}$) is then expressed as (Eq. 40):

$$\tilde{\sigma}_{ij} = \tilde{\sigma}_{ij}' - b_{asr} \cdot P_{asr} - b_w \cdot P_w \quad (40)$$

The effective stress increment in the sense of poro-mechanics is then calculated as (Eq. 41):

$$\dot{\tilde{\sigma}}_{ij}' = S_0 \cdot (\dot{\epsilon} - \dot{\epsilon}_{pl} - \dot{\epsilon}_{cr} - \dot{\epsilon}_{th}) \quad (41)$$

Where: S_0 is the stiffness matrix; $\dot{\epsilon}$, $\dot{\epsilon}_{pl}$, $\dot{\epsilon}_{cr}$ and $\dot{\epsilon}_{th}$ are the total strain increment, plastic strain increment, creep strain increment and thermal strain increment, respectively.

The total stress depends on the effective stress in the sense of damage ($\tilde{\sigma}_{ij}$) and on the two scalar damage variables regarding the damage caused by ASR (D_{ASR}) and the damage caused by structural loading (D_{struct}). Therefore, the total stress is written as (Eq. 42):

$$\sigma_{ij} = (1 - D_{ASR}) \cdot (1 - D_{struct}) \cdot \tilde{\sigma}_{ij} \quad (42)$$

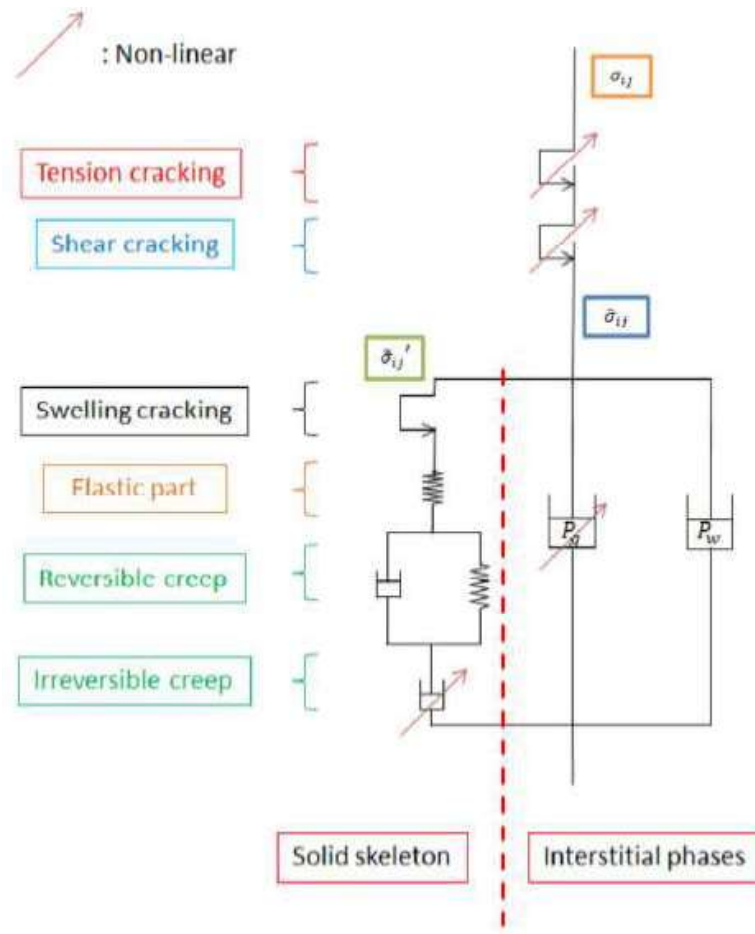


Figure 3.1. Rheological scheme (GRIMAL *et al.*, 2017).

3.2 CHEMICAL MODEL (MORENON, 2017)

The AAR is responsible for the appearance of newly formed phases in the porous matrix of the concrete. The lack of space at their disposal quickly puts the solid skeleton under pressure, which results in tensile stresses around the reactive sites (aggregates). Therefore, the theory of poro-mechanics allows to take into account the influence of this intrapore pressure on the solid skeleton of the concrete (MORENON, 2017). The physical

phenomena responsible for the degradation of the mechanical behavior of ASR-affected concrete structures can be listed as follows:

- 1) **Creation of the ASR gel:** A volume of intrapore swelling product (ASR gel) is created by chemical reactions;
- 2) **Creation of the intrapore pressure:** When all the porosity volume around the reactive site (silica aggregate) is filled with the reaction product, a intrapore pressure is generated;
- 3) **Diffuse cracking appearance:** The intrapore pressure produces a tensile stress in the cement paste, and basically, when the tensile strength is reached, diffuse cracks appear;
- 4) **Creep induced by the intrapore pressure:** As the gel pressure is maintained over time on the solid skeleton, creep will be generated;
- 5) **Localized cracks appearance:** When the concrete structure is subjected to external loading, localized cracks may be generated, which will facilitate the penetration of water and other pathologies agents (e.g. CO₂), and such water may accelerate or reactivate the swelling reaction (ASR).

According to Morenon (2017), the **advancement of the reaction** (A^{asr}) is based on the works of Poyet *et al.* (2006) and Grimal *et al.* (2008). The term A^{asr} ranges from 0 (before the reaction begins) to 1 (when the reaction is complete). The evolution of the advancement is written as follows (Eq. 43):

$$\frac{\delta A^{asr}}{\delta t} = \frac{1}{\tau_{ref}^{asr}} \cdot C^{T,asr} \cdot C^{W,asr} \cdot \langle Sr - A^{asr} \rangle^+ \quad (43)$$

Where: τ_{ref}^{asr} is the characteristic time (calibrated using a free swelling test); Sr is the saturation degree; $C^{T,asr}$ is the coefficient for temperature effect; $C^{W,asr}$ is the coefficient for humidity effect.

The **effect of temperature** ($C^{T,asr}$) is formulated with an Arrhenius' law (Eq. 44), as proposed by Ulm *et al.* (2000).

$$C^{T,asr} = \exp \left[-\frac{E^{asr}}{R} \cdot \left(\frac{1}{T} - \frac{1}{T_{ref}} \right) \right] \quad (44)$$

Where: E^{asr} is the thermal activation energy (40.000 J/mol - Larive, 1997); T_{ref} is the reference temperature (calibrated on the same test as τ_{ref}^{asr}); R is the perfect gas constant [8,1314 J/(mol.K)]; T is the temperature (Kelvin).

The **effect of humidity** ($C^{W,asr}$) is evaluated by a potential law (Eq. 45), which can describe the non-linear increase in the impact of humidity in ASR, specially the role of the saturation degree.

$$C^{W,asr} = \begin{cases} \left(\frac{Sr - Sr^{th,asr}}{1 - Sr^{th,asr}} \right)^2 & \text{if } Sr > Sr^{th,asr} \\ 0 & \text{if } Sr \leq Sr^{th,asr} \end{cases} \quad (45)$$

Where: $S_r^{th, asr}$ is the saturation degree threshold which is the minimum saturation degree to initiate the chemical reaction.

As a result of the chemical reactions, a **volume of ASR gel** (ϕ^{asr}) is created for a given time “ t ” (Eq. 46):

$$\phi^{asr}(t) = \phi^{asr, \infty} \cdot A^{asr}(t) \quad (46)$$

Where: $\phi^{asr, \infty}$ is the maximum volume ratio of gel that can be created, which is calibrated by the free swelling test (for the same condition as τ_{ref}^{asr}).

Next, on Table 1, there is a resume of the main material parameters used to calculate the volume of ASR gel, as well as the values range, its unities and the calibration tests required.

Table 1: Material parameters used to calculate the volume of gel (Morenon, 2017).

| Parameter | Signification | Range value in laboratory tests | Unity | Calibration test |
|----------------------|--|---------------------------------|-----------|---|
| $\phi^{asr, \infty}$ | Maximum volume ratio of ASR gel | $0 \sim 10^{-2}$ | m^3/m^3 | Free swelling test |
| τ_{ref}^{asr} | Characteristic time of ASR | $0 \sim 200$ | days | Free swelling test |
| $S_r^{th, asr}$ | Saturation degree threshold to activate ASR | $0 \sim 0,1$ | - | Swelling test for different hydric conditions |
| T_{ref} | Reference temperature at which the test is carried out | Temperature value | °C | - |
| E^{asr} | Activation energy for the kinetics of ASR | 40.000 (Larive, 1997) | J/mol | Swelling test for different temperature |

The volume of ASR gel produced is used to calculate **the intrapore pressure** (P_{asr}) induced by the swelling of the gel (Eq. 47). For each instant, the pressure is calculated by the difference between the volume of ASR gel produced (ϕ^{asr}) and the available volume for the gel to permeate (ϕ_{asr}^v).

$$P_{asr} = M_{asr} \cdot \langle \phi^{asr} - \phi_{asr}^v \cdot \left(\frac{P_{asr}}{\tilde{R}_I^t} \right) + b_{asr} \cdot tr(\varepsilon^e + \varepsilon^{cr}) + tr(\varepsilon^{p, asr}) \rangle^+ \quad (47)$$

Where: M_{asr} is the Biot modulus, which is responsible for the interaction between ASR gel and cement matrix; b_{asr} is the Biot coefficient used to take into account the increase in porosity volume due to the evolution of the intrapore pressure; ϕ_{asr}^v is the available voids volume; \tilde{R}_I^t is the micro-tensile strength of the material; $tr(\varepsilon^e + \varepsilon^{cr})$ is variation of the porosity due to concrete strain, and its composed by the trace of the elastic strains (ε^e) and creep strain (ε^{cr}) of the cement matrix; $tr(\varepsilon^{p, asr})$ is the variation of the porosity due to plastic strain, representing the volume of cracks produced by ASR and assumed to be completely filled by ASR gel, and its composed by the trace of the plastic strains ($\varepsilon^{p, asr}$) of the cement matrix; $\langle \rangle^+$ is the Macaulay bracket, which denotes the positive part operator.

The available volume for the permeation of the gel (ϕ_{asr}^v) is influenced by many factors, such as:

- Connected porosity;
- Increase or decrease in the volume of voids where the gel is formed (due to elastic strains or creep of the cement matrix)
- Volume of the cracks created by the ASR.

The formation of the available volume for gel percolation is illustrated in the Figure 3.2.

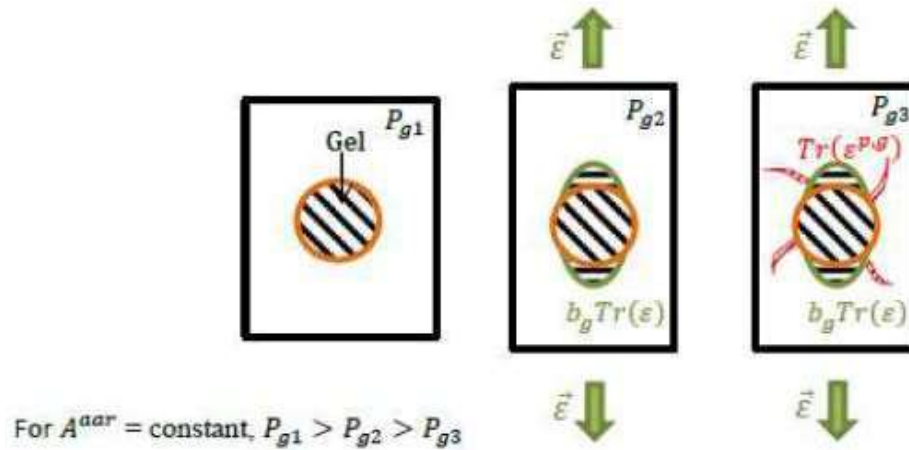


Figure 3.2. Strains effect on gel pressure (GRIMAL *et al.*, 2017).

Next, on Table 2, there is a resume of the main material parameters used to calculate the volume of ASR gel, as well as the values range, its unities and the calibration tests required.

Table 2: Material parameters to calculate the intrapore pressure (Morenon, 2017).

| Parameter | Signification | Range value in laboratory tests | Unity | Calibration test |
|----------------|--|---------------------------------|--------------------------------|--------------------------|
| ϕ_{asr}^v | Volume of porosity connected to the reactive sites | $\approx 10\%$ of ϕ^{asr} | m ³ /m ³ | Free swelling test |
| b_{asr} | Biot coefficient for ASR | 0,1 ~ 0,25 | - | Restrained swelling test |
| M_{asr} | Biot modulus for gel-matrix interaction | 27.700 | MPa | Free swelling test |

3.3 CREEP AND SHRINKAGE MODELS (SELLIER *et al.*, 2016)

The poro-mechanical creep and shrinkage models can be summarized in a rheological scheme (Figure 3.3) which contains two branches:

- **Left branch – Solid skeleton:** the elastic part (symbolized as a spring) is used to model the instantaneous behavior. The Kelvin module (symbolized as spring and a Newtonian dashpot in parallel) is used to model the reversible creep. The

non-linear Maxwell module (symbolized as a Newtonian dashpot) is used to model the permanent strains.

- **Right branch – Interstitial phases:** represents the effects of hydric forces (capillary pressure and variation of disjoining forces) and also the pressure generated by swelling products (e.g. AAR gel).

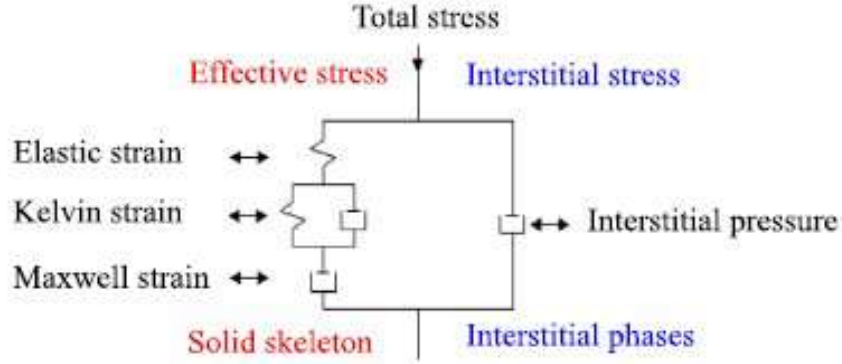


Figure 3.3. Idealized rheological scheme for poro-mechanical creep model (SELLIER *et al.*, 2016).

Although the concrete microstructure is not explicitly modelled, the constitutive equations reflect the several underlying phenomena induced by concrete heterogeneity. The viscous phenomenon is assumed to happen in the C-S-H interlayers, while the other hydrates and aggregates are considered as non-viscous elements.

3.3.1 Permanent Creep – Maxwell Strain

The permanent creep is modeled with a Maxwell module (Figure 3.3) and it's assumed to derive directly from the corresponding elastic strain components (ε_I^E). The proportionality between the creep velocity and the ε_I^E is supported by experimental data which shows that multiaxial creep starts with relative strain velocities in different directions (I) proportional to the ε_I^E . Therefore, the Maxwell strain component (ε_I^M) is written as (Eq. 48):

$$\frac{\partial \varepsilon_I^M}{\partial t} = \frac{\varepsilon_I^E}{\tau_I^M} \quad (48)$$

Where: τ_I^M is the characteristic time associated with the ε_I^M ; I is the eigenvalue to represent the main directions.

The characteristic time is then expressed as a function (Eq. 49) of the reference characteristic time (τ_{ref}^M), characterizing the initial material state, and also the consolidation function (C_I^C). The τ_{ref}^M is a fitting parameter which is inversely proportional to the initial creep velocity, under controlled conditions (temperature, humidity and mechanical loading), and the C_I^C considers the non-linear dependence of the creep potential on the loading rate.

$$\tau_I^M = \tau_{ref}^M \cdot C_I^C \quad (49)$$

As the consolidation function is written as an anisotropic formulation (Eq. 50), it considers the different consolidation velocities in the three main directions of creep. The objective of the consolidation function is to consider the decrease of the creep strain velocity with time without relying on the time variable itself.

$$C_I^C = \frac{1}{k} \cdot \exp \left(\frac{1}{k} \cdot \left\langle \frac{\varepsilon_I^M}{\varepsilon_I^E} \right\rangle^+ \right) \quad (50)$$

Where: k is the creep coefficient for the same conditions as τ_{ref}^M ; $\langle \rangle^+$ is the Macaulay bracket which denotes the positive part operator.

The creep coefficient is affected by physical conditions such as temperature (T), humidity (H) and mechanical loading (M), thus it can be expressed as (Eq. 51):

$$k = k_{ref} \cdot C^T \cdot C^H \cdot C^M \quad (51)$$

Where: k_{ref} is the reference creep coefficient; C^T , C^H and C^M are the functions related to the influence of temperature, humidity and mechanical loading, respectively.

The reference creep coefficient is then written as (Eq. 52):

$$k_{ref} = \frac{\varepsilon_{ref}^M}{\varepsilon_{ref}^E} \quad (52)$$

Where: ε_{ref}^E is the reference elastic strain which is a fitting parameter obtained for a given loading level applied on experimental test; ε_{ref}^M is the reference creep potential which is a fitting parameter related to the creep function amplitude, and it's defined for the same conditions as ε_{ref}^E .

The reference elastic strain is the immediate strain related to the creep test for a loading of 30% (or less) of its compressive strength. In the case of real structures which doesn't have creep tests performed, this strain is often estimated as a ration between the uniaxial compressive strength (R_c) and the Young's modulus (E), expressed as follows (Eq. 53):

$$\varepsilon_{ref}^E = \frac{\left(\frac{R_c}{3}\right)}{E} \quad (53)$$

The function related to the influence of humidity (C^H) is taken as equal to the saturation degree (S_r), written as (Eq. 54):

$$C^H = S_r \quad (54)$$

The function related to the influence of the temperature (C^T) is taken as a product of two functions (Eq. 55): the first is related to the influence of temperature in water viscosity (C_w^T) and the second is related to the influence of temperature in the differential dilatation between non-viscous and viscous phases (C_p^T).

$$C^T = C_w^T \cdot C_p^T \quad (55)$$

The two functions C_w^T and C_p^T are then written as Arrhenius laws as follows (Eq. 56 and Eq. 57):

$$C_w^T = \exp \left[-\frac{E_w^a}{R} \cdot \left(\frac{1}{T} - \frac{1}{T_{ref,creep}} \right) \right] \quad (56)$$

$$C_p^T = \begin{cases} \exp \left[-\frac{E_p^a}{R} \cdot \left(\frac{1}{T} - \frac{1}{T_{thr}} \right) \right] & \text{if } T > T_{thr} \\ 1 & \text{if } T \leq T_{thr} \end{cases} \quad (57)$$

Where: E_w^a is the activation energy of water viscosity (≈ 17000 J/mol); R is the perfect gas constant [8.1314 J/(mol.K)]; T is the environment temperature; $T_{ref,creep}$ is the reference temperature for which the τ_{ref}^M is fitted; E_p^a is the activation energy for differential dilatation between phases (≈ 25000 J/mol); T_{thr} is the temperature threshold ($\approx 45^\circ\text{C}$) for which the thermal damage appears and modifies the creep potential.

The function related to the influence of the mechanical loading (C^M) starts from 1 (for weakly loaded material) and diverges if the loading level reaches a critical value causing tertiary creep, which is believed to occur only in cases of micro-structure damage. Therefore, C^M is associated an equivalent Drucker-Prager criterion, and it's written as (Eq. 58):

$$C^M = \frac{\tau_{cr}^{DP}}{\tau_{cr}^{DP} - \tau^{DP}} ; \tau_{cr}^{DP} > \tau^{DP} \quad (58)$$

Where: τ_{cr}^{DP} is the critical stress leading to tertiary creep; τ^{DP} is the Drucker-Prager equivalent shear stress.

The two stresses (τ^{DP} and τ_{cr}^{DP}) are then expressed as follows (Eq. 59 and Eq. 60):

$$\tau^{DP} = \sqrt{\frac{\sigma^D : \sigma^D}{2}} + \delta \cdot \frac{tr(\sigma)}{3} \quad (59)$$

$$\tau_{cr}^{DP} = \frac{\sigma_{cr}}{\sqrt{3}} \cdot \left(1 - \frac{\delta}{\sqrt{3}} \right) \quad (60)$$

Where: σ^D is the deviatoric part of the stresses tensor; $tr(\sigma)/3$ is the hydrostatic pressure δ is the Drucker-Prager confinement coefficient; σ_{cr} is the uniaxial critical stress assumed as a compression.

The uniaxial critical stress is then written as (Eq. 61):

$$\sigma_{cr} = \frac{2}{3} \cdot \left(\frac{\chi^M}{\chi^M - 1} \right) \cdot R_c \quad (61)$$

Where: R_c is the uniaxial compressive strength; χ^M which is a fitting parameter responsible for the non-linear behavior when the specific creep amplification increases with the loading rate.

Next, on Table 3, there is a resume of the main material parameters used to calculate the reversible creep, as well as the values range and its unities.

Table 3: Material parameters to calculate the permanent creep (Sellier *et al.*, 2016).

| Parameter | Signification | Range value in creep tests | Unity |
|-----------------------|--|----------------------------|-------|
| τ_{ref}^M | Reference characteristic time associated with the Maxwell strain | ≈ 14 | days |
| E_w^a | Activation energy for water viscosity | 17.000 | J/mol |
| E_p^a | Activation energy for differential dilatation between phases | 25.000 | J/mol |
| $T_{ref,creep}$ | Reference temperature for which the τ_{ref}^M is fitted | 20 | °C |
| T_{thr} | Temperature threshold for which the thermal damage appears and modifies the creep potential | 40 | °C |
| χ^M | Fitting parameter responsible for the non-linear behavior when the specific creep amplification increases with the loading rate. | 2 | - |
| ε_{ref}^M | Reference creep coefficient | $0,9.10^{-4}$ | - |

3.3.2 Reversible Creep – Kelvin Strain

The reversible creep is modeled with a Kelvin module (Figure 3.3) and the asymptotic strain is assumed to be proportional to the elastic strain components (ε_{ij}^E). The directions ij correspond to the base in which the stress tensor is expressed. Therefore, the Kelvin strain component (ε_{ij}^K) is written as (Eq. 62):

$$\frac{\partial \varepsilon_{ij}^K}{\partial t} = \frac{1}{\tau^K} \cdot \left(\frac{\varepsilon_{ij}^E}{\psi^K} - \varepsilon_{ij}^K \right) \quad (62)$$

Where: τ^K is the characteristic time associated with the ε_{ij}^K ; ψ^K is a fitting parameter to control the kinetics modification, adjusting the final amplitude of the reversible creep, and it's obtained through creep test with strain recovery.

The characteristic time associated with the reversible creep has its velocity associated depends on the environmental condition, such as temperature – in the case of water viscosity (C_w^T) – and humidity (C^H). Therefore, it can be expressed as (Eq. 63):

$$\tau^K = \tau_{ref}^K \cdot C_w^T \cdot C^H \quad (63)$$

Where: τ_{ref}^K is the reference characteristic time associated with the ε_{ij}^K , calibrated for the same condition as ψ^K .

The authors (Sellier *et al.*, 2016) have shown through experimental test database that the value of the reversible creep (Kelvin strain) represents about 20 to 25% of the elastic strain.

Next, on Table 4, there is a resume of the main material parameters used to calculate the permanent creep, as well as the values range and its unities.

Table 4: Material parameters to calculate the reversible creep (Sellier *et al.*, 2016).

| Parameter | Signification | Range value in creep tests | Unity |
|----------------|---|----------------------------|-------|
| ψ^K | Fitting parameter to control the kinetics modification, adjusting the final amplitude of the reversible creep | 4 ~ 5 | - |
| τ_{ref}^K | Reference characteristic time associated with the Kelvin strain | 0,70 | days |

3.3.3 Shrinkage

The effects of intrapore water is modeled in a poro-mechanical framework because the water molecules presented in nanoscopic interlayers cause attractive or repulsive forces according to their environmental conditions (temperature, humidity and mechanical loading), impacting on the macroscopic scale, as already explained in the Chapter 2 (*Literature Review*). The hydric forces effects result in stress field heterogeneity, and subsequently damage induced by this stress gradient, as illustrated on the mesoscopic analyses presented in the Figure 3.4.

For the sake of simplicity, the different effects of water forces – capillary and disjoining forces – were combined into a single **equivalent capillary pressure** (p_w) which depends on the stress state (as illustrated in the Figure 3.4). As the capillary pressures will act when the conditions are unsaturated, a Van-Genuchten law was used to describe the relation between p_w and the saturation degree (Eq. 64):

$$p_w = -M_{shr} \cdot \left(S_r^{\left(\frac{-1}{m_{vg}} \right)} - 1 \right)^{(1-m_{vg})} \quad (64)$$

Where: M_{shr} and m_{vg} are fitting parameters calibrated from the work of Baroghel-Bouny *et al.* (1999) which controls the shape of the water retention curve, and their values are 41 MPa and 0.5, respectively.

Morenon (2017) re-wrote the previous Van-Genuchten law as follows (Eq. 65):

$$p_w = a \cdot \left(1 - S_r^{\left(1 - \frac{1}{b} \right)} \right)^{(1-b)} \quad (65)$$

Where: a and b are the fitting parameters calibrated from the work of Multon & Toutlemond (2006), and their values are 25 MPa and 0.42, respectively.

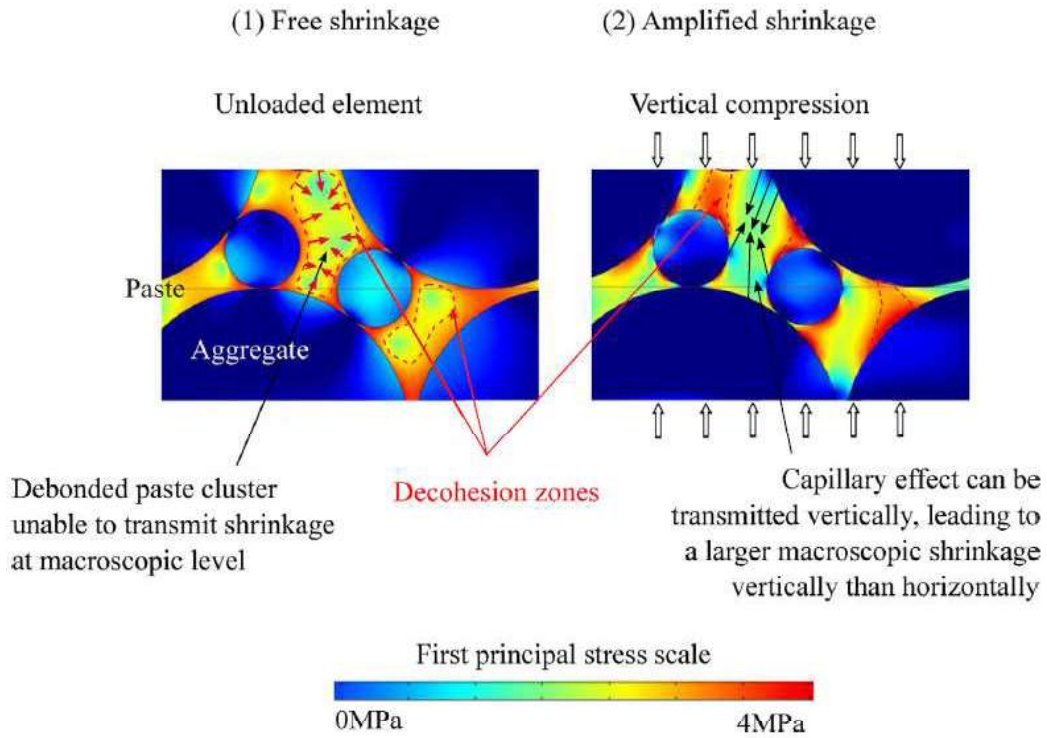


Figure 3.4. Stress field heterogeneity at meso-scale and consequences in terms of shrinkage forces transmission to macroscopic scale, for two conditions: (1) free shrinkage and (2) shrinkage amplified by external mechanical loading (**SELLIER *et al.*, 2016**).

3.4 IMPLEMENTATION IN COMSOL®

The models previously shown in this chapter were implemented in COMSOL Multiphysics® v. 5.5 (COMSOL AB, Stockholm, Sweden) a commercial multiphysics simulation platform. Firstly, the geometries of the concrete specimens were constructed by the graphic interface. The mechanical and chemical were realized by different models in COMSOL. These models were implemented through equation based modelling and they were transferred to different ordinary differential equations (ODEs) and combined into the solid mechanics interface, which can be solved using the nonlinear solver provided by COMSOL.

The Solid mechanics interface in COMSOL Multiphysics® is based on the standard momentum balance equation (Eq. 66), and for simplicity, inertial effects were neglected and displacements and strains were assumed to remain small (Eq. 67). Therefore, these two equations are complemented by appropriate boundary conditions and a constitutive law relating stresses and strains to complete the problem definition.

$$\nabla \cdot \sigma + F_V = 0 \quad (66)$$

$$\varepsilon = \frac{1}{2} \cdot (\nabla u + \nabla u^T) \quad (67)$$

Where: σ is the stress tensor; F_V contains the body forces; ε is the strain tensor; u are the displacements.

The results were analyzed using the post-processing functions provided by the software and verified from decoupling tests.

3.4.1 Implementation of the Chemical Model

First, it is needed to define the general parameters (environmental parameters, loading and time) and the model parameters. The definition of such parameters is shown in the Figure 3.5 and Figure 3.6. The internal variables of the problem are shown in the Figure 3.7. The advancement of the reaction (A^{asr}) was implemented as a domain ODE, and it's shown in the Figure 3.8.

Parameters

Label: Parameters - General

Parameters

| Name | Expression | Value | Description |
|-------|--------------------|------------------|--------------------------|
| Sr | 0.99 | 0.99 | Saturation Degree |
| T | 273.15+25 [K] | 298.15 K | Temperature |
| R | 8.1314 [J/(mol*K)] | 8.1314 J/(mol*K) | Perfect Gas Constant |
| Fy | 5 [MPa] | 5E6 Pa | Pressure applied on test |
| Delta | 0.1 [d] | 8640 s | Timestep |
| tf | Delta*500 | 4.32E6 s | Total time |

Figure 3.5. General parameters – environmental conditions, loading and total time of simulation.

Parameters

Label: Parameters - Chemical model

Parameters

| Name | Expression | Value | Description |
|---------|---------------|-------------|--|
| tau_ref | 50*24*3600[s] | 4.32E6 s | Characteristic time of ASR |
| Sr_th | 0.1 | 0.1 | Saturation degree threshold to activate ASR |
| T_ref | 38+273.15[K] | 311.15 K | Reference temperature for Free Swelling Test calibration |
| E_asr | 40000[J/mol] | 40000 J/mol | Activation energy for ASR |
| phi_inf | 5e-3 | 0.005 | Maximum volume ratio of ASR gel |
| M_asr | 27700[MPa] | 2.77E10 Pa | Biot Modulus for ASR gel-cement matrix interaction |
| b_asr | 0.25 | 0.25 | Biot Coefficient for ASR |
| h_asr | 0.03 | 0.03 | plastic hardening law ratio |

Figure 3.6. Chemical model parameters.

Variables

Label: Variables - Chemical model

Geometric Entity Selection

Geometric entity level: Entire model

Variables

| Name | Expression | Unit | Description |
|---------------|--|------|---|
| CT | $\exp(-E_{asr}/R*(1/T-1/T_{ref}))$ | | Coefficient of temperature effect |
| CW | $((Sr-Sr_{th})/(1-Sr_{th}))^2*(Sr>Sr_{th})+0*(Sr\leq Sr_{th})$ | | Coefficient of humidity effect |
| phi_asr | $\phi_{inf}*A_{asr}$ | | Volume ratio of ASR gel |
| phi_availa... | $0.1*\phi_{asr}$ | | Volume of porosity connected to the reactive sites (available void... |
| Rt_micro | $Rt+(h_{asr}+material.E)$ | Pa | Evolution of the micro tensile strength |

Figure 3.7. Internal variables of the chemical model.

Global Equations

Label: A_asr

Global Equations

$f(u, u_t, u_{tt}, t) = 0, u(t_0) = u_0, u_t(t_0) = u_{t0}$

| Name | $f(u, u_t, u_{tt}, t)$ (1/s) | Initial value (u) | Initial | Description |
|-------|---|-------------------|---------|-----------------------------|
| A_asr | $d(A_{asr}, t) - ((CT * CW) / \tau_{ref}) * (abs(Sr - A_{asr}) * (A_{asr} \leq Sr) + 0 * (A_{asr} > Sr))$ | 0 | 0 | Advancement of the Reaction |

Name: A_asr

$f(u, u_t, u_{tt}, t)$ (1/s):

$d(A_{asr}, t) - ((CT * CW) / \tau_{ref}) * (abs(Sr - A_{asr}) * (A_{asr} \leq Sr) + 0 * (A_{asr} > Sr))$

Figure 3.8. Advancement of the reaction written as a domain ODE.

3.4.2 Implementation of the Shrinkage Model

The definition of the general parameters (Figure 3.5) is the same as before. The model parameters are shown in Figure 3.9, the internal variables of the model are shown in Figure 3.10. The capillary pressure (shrinkage stress) was applied as a pore-pressure (Figure 3.11), regarding the poro-mechanical theory, using the *External Stress* subnode which allows the user to specify an additional stress contribution to the material which is not part of the constitutive relation. The external stress can be added to the total stress tensor, or act only as an extra load contribution. When the *Pore Pressure* option is selected, there is no contribution to the stress tensor and the only effect of the pressure is as a load.

Parameters

Label: Parameters - Shrinkage model

Parameters

| Name | Expression | Value | Description |
|-------|------------|----------|---|
| b_w | 0.25 | 0.25 | Biot coefficient for water |
| b_shr | 0.42 | 0.42 | fitting parameter "b" - Van-Genuchten law |
| a_shr | 25 [MPa] | 2.5E7 Pa | fitting parameter "a" - Van-Genuchten law |

Figure 3.9. Shrinkage model parameters.

Variables

Label: Variable - Shrinkage model

Geometric Entity Selection

Geometric entity level: Entire model

Variables

| Name | Expression | Unit | Description |
|------|--|------|--------------------|
| Pw | $b_w(a_{shr}(1-Sr^{1-(1/b_{shr})})^{1-b_{shr}})$ | Pa | Capillary Pressure |

Figure 3.10. Internal variables of the shrinkage model.

External Stress

Label: Shrinkage and Capillary Pressure (Pw)

Domain Selection

Override and Contribution

Equation

Show equation assuming:

Study 1, Time Dependent

$$0 = \nabla \cdot \mathbf{F} \left(\mathbf{S} + J \mathbf{F}^{-1} \sigma_{ext} \mathbf{F}^{-T} \right) + \mathbf{F}_v$$

Coordinate System Selection

External Stress

Stress input:

Stress tensor (Spatial)

External stress tensor:

σ_{ext} Pw N/m²

Isotropic

Contribution type:

Load contribution only

Figure 3.11. Capillary pressure (shrinkage stress).

3.4.3 Implementation of the Creep Model

The definition of the general parameters (Figure 3.5) is the same as before. First, it's presented the implementation of the Maxwell module (permanent creep) and after it's presented the implementation of the Kelvin module (reversible creep). Both strains were applied using the *External Strain* subnode which allows the user to provide inelastic strain contributions to the material on a variety of formats, including using external coded functions. For both modules (Maxwell and Kelvin), the external coded functions were implemented as ODEs to calculate the strains components in the main directions ($a_{ij} = a_{11}, a_{22}$) regarding the 2D application.

MAXWELL MODULE (PERMANENT CREEP):

The model parameters are shown in Figure 3.12, the internal variables of the model are shown in Figure 3.13. The internal variables for the function to consider the non-linearity dependence on loading levels are shown in Figure 3.14. The coded function (ODE) to calculate the Maxwell strain is presented in Figure 3.15 (discretization) and Figure 3.16 (code), and the main components used as *External Strain* are shown in Figure 3.17.

| Parameters | | | |
|-----------------------------------|----------------|-------------|---|
| Label: Parameters - Maxwell model | | | |
| Parameters | | | |
| Name | Expression | Value | Description |
| strain_ref_M | 10e-5 | 1E-4 | Reference Creep Potential (Creep Strain for a loading used to determine th... |
| Eaw | 17000 [J/mol] | 17000 J/mol | Activation Energy for water viscosity |
| Eap | 25000 [J/mol] | 25000 J/mol | Activation Energy for differential dilatation between phases |
| Trefc | 273.15+20 [K] | 293.15 K | Reference Temperature for creep |
| Tthr | 273.15+45 [K] | 318.15 K | Temperature threshold |
| tauMref | 15*24*3600 [s] | 1.296E6 s | Reference Characteristic Time for Maxwell Model |

Figure 3.12. Maxwell module parameters.


| Variables | | | |
|---|--|------|--|
| Label: Variables - Maxwell model (Permanent Creep) | | | |
| Geometric Entity Selection | | | |
| Geometric entity level: Entire model | | | |
|  | | | |
| Variables | | | |
| Name | Expression | Unit | Description |
| tauM1 | tauMref*CC1 | s | Characteristic time associated with the Maxwell strain component (11) |
| tauM2 | tauMref*CC2 | s | Characteristic time associated with the Maxwell strain component (22) |
| CC1 | $(1/k) \cdot \exp(1/k \cdot \text{abs}(Ga1/\text{solid.eel11}))$ | | Consolidation Function (11) |
| CC2 | $(1/k) \cdot \exp(1/k \cdot \text{abs}(Ga2/\text{solid.eel22}))$ | | Consolidation Function (22) |
| strain_ref_E | $(Rc/3)/\text{material.E}$ | | Reference Elastic Strain (corresponding to the loading level used to define... |
| kref | strain_ref M/strain_ref E | | Reference Creep Coefficient |
| k | kref*CT_maxwell*CH*CM | | Creep Coefficient |
| CH | Sr | | Influence of the Humidity (Humidity Function) |
| CT_maxwell | CTw*CTp | | Influence of the Temperature (Temperature Function) |
| CTw | $\exp(-Eaw/R \cdot (1/T - 1/Trefc))$ | | Influence of Temperature on Water Viscosity |
| CTp | $\exp(-Eap/R \cdot (1/T - 1/Tthr)) \cdot (T > Tthr) + 1 \cdot (T \leq Tthr)$ | | Influence of Temperature on Creep Potential |
| CM | $\text{Tau_DP_cr}/(\text{Tau_DP_cr} - \text{Tau_DR})$ | | Influence of the Mechanical Loading (Specific Creep Amplification Funct... |

Figure 3.13. Internal variables of the Maxwell module.


| Variables | | | |
|---|---|------------------|---|
| Label: Variable - Function for the non-linearity dependance on loading | | | |
| Geometric Entity Selection | | | |
| Geometric entity level: Entire model | | | |
|  | | | |
| Variables | | | |
| Name | Expression | Unit | Description |
| Tau_DP_cr | $(\text{Sigma_cr}/\text{sqrt}(3)) \cdot (1 - (\text{Coef_DP}/\text{sqrt}(3)))$ | Pa | Critical Stress leading to tertiary creep |
| Tau_DR | $\text{sqrt}(\text{solid.II2s}/2 + \text{eps}) + \text{Coef_DP} \cdot \text{solid.II1s}/3$ | N/m ² | Equivalent Drucker-Prager shear stress |

Figure 3.14. Internal variables of the function to consider the non-linearity dependance on loading level.

Domain ODEs and DAEs

Label: Maxwell Model

Name: Ga

Domain Selection

Units

Discretization

Shape function type:
Discontinuous Lagrange

Element order:
Quadratic

Value type when using splitting of complex variables:
Complex

Frame:
Spatial

Dependent Variables

Field name: Ma

Number of dependent variables: 2

Dependent variables: Ma11, Ma22

Figure 3.15. Discretization of the Maxwell module applied as an ODE.

Distributed ODE

Label: Maxwell model

Domain Selection

Override and Contribution

Equation

Show equation assuming:
Study 1, Time Dependent

$$e_a \frac{\partial^2 \mathbf{u}}{\partial t^2} + d_a \frac{\partial \mathbf{u}}{\partial t} = \mathbf{f}$$

$$\mathbf{u} = [Ma11, Ma22]^T$$

Source Term

\mathbf{f} : solid.eel11/tauM1 (1/s), solid.eel22/tauM2 (1/s)

Damping or Mass Coefficient

d_a : 1, 0, 0, 1, 0, 1

Mass Coefficient

e_a : 0, 0, 0, 0, 0, 0

Figure 3.16. Coded function of the Maxwell module applied as an ODE.

External Strain

Label: External Strain - Maxwell model

Domain Selection

Override and Contribution

Equation

Show equation assuming:

Study 1, Time Dependent

$F_{inel}^{-1} \rightarrow F_{ext}^{-1} F_{inel}^{-1}$

$F_{ext} = I + \epsilon_{ext}$

Model Input

Coordinate System Selection

External Strain

Strain input:

Strain tensor

Strain tensor:

ϵ_{ext} User defined

| | | |
|------|------|---|
| Ma11 | 0 | 0 |
| 0 | Ma22 | 0 |
| 0 | 0 | 0 |

Figure 3.17. Maxwell strains applied *External Strain*.

KELVIN MODULE (REVERSIBLE CREEP):

The model parameters are shown in Figure 3.18, the internal variables of the model are shown in Figure 3.19. The coded function (ODE) to calculate the Kelvin strain is presented in Figure 3.20 (discretization) and Figure 3.21 (code), and the main components used as *External Strain* are shown in Figure 3.22.

Parameters

Label: Parameters - Kelvin model

Parameters

| Name | Expression | Value | Description |
|---------|-----------------------------|-----------|---|
| tauKref | $2 \cdot 24 \cdot 3600$ [s] | 1.728E5 s | Reference Characteristic Time for Maxwell Model |
| PsiK | 4 | 4 | Coefficient for Kinetics modification in Kelvin model (Kelvin stiffness/Young module Ratio) |


Figure 3.18. Kelvin module parameters.

Variables

Label: Variables - Kelvin model (Reversible Creep)

Geometric Entity Selection

Geometric entity level: Entire model



Variables

| Name | Expression | Unit | Description |
|------|----------------|------|---|
| tauK | tauKref*CTw*CH | s | Characteristic time associated with the Kelvin strain component |

Figure 3.19. Internal variables of the Kelvin module.

Domain ODEs and DAEs

Label: Kelvin Model

Name: Ka

Domain Selection

Units

Discretization

Shape function type: Discontinuous Lagrange

Element order: Quadratic

Value type when using splitting of complex variables: Complex

Frame: Spatial

Dependent Variables

Field name: Ka

Number of dependent variables: 2

Dependent variables: Ka11, Ka22

Figure 3.20. Discretization of the Kelvin module applied as an ODE.

Distributed ODE

Label:

Domain Selection

Override and Contribution

Equation

Source Term

f 1/s

1/s

Damping or Mass Coefficient

d_a 1 1

1 1

Mass Coefficient

e_a s s

s s

Figure 3.21. Coded function of the Maxwell module applied as an ODE.

External Strain

Label:

Domain Selection

Override and Contribution

Equation

Show equation assuming:

$F_{inel}^{-1} \rightarrow F_{ext}^{-1} F_{inel}^{-1}$

$F_{ext} = I + \epsilon_{ext}$

Model Input

Coordinate System Selection

External Strain

Strain input:

Strain tensor:

ϵ_{ext}

| | | | |
|------|------|---|---|
| Ka11 | 0 | 0 | 1 |
| 0 | Ka22 | 0 | |
| 0 | 0 | 0 | |

Figure 3.22. Maxwell strains applied *External Strain*.

CHAPTER 4

4. RESULTS AND DISCUSSION

In this chapter is presented the main simulations and the respective results of the models separately. The implementation in COMSOL was done by two different types of calibration: theoretical and experimental.

First, is presented the theoretical evolution of the advancement of the reaction in a parametric study, comparing with the results shown by Morenon (2017).

The second part is dedicated to present the results of the creep model. First is presented the theoretical behavior of a concrete specimen subjected to a loading, followed by unloading, compared to the theoretical behavior shown by Mehta & Monteiro (2014) – see Figure 2.26. Next, the creep model was compared to the numerical benchmark shown by Sellier *et al.* (2016), which is focused in the comparison with experimental data found in the literature. An advantage of this procedure is the fact that the parameters were already calibrated by the developer of the model.

For the sake of simplicity, the chemical model was evaluated through simulations in a 0-D framework, and for the creep model, the simulations were done in a 2-D framework.

4.1 RESULTS OF THE CHEMICAL MODEL

In order to evaluate the implementation of the chemical model in COMSOL Multiphysics®, it was analyzed the evolution of the advancement of the reaction (A^{asr}), the main vector in the chemical model to produce a volume of gel (Morenon, 2017). It was done a parametric study regarding to the influence of the three main parameters which influences on the advancement of the reaction: (i) characteristic time (τ_{ref}^{asr}); (ii) temperature (T); (iii) saturation degree (Sr). The main material parameters are available in Table 1.

This first approach was modeled in a 0-D framework, without explicitly modeling a material such as concrete. Actually, the material is substituted by a point, and the chemical response is observed regardless of the material behavior. It was done in a way to analyze and validate the chemical model only.

In the Figure 4.1, it's presented the parametric study on the characteristic time (τ_{ref}^{asr}), which this material parameter was set in 50, 100, 150 and 200 days. The saturation degree was set in 100% and the temperature was set in 38° C. The evolution of A^{asr} is in very good agreement with the results shown by Morenon (2017).

In the Figure 4.2, it's presented the parametric study on the temperature (T), which this environmental parameter was set in 10, 20, 30 and 40° C. The saturation degree was set in 100% and the characteristic time was set in 50 days. The evolution of A^{asr} is in very good agreement with the results shown by Morenon (2017).

In the Figure 4.3, it's presented the parametric study on the saturation degree (Sr), which this environmental parameter was set in 25, 50, 75 and 100%. The temperature was set in 38° C and the characteristic time was set in 50 days. The evolution of A^{asr} is slower than shown by Morenon (2017). This discrepancy can be due to an alteration of the parameters presented by Morenon, because the curves for the same parameters ($Sr = 100\%$, $T = 38^\circ \text{C}$, $\tau_{ref}^{asr} = 50 \text{ days}$) don't match, as seen in Figure 4.4.

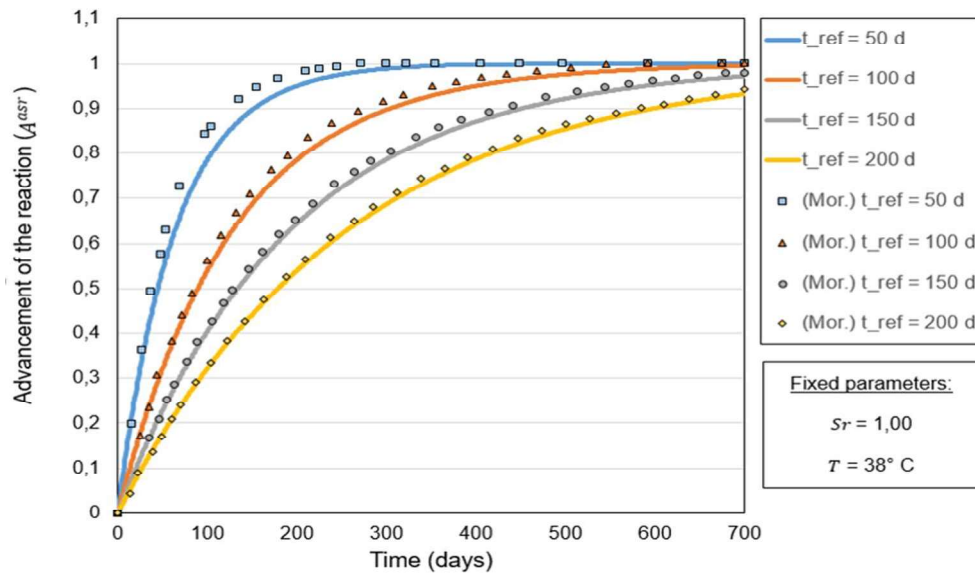


Figure 4.1. Effects of the characteristic time over the advancement of the reaction – comparison with the results shown by Morenon (2017).

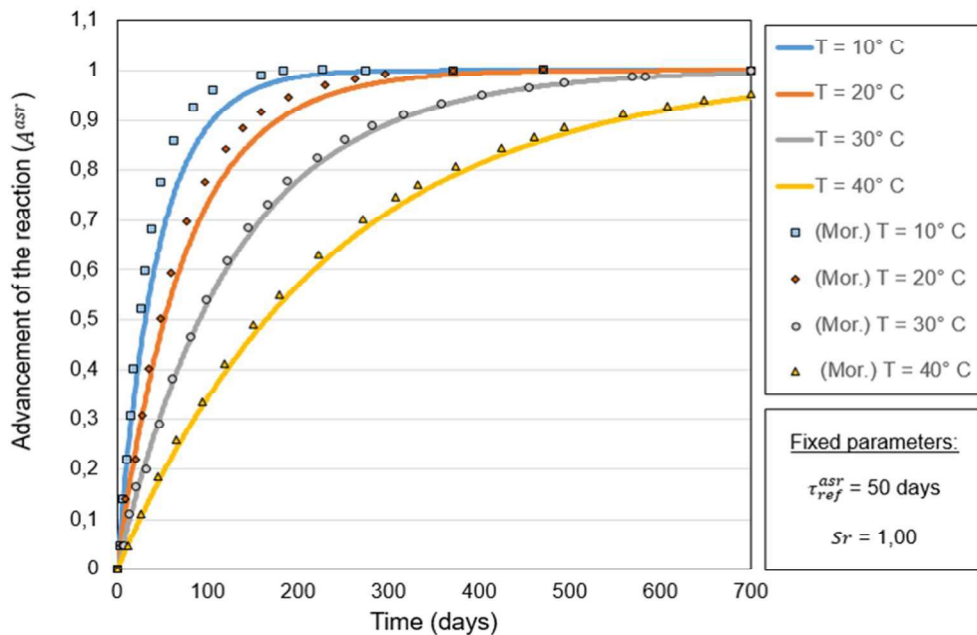


Figure 4.2. Effects of the temperature over the advancement of the reaction – comparison with the results shown by Morenon (2017).

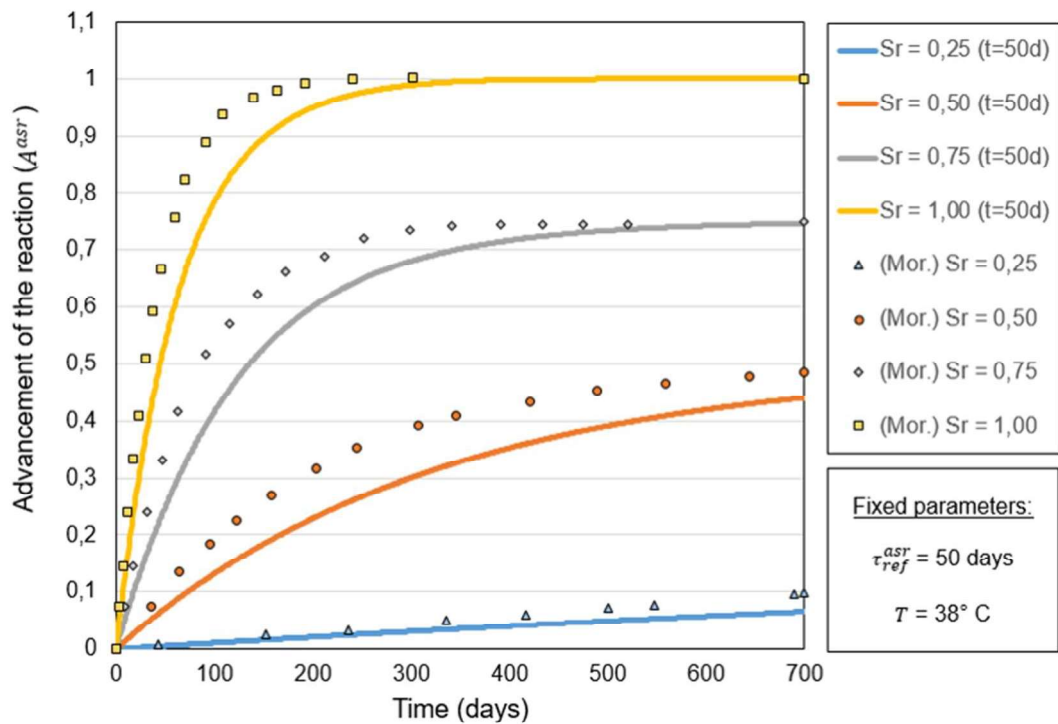


Figure 4.3. Effects of the saturation degree over the advancement of the reaction – comparison with the results shown by Morenon (2017).

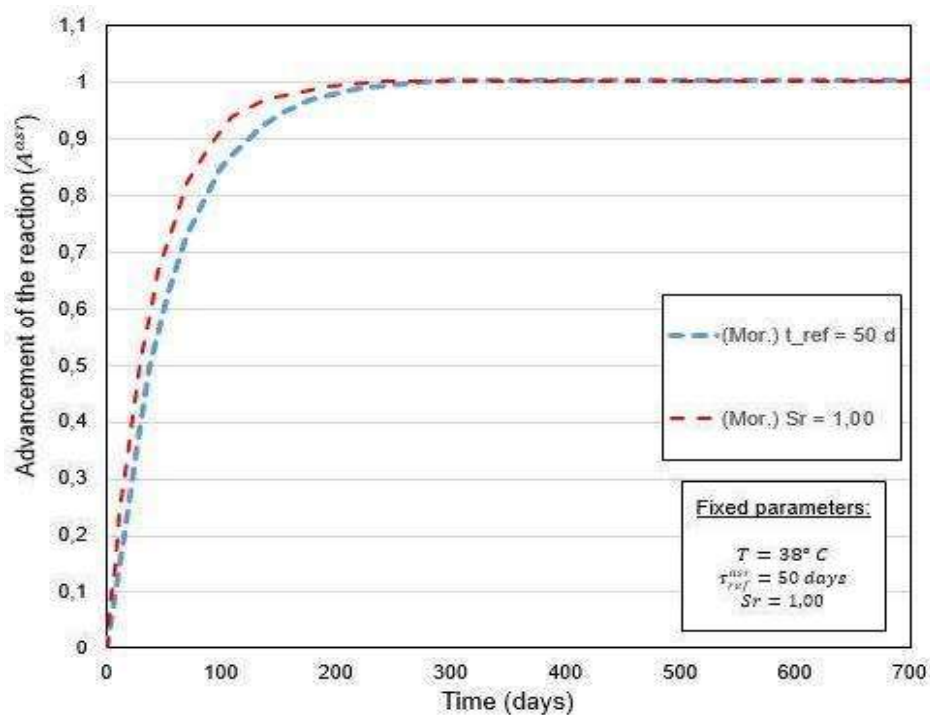


Figure 4.4. Difference of the evolution of the advancement of the reaction for the same main parameters, shown by Morenon (2017).

4.2 RESULTS OF THE CREEP MODEL

In order to evaluate the implementation of the creep model in COMSOL Multiphysics®, it was necessary to simulate the creep tests performed by Kim *et al.* (2005) and Ladaoui *et al.* (2013). Sellier *et al.* (2013) calibrated the main material parameters and compared the results of their model with the experimental data, and the results presented were in very good agreement.

Multiaxial creep test:

The tests performed by Kim *et al.* (2005) consist of multiaxial creep tests of 27 cubic concrete specimens (200mm x 200mm x 200mm) with different strengths (26, 44 and 54 MPa), and the creep strains were measured in three principal directions. The tests were divided in uniaxial compression, biaxial compression and triaxial compression. For the sake of simplicity, the numerical simulation was performed only for uniaxial and biaxial compression, as the simulation was done in a 2-D framework.

The geometry and boundary conditions of the simulation are presented in Figure 4.5, for both uniaxial (Figure 4.5 b) and biaxial compression (Figure 4.5 c). The test was performed for three different types of concrete (C1, C2 and C3) which had different material parameters. The loading scenarios varied for each type of concrete and also for uniaxial (U1 and U2) and biaxial compression (B1, B2 and B3). Next, on Table 5, it's presented the loading configuration for each scenario and type of concrete.

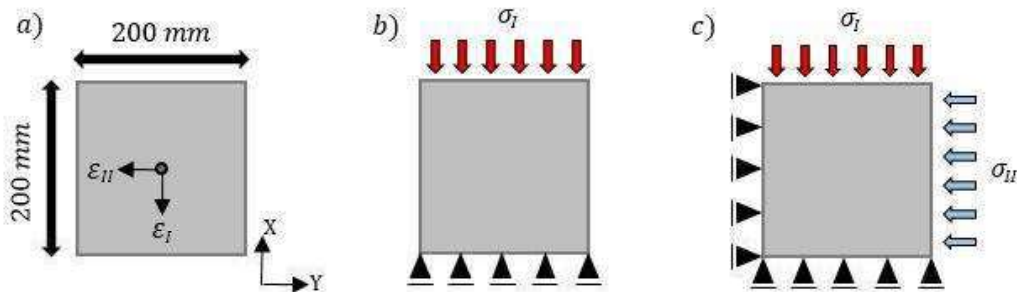


Figure 4.5. (a) Geometry of the problem; (b) Boundary conditions for uniaxial compression; (c) Boundary conditions for biaxial compression.

Table 5: Loading scenarios for the multiaxial creep tests by Kim *et al.* (2005).

| Concrete Type | Uniaxial Compression | | Biaxial Compression | | |
|---------------|----------------------|--------------------|---|---|--|
| | U1 (MPa) | U2 (MPa) | B1 (MPa) | B2 (MPa) | B3 (MPa) |
| C1 | $\sigma_I = 4,9$ | $\sigma_I = 9,8$ | $\sigma_I = 4,9$ $\sigma_{II} = 0,98$ | $\sigma_I = 4,9$ $\sigma_{II} = 1,96$ | $\sigma_I = 9,8$ $\sigma_{II} = 1,96$ |
| C2 | $\sigma_I = 7,35$ | $\sigma_I = 9,8$ | $\sigma_I = 7,35$ $\sigma_{II} = 1,47$ | $\sigma_I = 7,35$ $\sigma_{II} = 2,94$ | $\sigma_I = 9,8$ $\sigma_{II} = 2,94$ |
| C3 | $\sigma_I = 9,8$ | $\sigma_I = 12,25$ | $\sigma_I = 9,8$ $\sigma_{II} = 1,96$ | $\sigma_I = 9,8$ $\sigma_{II} = 3,92$ | $\sigma_I = 12,25$ $\sigma_{II} = 3,92$ |

Next, on Table 6, there is a resume of the calibrated parameters used to simulate the creep tests performed by Kim et al. (2005).

Table 6: Main material parameters to simulate the multiaxial creep tests performed by Kim et al. (2005).

| Concrete Type | Parameter | Value | Unity |
|---------------|-----------------------|--------------|-------|
| C1 | Rc | 26 | MPa |
| | E | 24.010 | MPa |
| | ν | 0,18 | - |
| | τ_{ref}^K | 2 | days |
| | τ_{ref}^M | 15 | days |
| | ε_{ref}^M | $10.e^{-5}$ | - |
| | ψ^K | 4 | - |
| | ε_{ref}^E | $211.e^{-6}$ | - |
| C2 | Rc | 44,1 | MPa |
| | E | 29.841 | MPa |
| | ν | 0,18 | - |
| | τ_{ref}^K | 2 | days |
| | τ_{ref}^M | 15 | days |
| | ε_{ref}^M | $9.e^{-5}$ | - |
| | ψ^K | 4 | - |
| | ε_{ref}^E | $246.e^{-6}$ | - |
| C3 | Rc | 54,3 | MPa |
| | E | 34.006 | MPa |
| | ν | 0,18 | - |
| | τ_{ref}^K | 3 | days |
| | τ_{ref}^M | 20 | days |
| | ε_{ref}^M | $7,5.e^{-5}$ | - |
| | ψ^K | 4 | - |
| | ε_{ref}^E | $288.e^{-6}$ | - |

The results for the uniaxial compression for concrete C1, C2 and C3 are presented in the Figure 4.6, Figure 4.7 and Figure 4.8, respectively. The maximum discrepancy between the simulation and experimental results is approximately 10%, which is considered satisfactory for numerical simulation of experimental benchmark.

The results for the biaxial compression for concrete C1, C2 and C3 are presented in the Figure 4.9, Figure 4.10 and Figure 4.11, respectively. The maximum discrepancy was approximately 13%, very close to the one found in uniaxial compression comparison.

The discrepancy observed on the results of the strain ε_I – parallel to the load σ_I – was higher than observed on the strain ε_{II} – parallel to the load σ_{II} . It can be inferred that higher loads induces to higher discrepancy, as σ_I was 2.5 and 5 times higher than σ_{II} . Also it can be seen that the discrepancy is higher for longer periods of time, as the creep strain increases with time.

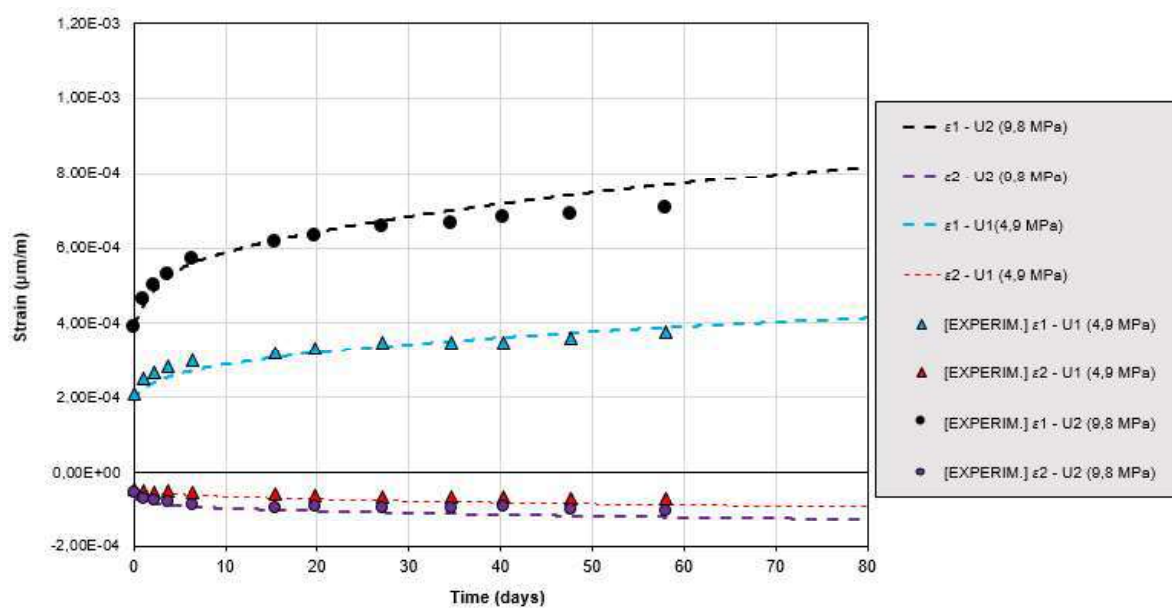


Figure 4.6. Evolution of the total strain for concrete type C1 under uniaxial compression.

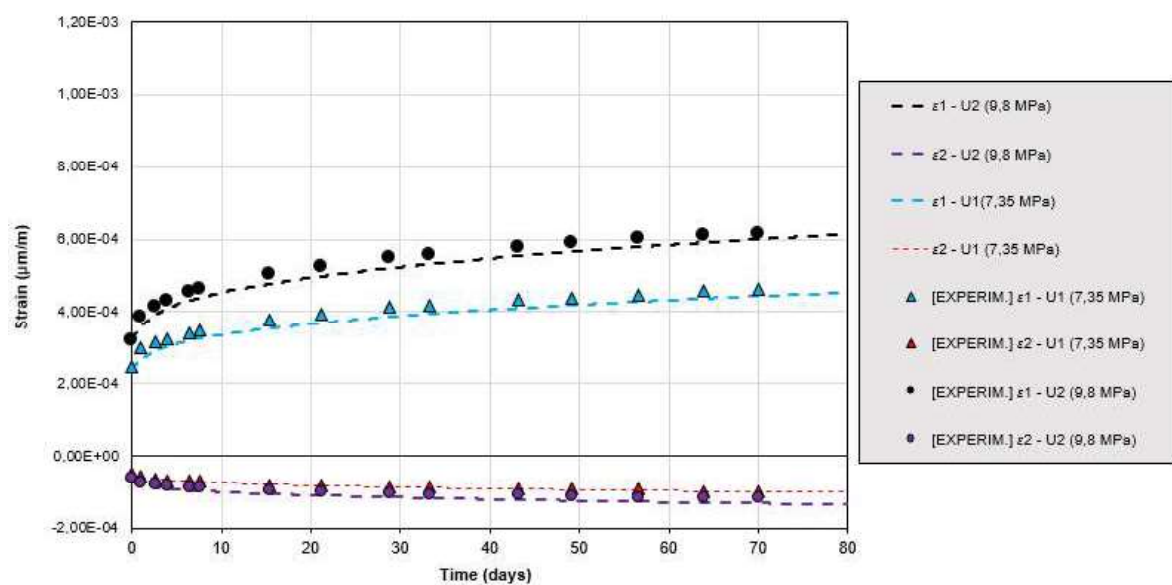


Figure 4.7. Evolution of the total strain for concrete type C2 under uniaxial compression.

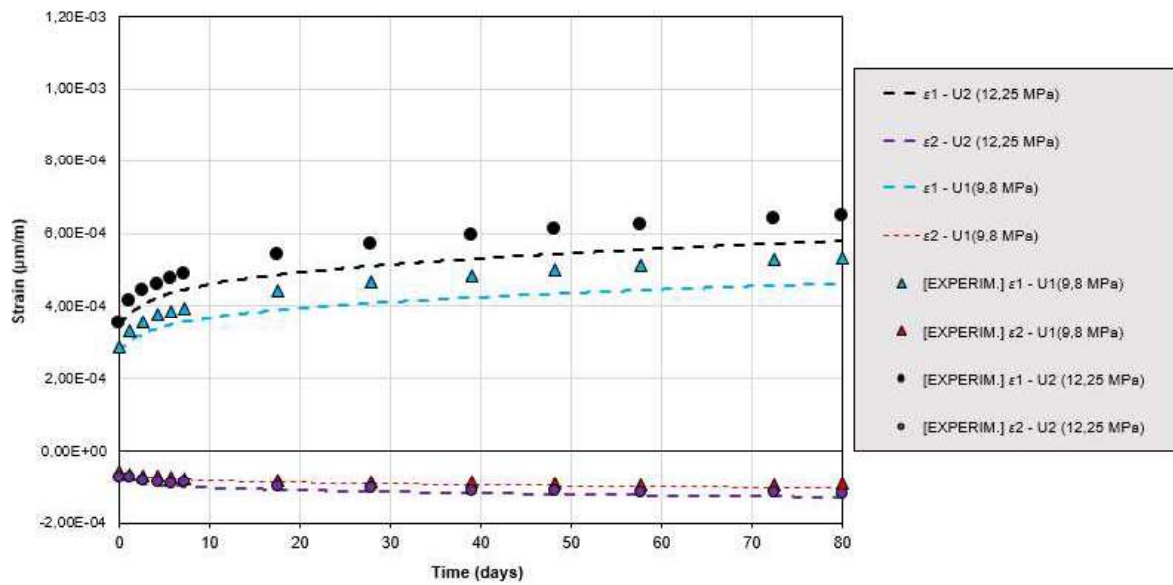


Figure 4.8. Evolution of the total strain for concrete type C3 under uniaxial compression.

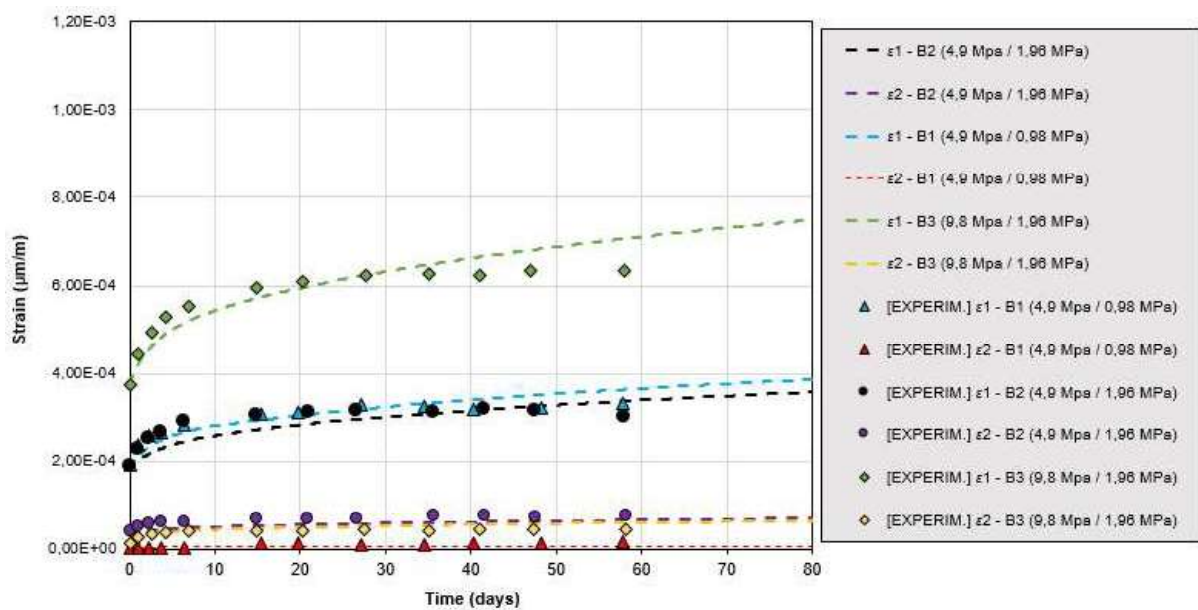


Figure 4.9. Evolution of the total strain for concrete type C1 under biaxial compression.

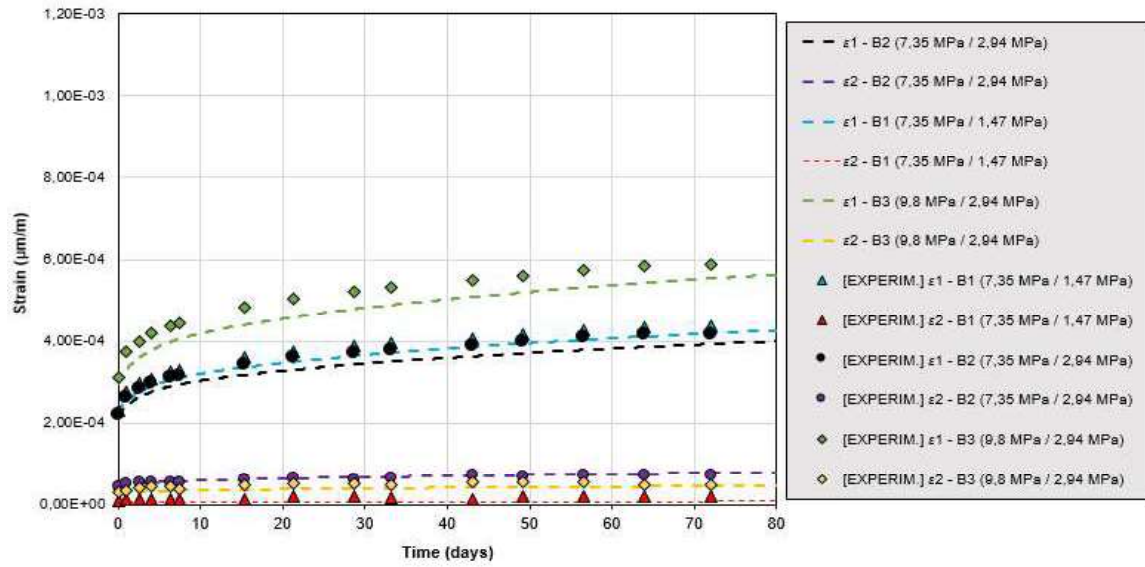


Figure 4.10. Evolution of the total strain for concrete type C2 under biaxial compression.

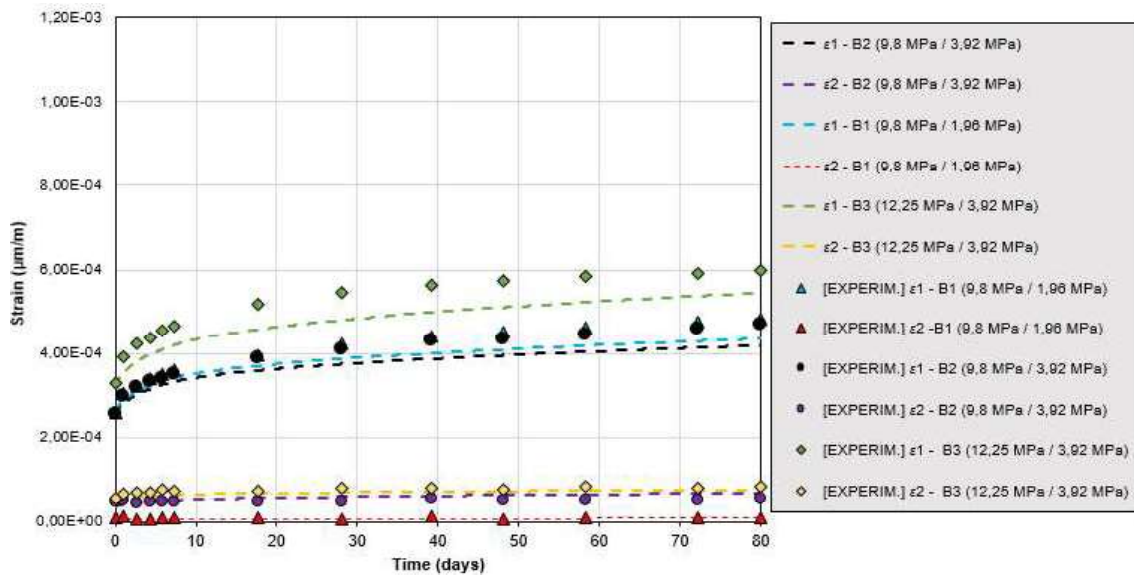


Figure 4.11. Evolution of the total strain for concrete type C3 under biaxial compression.

Uniaxial creep test in different temperatures conditions:

The tests performed by Ladaoui *et al.* (2013) consist in a uniaxial creep test in different temperature conditions of 24 cylindrical specimens (220mm x 110mm) of high performance concrete (HPC), with 86 MPa of compressive strength and 45 MPa of Young's modulus. The creep strains were measured in the principal direction (direction of the loading). After one year of curing, an uniaxial compression stress of 26 MPa was applied for specimens under 20, 50 and 80°C. For the sake of simplicity, the numerical simulation was performed only for uniaxial and biaxial compression, because it was done in a 2D-axisymetric framework. The geometry and boundary conditions of the simulation are presented in Figure 4.12.

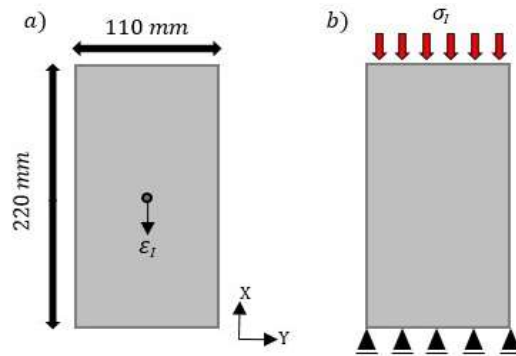


Figure 4.12. (a) Geometry of the problem; (b) Boundary conditions for uniaxial compression.

Next, on Table 7, there is a resume of the calibrated parameters used to simulate the creep tests performed by Ladaoui et al. (2013).

Table 7: Main material parameters to simulate the creep tests performed by Ladaoui et al. (2013).

| Parameter | Value | Unity |
|-----------------------|---------------------|-------|
| R_c | 86 | MPa |
| E (T=20°C) | 34.800 | MPa |
| E (T=50°C) | 41.600 | MPa |
| E (T=80°C) | 45.450 | MPa |
| ν | 0,28 | - |
| E_p^a | 23.700 | J/mol |
| τ_{ref}^K | 5 | days |
| τ_{ref}^M | 10 | days |
| ε_{ref}^M | $5,5 \cdot 10^{-5}$ | - |
| ψ^K | 5 | - |
| ε_{ref}^E | $590 \cdot 10^{-6}$ | - |

The influence of the temperature in the creep tests can be visualized through the results of the simulation for the temperatures of 20, 50 and 80 °C. The results are presented in Figure 4.13. The experimental results for the temperature of 80°C after 56 days were not given due to a malfunction in the strain measurer, because the high temperature condition lead to a failure on the electric parts of the measurer.

The curves for 20° e 50°C presents higher discrepancy for longer periods of time, as expected regarding the results for multiaxial creep test. The maximum discrepancy was approximately 6% which can be considered in a very good agreement with the experimental benchmark.

In the other hand, the curves for 80°C already presents discrepancy of approximately 5% already at the early days (56 days). If the experimental results were available, it would be possible to check if the maximum discrepancy overtime would be much higher than the ones calculated for the curves of the other temperature conditions.

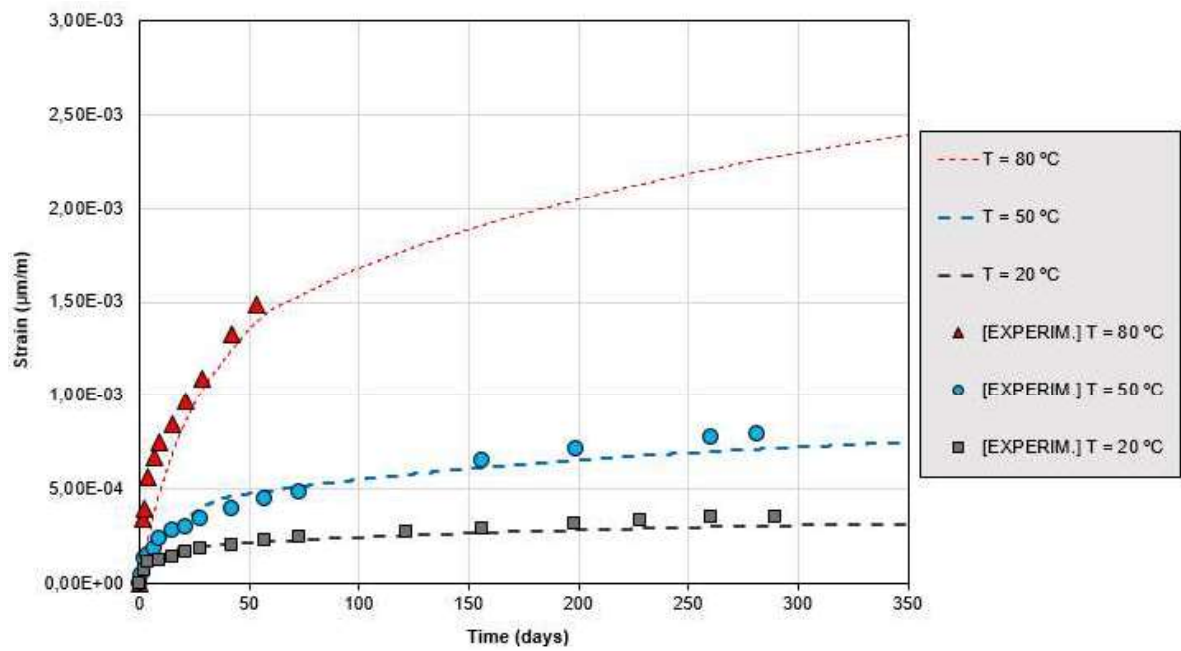


Figure 4.13. Evolution of the total strain for the different temperatures in the creep test performed by Ladaoui *et al.* (2013).

CHAPTER 5

5. CONCLUSIONS AND SUGGESTION FOR FUTURE WORKS

In this chapter is discussed the main conclusions about the results presented on the previous chapter, and also about the limitations of the work. At the end, some suggestions and perspectives are presented in order to serve as a guideline for the next works in this same subject.

Analyzing the results, both chemical and creep models seems to work properly well, with low error values for numerical simulations. The method to compare the simulation results with the experimental benchmark - proposed by the developers of the models – guarantees that the implementation of such models in COMSOL Multiphysics® was a success.

Although such models require a huge number of material parameters that must be calibrated by the user. The values of those parameters can be found in the papers published by the developers of the models, but to implement in a real concrete structure assessment, there must be done a careful investigation over the structure. If those models are used still in the design phase of such structures, a parametric study is necessary to verify the variation in the mechanical response due to the variation of such material parameters.

First, as the reader was capable to observe, the chemical and creep model were not coupled. The attempts to do this result in numerical instability regarding time. The author was not capable to verify the reason behind it, neither identify which condition must be satisfied in order to do this.

Secondly, the pressure of the gel was not calculated, because to do so is necessary the creep strains and also the diffuse cracking (micro-plastic cracks) in order to generate this intrapore pressure.

Thirdly, the shrinkage model was not resulting in any significant strain, therefore it was not even compared to any experimental benchmark. Probably is due to the increment on the effective stress, which formulation in COMSOL Multiphysics® seems to be different from the formulation proposed by Sellier *et al.* (2016). More tests must be done to look carefully how to reproduce shrinkage in concrete materials.

Finally, to fully reproduce a concrete structure subjected to AAR, is necessary to implement a coupled chemo-creep-damage model. The author tried to use the isotropic damage model proposed by Gasch & Ansell (2016), which was already developed in COMSOL Multiphysics® (*Damage* subnode for elastic materials). The creep model somehow doesn't converge with the damage model, mostly because numerical instability over time due to plastic strains interacting with creep strains. A lot of effort was put on the resolution of this problem, but no significant results were achieved.

Therefore, the next works in this subject must have as the principal aim the coupling of such models, comparing with numerical and experimental benchmark, firstly in a 2D approach for the sake of simplicity, and once the numerical stability is reached, the models must be tested in a 3D framework. The first approach on more complex

simulations regarding AAR-affected concrete structures must verify the experimental and numerical benchmark, found in the works of Morenon (2017) and Sellier (2018).

The author of this work is currently working on the execution of subnodes for COMSOL, using the Model Builder tool in order to pre-set the equations and set of parameters, making them available for all users in an easy way, regarding all the careful measures which are necessary to use such models.

REFERENCES

_____. **NBR 15577-1: Agregados – Reatividade álcali-agregado – Parte 1: Guia para avaliação da reatividade potencial e medidas preventivas para uso de agregados em concreto.** São Paulo, 2008.

_____. **NBR 15577-4: Agregados – Reatividade álcali-agregado – Parte 4: Determinação da expansão em barras de argamassa pelo método acelerado.** São Paulo, 2008.

Abdellatef, M.; Alnaggar, M.; Boumakis, G.; Cusatis, G.; Di-Luzio, G.; Wendner, R. **Lattice Discrete Particle Modeling for coupled concrete creep and shrinkage using Solidification Microprestress Theory.** *CONCREEP 10: Mechanics and Physics of Creep, Shrinkage, and Durability of Concrete and Concrete Structures.* Vienna, Austria: p. 21-23, 2015.

ACI 209. **Guide for Modeling and Calculating Shrinkage and Creep in Hardened Concrete.** Farmington Hills, USA: *American Concrete Institute (ACI)*, 2008.

Alcantara Jr., N. P.; Gonçalves Jr., L. **Simulation of an ECT Sensor to Inspect the Reinforcement of Concrete Structures.** *Proceedings of the 2015 COMSOL Conference.* Curitiba, Brazil: p. 6, 2015.

Andrade, T. **Histórico de casos de RAA ocorridos recentemente em fundações de edifícios na região metropolitana de Recife.** *2º Simpósio sobre Reação Álcali-Agregado em Estruturas de Concreto.* Anais... Rio de Janeiro: IBRACON, p.1-16, 2006.

Andrade, T.; Silva, J. J. R.; Hasparyk, N.; Silva, C. M. **Investigação do potencial de reatividade para o desenvolvimento de RAA dos agregados miúdos e graúdos comercializados na região metropolitana do Recife.** *2º Simpósio sobre Reação Álcali-Agregado em Estruturas de Concreto.* Anais... Rio de Janeiro: IBRACON, p.1-16, 2006b.

Andrade, T.; Silva, J. J. R.; Almeida, R.; Patrocínio, J.; Kihara, Y.; Pecchio, M. **Diagnóstico de reação álcali-agregado em blocos de fundação de um edifício público situado na cidade de Recife/PE.** *2º Simpósio sobre Reação Álcali-Agregado em Estruturas de Concreto.* Anais... Rio de Janeiro: IBRACON, p.1-15, 2006a.

Andriolo, F. R. **AAR dams affected in Brazil report on the current situation.** *Proceedings of the 11th International Conference on Alkali-Aggregate Reaction in Concrete.* Quebec: p.1243-1252, 2000.

Ayub, T.; Khan, S. U.; Memon, F. A. **Mechanical Characteristics of Hardened Concrete with Different Mineral Admixtures: A Review.** *The Scientific World Journal*, v. 2014, p. 1-15, 2014.

Balabuch, T. J. R. **Análise numérica das deformações do concreto sujeito à reação álcali-agregado considerando os efeitos de retração e fluência.** *Master Thesis – Escola de Engenharia de São Carlos, Universidade de São Paulo (USP).* Brasil: p. 114, 2018.

Baroghel-Bouny, V.; Mainguy, M.; Lassabatere, T.; Coussy, O. **Characterization and identification of equilibrium and transfer moisture properties for ordinary and high-performance cementitious materials.** *Cement and Concrete Research*, v. 29, p. 1225-1238, 1999.

Bazănt, Z. P.; Baweja, S. **Creep and Shrinkage Prediction Model for Analysis and Design of Concrete Structures: Model B3.** *ACI Adam Neville Symposium: Creep and Shrinkage – Structural Design Effects*. Farmington Hills, USA: American Concrete Institute (ACI), p. 1-83, 2000.

Bazănt, Z. P.; Panula, L. **Practical prediction of time-dependent deformations of concrete – Part II: Basic creep.** *Matériaux et Construction*, v. 11, p. 317-328, 1978.

Bazănt, Z. P.; RILEM. **RILEM draft recommendation: TC-242-MDC multi-decade creep and shrinkage of concrete: material model and structural analysis Model B4 for creep, drying shrinkage and autogenous shrinkage or normal and high-strength concretes with multi-decade applicability.** *Materials and Structures*, v. 48, p. 753-770, 2015.

Bazănt, Z. P.; Steffens, A. **Mathematical model for kinetics of alkali-silica reaction in concrete.** *Cement and Concrete Research*, 30(3), p.419-428, 2000.

Bazănt, Z. P.; Zi, G.; Meyer, C. **Fracture mechanics of ASR in concretes with waste glass particles of different sizes.** *Journal of Engineering Mechanics*, 126(3), p.226-232, 2000.

Ben Haha, M.; Gallucci, E.; Guidoum, A.; Scrivener, K. L. **Relation of expansion due to alkali silica reaction to the degree of reaction measured by SEM image analysis.** *Cement and Concrete Research*, 37(8), p.1206-1214, 2007.

Berra, M.; Mangialardi, T.; Paolini, A. E. **Alkali-silica reactivity criteria for concrete aggregates.** *Materials and Structures*, v. 38, p. 373-380, 2005.

Bérubé, M.-A.; Duchesne, J.; Dorion, J. F.; Rivest, M. **Laboratory assessment of alkali contribution by aggregates to concrete and application to concrete structures affected by alkali-silica reactivity.** *Cement and Concrete Research*, v. 32, p. 1215-1227, 2002.

Biot, M. A. **General Theory of Three-Dimensional Consolidation.** *Journal of Applied Physics*, v. 12, p. 155-164, 1941.

Bournazel, J.P. **Modelling of the development of microcracks due to alkali-aggregate reaction.** *Engineering and Transport Properties of the Interfacial Transition Zone in Cementitious Composites*. France: RILEM 20th Report, 1999.

Brito Júnior, A.; Ferro, I. P. **Reação Álcali-Agregado: Um breve estudo da ocorrência nos blocos da Ponte Paulo Guerra - Recife/PE.** *Congresso Brasileiro de Patologia das Construções – CBPAT. Anais...* Belém: ISSN. p. 2448-1459, 2016.

Broekmans, M. A. T. M. **The alkali-silica reaction: mineralogical and geochemical aspects of some Dutch concretes and Norwegian mylonites.** PhD Thesis – University of Utrecht. Netherlands: p. 144, 2002.

Capra, B. Bournazel, J. P. **Modeling of Induced Mechanical Effects of Alkali-Aggregate Reactions.** *Cement and Concrete Research*, 28(2), p.251-260, 1998.

- Capra, B. **Modelisation des effets mécaniques induits par les reaction alkali-granulats**. PhD thesis – ENS Cachan. France: p. 194, 1997.
- Capra, B.; Sellier, A. **Orthotropic modelling of alkali-aggregate reaction in concrete structures: Numerical simulations**. *Mechanics of Materials*, 35(8), p.817-830, 2003.
- Carasek, H.; Cascudo, O.; Caetano, G. **Contribuição à previsão de danos para estruturas de concreto atacadas pela reação álcali-sílica**. Brasil: *Concreto e Construções*, v. 44, n. 83, p.30-38, 2016.
- Charpin, L.; Ehrlacher, A. **Microporomechanics study of anisotropy of ASR under loading**. *Cement and Concrete Research*, v. 63, p. 143-157, 2014.
- Collins, R. J.; Bareham, P. D. **Alkali-silica reaction: suppression of expansion using porous aggregate**. *Cement and Concrete Research*, v. 17, n. 1, p. 89-96, 1987.
- Comby-Peyrot, I; Bernard, F.; Bouchard, P. O.; Bay, F.; Garcia-Diaz, E. **Development and validation of a 3D computational tool to describe concrete behavior at mesoscale. Application to the alkali-silica reaction**. *Computational Materials Science*, 46(4). p.1163-1177, 2009.
- Comi, C.; Fedele, R.; Perego, U. **A chemo-thermo-damage model for the analysis of concrete dams affected by alkali-silica reaction**. *Mechanics of Materials*, v. 41, p. 210-230, 2009.
- Comi, C.; Perego, U. **Anisotropic Damage Model for Concrete Affected by Alkali-Aggregate Reaction**. *International Journal of Damage Mechanics*, v. 20, n. 4, p. 598-617, 2011.
- Coussy, O. **Mécanique des milieu poreux**. Editions Technip, 1991.
- De Melo, S. K. **Estudo da formação da etringita tardia em concreto por calor de hidratação do cimento**. Goiânia: Thesis (MSc in Civil Engineering) – Universidade Federal de Goiás, p.286, 2010.
- Dent Glasser, L. S. **Osmotic pressure and the swelling of gels**. *Cement and Concrete Institute*, 9(4), p.515-517, 1979.
- Dent Glasser, L. S.; Kataoka, N. N. K. **On the role of calcium in the alkali-aggregate reaction**. *Cement and Concrete Research*, 12(3), p.321-331, 1982.
- Dent Glasser, L. S.; Kataoka, N. N. K. **The chemistry of alkali-aggregate reaction**. *Cement and Concrete Research*, 1981, 11(1). p.1-9, 1981.
- Deschenes, D. J. **ASR/DEF-Damaged bent caps: shear tests and field implications**. *Master of Science Engineering – The University of Texas*. Austin: p. 295, 2009.
- Diamond, S. **Alkali Aggregate Reactions in Concrete – Pore Solution Effects**. In: *Proceedings of the 6th International Conferente of Alkalis in Concrete*. Copenhagen: p. 155, 1983.
- Diamond, S. **ASR - another look at mechanisms**. In: *Proceedings of the 8th International Conference on Alkali-Aggregate Reaction*. Kyoto, Japan: p. 83-94, 1989.
- Diamond, S.; Barneyback Jr., R. S.; Struble, L. J. **On the physics and chemistry of alkali-silica reactions**. *Purdue University – School of Civil Engineering*. Indiana, USA: p. 10, 1981.

Dormieux, L.; Lemarchand, E.; Kondo, D.; Fairbairn, E. **Elements of poro-mechanics applied to concrete**. *Materials and Structures*, v. 37, p. 31-42, 2004.

Dron, R.; Brivot, F. **Thermodynamic and kinetic approach to the alkali-silica reaction – Part 2: Experiment**. *Cement and Concrete Research*, 23(1), p.93-103, 1993.

Dunant, C. F.; Scrivener, K. L. **Micro-mechanical modelling of alkali-silica-reaction-induced degradation using the AMIE framework**. *Cement and Concrete Research*, 40(4), p.517-525, 2010.

Durand, B. Roux, R. Houde, J. Blanchette, A. **Free expansions and stresses in concrete related to alkali aggregate reaction**. *Proceedings of 9th ICAAR*. London: p.298-310, 1992.

Dyer, T. **A Durabilidade do Concreto**. Rio de Janeiro, Brazil: Editora Ciência Moderna, 2015.

Esposito, R.; Hendriks, M. A. **A multiscale micromechanical approach to model the deteriorating impact of alkali-silica reaction on concrete**. *Cement and Concrete Composites*, v. 70, p. 139-152, 2016.

Esposito, R.; Hendriks, M. A. **Literature review of modelling approaches for ASR in concrete: a new perspective**. *European Journal of Environmental and Civil Engineering*, 23:11, p. 1311-1331, 2019.

FIB. **Model Code 2010**. 65th Ed. Lausanne, Switzerland: *International Federation for Structural Concrete (FIB)*, v. 1, 2012.

Furusawa, Y. Ohga, H. Uomoto, T. **An analytical study concerning prediction of concrete expansion due to alkali-silica reaction**. *American Concrete Institute*, SP 145, p.757-780, 1994.

Gameleira, C. M. T. M.; Nunes, V. Q. G.; Régis, P. A.; Oliveira, R. A. **Structural Analysis of Pile Caps, Used in Bridge Foundation, Subject to AAR**. *Maintenance, Monitoring, Safety, Risk and Resilience of Bridges and Bridge Networks*. Florida, USA: CRC Press, p. 616, 2016.

Gao, X. X.; Multon, S.; Cyr, M.; Sellier, A. **Alkali-silica reaction (ASR) expansion: Pessimism effect versus scale effect**. *Cement and Concrete Research*, v. 44, p. 25-33, 2013.

Garcia-Diaz, E.; Riche, J.; Bulteel, D.; Vernet, C. **Mechanism of damage for the alkali-silica reaction**. *Cement and Concrete Research*, 36(2), p.395-400, 2006.

Gardner, N. J. **Comparison of prediction provisions for drying shrinkage and creep of normal-strength concretes**. *Canadian Journal of Civil Engineering*, v. 31, n. 5, p. 767-775, 2004.

Gardner, N. J.; Lockman, M. J. **Design provisions for drying shrinkage and creep of normal-strength concrete**. *ACI Materials Journal*, v. 98, p. 159-167, 2001.

Grimal, E. **Caractérisation des effets du gonflement provoqué par la réaction alcali-silice sur le comportement mécanique d'une structure en béton**. *PhD Thesis – Université Paul Sabatier Toulouse*. France, 2007.

Grimal, E.; Morenon, P.; Sellier, A.; Multon, S.; Bourdarot, E. **AAR and DEF Structural Effects Modelling**. *Swelling Concrete in Dams and Hydraulic Structures: DSC 2017*. 1st Edition published by ISTE Ltd and John Wiley & Sons, 2017.

Grimal, E.; Sellier, A.; Le Pape, Y.; Bourdarot, E. **Creep, Shrinkage, and Anisotropic Damage in Alkali-Aggregate Reaction Swelling Mechanism – Part I: A Constitutive Model.** *ACI Materials Journal*. Toulouse: p.227-235, 2007.

Hansen, W. C. **Studies relating to the mechanism by which the alkali-aggregate reaction produces expansion in concrete.** *Journal of the American Concrete Institute*, v. 15, p. 213-227, 1944.

Hasparyk, N. P. **Reação álcali-agregado no concreto.** In: ISAIA, C. G. *Concreto: ciência e tecnologia*. São Paulo: IBRACON, Cap. 27, p.933-1001, 2011.

Hawlett, P. **Lea's chemistry of cement and concrete.** *Butterworth-Heinemann: 4th edition*, p. 1092, 2003.

Heinz, D.; Kalde, M.; Ludwig, U.; Ruediger, I. **Present state of investigation on damaging late ettringite formation (DLEF) in mortars and concretes.** *Ettringite: the sometimes host of destruction*. Michigan, USA: American Concrete Institute, p.1-13, 1999.

Hobbs, D. W. **Alkali-silica reaction in concrete.** Londres: Thomas Telford, p. 183, 1988.

Hobbs, D.W. **Expansion and cracking in concrete associated with delayed Ettringite formation.** *Ettringite: the sometimes host of destruction*. Michigan, USA: American Concrete Institute, p.159-182, 1999.

Ichikawa, T.; Miura, M. **Modified model of alkali-silica reaction.** *Cement and Concrete Research*, 37(9), p.1291-1297, 2007.

Idorn G. M. **A discussion of the paper “Mathematical model for kinetics of alkali-silica reaction in concrete” by Zdenek P. Bazant and Alexander Steffens.** *Cement and Concrete Research*, 31(7). p.1109-1110, 2001.

Jensen, V. **Alkali-silica reaction damage to Elgeseter Bridge, Trondheim, Norway: a review of construction, research and repair up to 2003.** *Materials Characterization*, v. 53, n. 2-4, p. 155-1770, 2004.

Joshaghani, A.; Balapour, M.; Ramezaniapour, A. **Effect of controlled environmental conditions on mechanical, microstructural and durability properties of cement mortar.** *Construction and Building Materials*, v. 164, p. 134-139, 2018.

JSCE. **Standard Specifications for Concrete Structures – 2007. Design.** Tokyo, Japan: *Japan Society of Civil Engineers (JSCE)*, v. 15, 2010.

Kim, S. Y.; Kim, J. K.; Kim, Y. Y.; Kwon, S. H. **Experimental studies on creep of sealed concrete under multiaxial stresses.** *Magazine of Concrete Research*, v. 57, p. 623-634, 2005.

Kuperman, S. C. **Considerações sobre fluência de concretos.** *Téchne – Revista de Tecnologia da Construção*, v. 125, p. 58-63, 2007.

Kuperman, S. C. **Curso sobre Reação Álcali-Agregado.** Recife: 2007.

Ladaoui, W.; Vidal, T.; Sellier, A.; Bourbon, X. **Analysis of interactions between damage and basic creep of HPC and HPFRC heated between 20 and 80 °C.** *Materials and Structures*, v. 46, p. 13-23, 2013.

Langer, S. A.; Fuller, E.; Carter, W. C. **OOF: An Image-Based Finite-Element Analysis of Material Microstructure**. *Computing in Science and Engineering*, v. 3, p. 15-23, 2001.

Larive, C. **Apports combinés de l'expérimentation et de la modélisation à la compréhension de l'alcali-réaction et de ses effets mécaniques**. PhD Thesis – *Ecole Nationale des Ponts et Chaussées*. Paris, France: p. 335, 1997.

Larive, C. **Combined contribution of experiments and modeling to the understanding of alkali-aggregate reaction and its mechanical consequences**. *Laboratoire Central des Ponts et Chaussées, Report OA 28*. Paris, France: 1998.

LCPC. **Recommandations pour la prevention des désordres dus à l'alcali-réaction**. 1994.

Léger, P.; Côté, P.; Tinawi, R. **Finite element analysis of concrete swelling due to alkali-aggregate reactions in dams**. *Computers & Structures*, v. 60, p. 601-611, 1996.

Lemarchand, E.; Dormieux, L.; Ulm, F.-J. **Micromechanics investigation of expansive reactions in chemoelastic concrete**. *Philosophical Transactions of the Royal Society: A Mathematical, Physical and Engineering Sciences*, v. 363 (1836):2581, 2005.

Leonhardt, F.; Mönning, E. **Construções de Concreto. Princípios Básicos do Dimensionamento de Estruturas de Concreto Armado**. 2ª ed. Rio de Janeiro: Interciência Ltda., v. I, 1977.

Lindgård, J.; Andiç-Çakir, Ö.; Fernandes, I.; Rønning, T. F.; Thomas, M. D. **Alkali-Silica Reactions (ASR): literature review on parameters influencing laboratory performance testing**. *Cement and Concrete Research*, v. 42, p. 223-243, 2012.

Lindgård, J.; Nixon, P. J.; Borchers, I.; Schouenborg, B.; Wigum, B. J.; Haugen, M.; Åkesson, U. **The EU "PARTNER" Project – European standard tests to prevent alkali reactions in aggregates: Final results and recommendations**. *Cement and Concrete Research*, v. 40, p. 611-635, 2010.

Lindgård, J.; Thomas, M. D. A.; Sellevold, E. J.; Pedersen, B.; Andiç-Çakir, Ö.; Justnes, H.; Rønning, T. F. **Alkali-silica reaction (ASR) – performance testing: Influence of specimen pre-treatment, exposure conditions and prism size on alkali leaching and prism expansion**. *Cement and Concrete Research*, v. 53, p. 68-90, 2013.

Lombardi, J.; Massard, P.; Perruchot, A. **Mesure expérimentale de la cinétique de formation d'un gel silicocalcique, produit de la réaction alcalis-silice**. *Cement and Concrete Research*, v. 27, p. 1379-1391, 1997.

Macgowan, J. K.; Vivian, H. E. **Studies in cement-aggregate reaction: Correlation between crack development and expansion of mortars**. *Australian Journal of Applied Science*, v. 3, p. 228-232, 1952.

Madureira, E. L. **Simulação Numérica do Comportamento Mecânico de Elementos de Concreto Armado Afetados pela Reação Álcali-Agregado**. Thesis (DSc in Civil Engineering) – *Universidade Federal de Pernambuco*. Recife: p. 219, 2007.

Martin, R. P.; Bazin, C.; Toutlemonde, F. **Alkali aggregate reaction and delayed ettringite formation: common features and differences**. *14th International Conference on Alkali-Aggregate Reaction (ICAAR14)*. Austin, USA: p. 10, 2012.

Martin, R. P.; Metalssi, O. O.; Toutlemonde, F. **Modelling of concrete structures affected by internal swelling reactions: couplings between transfer properties, alkali leaching and expansion.** *2nd International conference on microstructure related durability of cementitious.* Amsterdam, Netherlands: p. 8, 2012.

Mazloom, M.; Ramezani pour, A. A.; Brooks, J. J. **Effect of silica fume on mechanical properties of high-strength concrete.** *Cement and Concrete Composites*, v. 26, n. 4, p. 347-357, 2004.

Mehta, P. K.; Monteiro, P. J. M. **Concreto: estrutura, propriedades e materiais.** 2^a ed. Reviewers: Nicole P. Hasparyk, Paulo Helene & Vladimir A. Paulon, Translate of the 4th edition in English with the title - *Concrete: Microstructure, Properties and Materials.* São Paulo: IBRACON, 2014.

Morenon, P. **Modélisation des réactions de gonflement interne des bétons avec prise en compte des couplages poro-mécaniques et chimiques.** *PhD Thesis – Université Toulouse 3 Paul Sabatier.* France: p. 272, 2017.

Morenon, P.; Multon, S.; Sellier, A.; Grimal, E.; Hamon, F.; Kolmayer, P. **Flexural performance of reinforced concrete beams damaged by Alkali-Silica Reaction.** *Cement and Concrete Composites*, 104(3), p.103412, 2019.

Multon, S. **Évaluation expérimentale et théorique des effets mécaniques de l'alcali-réaction sur des structures modèles.** *PhD Thesis – Université de Marne-la-Vallée.* France: p. 423, 2003.

Multon, S.; Cyr, M.; Sellier, A.; Diederich, P.; Petit, L. **Effects of aggregate size and alkali content on ASR expansion.** *Cement and Concrete Research*, v. 38, p. 350-359, 2010.

Multon, S.; Cyr, M.; Sellier, A.; Leklou, N.; Petit, L. **Coupled effects of aggregate size and alkali content on ASR expansion.** *Cement and Concrete Research*, v. 40, p. 508-516, 2008.

Multon, S.; Seignol, J.-F.; Bourdarot, E.; Jeanpierre, A.; Toutlemonde, F. **Effets structuraux de l'alcali-réaction : Apports d'une expérimentation sur éléments de structures à la validation de modèles.** *Revue Européenne de Génie Civil*, v. 9, p. 1219-1247, 2005.

Multon, S.; Sellier, A. **Multi-scale analysis of alkali-silica reaction (ASR): Impact of alkali leaching on scale effects affecting expansion tests.** *Cement and Concrete Research*, v. 81, p. 122-133, 2016.

Multon, S.; Sellier, A.; Cyr, M. **Chemo-mechanical modelling for prediction of alkali silica reaction (ASR) expansion.** *Cement and Concrete Research*, v. 39, p. 490-500, 2009.

Multon, S.; Toutlemonde, F. **Effect of applied stresses on alkali-silica reaction induced expansions.** *Cement and Concrete Research*, v. 36, p. 912-920, 2006.

Neville, A. M.; Brooks, J. J. **Tecnologia do Concreto.** Porto Alegre, Brazil: Bookman, 2013.

Nguyen, M.; Timothy, J.; Meschke, G. **Numerical analysis of multiple ion species diffusion and alkali-silica reaction in concrete.** In: *Computational Modellings of Concrete Structures (EURO-C)*. St Anton am Alberg: CRC Press, Taylor & Francis Group, 2014.

Nguyen, V. P.; Stroeve, M.; Sluys, L. J. **Multiscale failure modeling of concrete: Micromechanical modeling, discontinuous homogenization and parallel computations.** *Computer Methods in Applied Mechanics and Engineering*, v. 201, p. 139-156, 2012.

Oberholster, R. E. **Alkali reactivity of siliceous rock aggregates: Diagnosis of the reaction, testing of cement and aggregate and prescription of preventive measures.** In: *Proceedings of the 6th International Conference Alkalis in Concrete – Research and Practice*. Copenhagen: 1983.

Pacelli, W. A. **Tema II: Casos Históricos – Barragens e outras estruturas.** *Relatório Final – 1º Simpósio sobre Reatividade Álcali-Agregado em Estruturas de Concreto*. Annals... Goiânia: CBGB/FURNAS, 1999.

Pan, J. W.; Feng, Y. T.; Wang, J. T.; Sun, Q. C.; Zhang, C. H.; Owen, D. R. J. **Modeling of alkali-silica reaction in concrete: a review.** *Structural Civil Engineering*, v. 6, p.1-18, 2012.

Pecchio, M.; Kihara, Y.; Battagin, A. F.; Andrade, T. **Produtos da reação álcali-silicato em concretos de edificações da região metropolitana de Recife.** *2º Simpósio sobre Reação Álcali-Agregado em Estruturas de Concreto*. Anais... Rio de Janeiro: IBRACON, p. 1-16, 2006.

Pignatelli, R. **Modeling of degradation induced by alkali-silica reaction in concrete structures.** *PhD Thesis – Politecnico di Milano*. Italy: p.163, 2012.

Pignatelli, R.; Comi, C.; Monteiro, P. **A coupled mechanical and chemical damage model for concrete affected by alkali-silica reaction.** *Cement and Concrete Research*, v. 53, p. 196-210, 2013.

Pomarico, A. A.; Roselli, G.; Caltabiano, D. **Modelling of Viscoelastic Phenomena in Concrete Structures.** *Proceedings of the 2016 COMSOL Conference*. Munich, 2016.

Ponce, J.; Batic, O. **Different manifestations of the alkali-silica reaction in concrete according to the reaction kinetics of the reactive aggregate.** *Cement and Concrete Research*, v. 36, p.1148-1156, 2006.

Poole, A. B. **Alkali-silica reactivity mechanisms of gel formation and expansion.** In: *Proceedings of the 9th International Conference on Alkali-Aggregate Reaction*. London, England: p. 782-789, 1992.

Pourbehi, M. S.; Van Zijl, G. P. A. G.; Strasheim, J. A. v. B. **Modelling of Alkali Silica Reaction in concrete structures for rehabilitation intervention.** Cape Town, South Africa: *5th International Conference on Concrete Repair, Rehabilitation and Retrofitting (ICCRRR)*. MATEC Web of Conferences 199, 03007, 2018.

Powers, T. C.; Steinour H. H. **An interpretation of some published researchers on alkali-aggregate reaction: Part 1 – the chemical reactions and mechanism of expansion.** *American Concrete Institute - Journal Proceedings*, v. 51, p. 497-516, 1955a.

Powers, T. C.; Steinour H. H. **An interpretation of some published researchers on alkali-aggregate reaction: Part 2 – a hypothesis concerning safe and unsafe reactions with reactive silica in concrete.** *American Concrete Institute - Journal Proceedings*, v. 51, p. 785-812, 1955b.

Poyet, S. **Etude de la dégradation des ouvrages en béton atteints par la réaction alkali-silice – approche expérimentale et modélisation numérique des dégradations dans un environnement hydro-chemo-mécanique variable.** *PhD Thesis – Université de Marne la Vallée*. France: p. 237, 2003.

Poyet, S.; Sellier, A.; Capra, B.; Thèvenin-Foray, G.; Torrenti, J.-M.; Tournier-Cognon, H.; Bourdarot, E. **Influence of Water on Alkali-Silica Reaction: Experimental Study and Numerical Simulations.** *Journal of Materials in Civil Engineering*, v. 18, p. 588-596, 2006.

Rajabipour, F.; Giannini, E.; Ideker, J. H.; Dunant, D. F. **Alkali-silica reaction: Current understanding of the reaction mechanisms and the knowledge gaps.** *Cement and Concrete Research*, v. 76, p. 130-146, 2015.

Rüsch, H.; Jungwirth, D.; Hilsdorf, H. K. **Creep and Shrinkage – Their Effect on the Behavior of Concrete Structures.** *1st Edition, Springer-Verlag*. New York, USA: p. 284, 1983.

Sahu, S.; Thaulow, N. **Delayed ettringite formation in Swedish concrete railroad ties.** *Cement and concrete research*, v.34, p.1675-1681, 2004.

Sanchez, L. F. M.; Fournier, B.; Jolin, M.; Duchesne, J. **Reliable quantification of AAR damage through assessment of the Damage Rating Index (DRI).** *Cement and Concrete Research*, v. 67, p. 74-92, 2015.

Sanchez, L.; Multon, S.; Sellier, A.; Cyr, M.; Fournier, B.; Jolin, M. **Comparative study of a chemo-mechanical modelling for alkali silica reaction (ASR) with experimental evidences.** *Construction and Building Materials*, v. 72, p. 301-315, 2014.

Saouma, V. E.; Martin, R.A.; Hariri-Ardebili, M.A.; Katayama, T.A. **A mathematical model for the kinetics of the alkali-silica chemical reaction.** *Cement and Concrete Research*, v. 68, p. 184-195, 2015.

Scrivener, K. L. **Importance of microstructural understanding for durable and sustainable concrete.** *Concrete Repair, Rehabilitation and Retrofitting II*, p. 13-20, 2009.

Sellier, A. **Anisotropic Damage and Visco-Elasto-Plasticity Applied to Multiphasic Materials.** [Research Report] LMDC – Laboratoire Matériaux et Durabilité des Constructions de Toulouse; Université de Toulouse III – Paul Sébatier; INSA de Toulouse. 2018.

Sellier, A. **Modélisations probabilistes du comportement des matériaux et structures en génie civil.** Ph.D. Thesis – LMT – ENS Cachan. France: p. 160, 1995.

- Sellier, A.; Bournazel, J. P.; Mébarki, A. **Modeling the alkali-aggregate reaction with descriptions of the local destructive phenomena involved.** *Materials and Structures*, v. 28, p. 373-383, 1995a.
- Sellier, A.; Casaux-Ginestet, G.; Buffo-Lacarrière, L.; Bourbon, X. **Orthotropic damage coupled with localized crack reclosure processing – Part I: constitutive laws.** *Engineering Fracture Mechanics*, v. 971, p.148-167, 2013.
- Sellier, A.; Multon, S.; Buffo-Lacarrière, L.; Vidal, T.; Bourbon, X; Guillaume, C. **Concrete creep modelling for structural applications: non-linearity, multi-axiality, hydration, temperature and drying effects.** *Cement and Concrete Research*, Elsevier, v. 79, p. 301-315, 2016.
- Shin, J. H. **Modeling alkali-silica reaction using image analysis and finite element analysis.** Dissertation Tip, University of Illinois at Urbana-Champaign, 2009.
- Shin, J.; Jee, N.; Struble, L. J.; Kirkpatrick, R. J. **Modeling Alkali-Silica Reaction Using Image Analysis and Finite Element Analysis.** *Advanced Materials Research*, vols.(250-253). p. 1050-1053, 2011.
- Silva, N. G.; Collodetti, G.; Pichetti, D. Z. C. M.; Gleize, P. J. P. **Efeitos do ar incorporado nas propriedades do estado endurecido em argamassas de cimento e areia.** In: *Anais do 51º Congresso Brasileiro do Concreto (CBC)*, 2009.
- Silveira, J. F. A. **A Expansão do Concreto em Barragens Afetadas pela RAA e a Importância das Tensões Confinantes.** 1º *Simpósio sobre Reatividade Alcali-Agregado em Estruturas de Concreto*. Annals... Goiânia: CBGB/FURNAS, 1997.
- Simo, J. **Numerical analysis and simulation of plasticity.** *Handbook of Numerical Analysis*, Holland: VI, 1998.
- Stanton, T. E. **Expansion of Concrete Through Reaction Between Cement and Aggregates.** New York: *Proceedings of ASCE*, 66(10), p.1781-1811, 1940.
- Suwito, A.; Jin, W.; Xi, Y.; Meyer, C. **A mathematical model for the pessimum effect of ASR in concrete.** *Concrete Science and Engineering*, RILEM, v.4. p.23-2, 2002.
- Taylor, H. F. W. **Cement chemistry.** London: Thomas Telford, 2nd edition, 1997.
- Taylor, H.F.W.; Famy, C.; Scrivener, K.L. **Delayed ettringite formation.** *Cement and concrete research*, v. 31, p .683-693, 2001.
- Thaulow, N.; Johansen, V.; Jakobsen, U. H. **What causes Delayed Ettringite Formation?** In: *Mechanisms of chemical degradation of cement-based systems*. Boston, USA: E&FN SPON, p .219-226, 1997.
- Thomas M. D. A.; Fournier, B.; Folliard, K. J. **Alkali-Aggregate Reactivity (AAR) Facts Book.** Springfield, VA: *U.S. Department of Transportation – Federal Highway Administration*, Report no. FHWA-HIF-13-019, p. 211, 2013.
- Thomas, M.; Folliard, K.; Drimalas, T.; Ramlochan, T. **Diagnosing delayed ettringite formation in concrete structure.** *Cement and concrete research*, v.28. p. 841-847, 2008.
- Tiecher, F. **Reação álcali-agregado: avaliação do comportamento de agregados do sul do Brasil quando se altera o cimento utilizado.** *Master Thesis – Universidade Federal do Rio Grande do Sul*. Porto Alegre, Brazil: p. 182, 2006.

- Troxell, G. E.; Raphael, J. M.; Davis, R. E. **Long-Time Creep and Shrinkage Tests of Plain and Reinforced Concrete.** *Proceedings of ASTM International*, v. 58, p. 1101-1120, 1958.
- Ulm, F.-J.; Coussy, O.; Larive, C.; Kefei, L. **Thermo-Chemo-Mechanics of ASR Expansion in Concrete Structures.** *Journal of Engineering Mechanics*, v. 126, p. 233-242, 2000.
- Wawrzeczyk, J.; Molendowska, A. **Impact of Air Entraining Method on the Resistance of Concrete to Internal Cracking.** *IOP Conference Series: Materials Science and Engineering*, 245, 2017.
- Wendner, R.; Hubler, M. H.; Bazănt, Z. P. **Statistical justification of model B4 for multidecade concrete creep using laboratory and bridge databases and comparisons to other models.** *Materials and Structures*, v. 48, p. 815-833, 2015.
- Wood, J. G.; Young, J. S.; Ward, D. E. **The structural Effects of Alkali-Aggregate Reaction on Reinforced Concrete.** In: *Concrete Alkali-Aggregate Reactions, Proceeding of the 7th International Conference.* Edited by Graham-Bellew, Patrick E. Noyes Publications, Park Ridge, New Jersey. Ottawa, Canada: 1987.
- Wu, T.; Temizer, I.; Wriggers, P. **Multiscale hydro-thermo-chemo-mechanical coupling: Application to alkali-silica reaction.** *Computational Materials Science*, v. 84, p. 381-395, 2014.
- Xi, Y.; Suwito, A.; Wen, X.; Meyer, C.; Jin, W. **Testing and modeling alkali-silica reaction and the associated expansion of concrete.** *Mechanics of Quasi-Brittle Materials and Structures, Proceedings of International Workshop in honor of Prof Z. P. Bazănt 60th birthday.* Paris: Hermes Science Publications, 1998.
- Zhang, C.; Wang, A. Q.; Tang, M. S.; Wu, B. Q.; Zhang, N. S. **Influence of aggregate size and aggregate size grading on ASR expansion.** *Cement and Concrete Research*, v. 29, n. 9, p. 1393-1396, 1999.
- Zhang, M. H.; Malhotra, V. M. **Characteristics of a thermally activated aluminosilicate pozzolanic material and its use in concrete.** *Cement and Concrete Research*, v. 25, n. 8, p. 1713-1725, 1995.

